Tesis Doctoral

Estructura electrónica y reactividad de nitrosilos en complejos de metales de transición

Roncaroli, Federico

2004

Tesis presentada para obtener el grado de Doctor de la Universidad de Buenos Aires en Ciencias Químicas de la Universidad de Buenos Aires

Departamento de Química Inorgánica, Analítica y Química Física
Facultad de Ciencias Exactas y Naturales
Universidad de Buenos Aires

Estructura Electrónica y Reactividad de Nitrosilos en Complejos de Metales de Transición

Federico Roncaroli

Director: Prof. José A. Olabe

Tesis presentada para optar al Título de Doctor de la Universidad de Buenos Aires.

Buenos Aires, Diciembre de 2004.

Departamento de Química Inorgánica, Analítica y Química Física
Facultad de Ciencias Exactas y Naturales
Universidad de Buenos Aires

Electronic Structure and Reactivity of Nitrosyls in Transition Metal Complexes

Federico Roncaroli

Director: Prof. José A. Olabe

Dissertation submitted in partial satisfaction of the requirements for the degree of:
Doctor de la Universidad de Buenos Aires.

Buenos Aires, December 2004.

A mis padres

"Trabaja y persevera!
Nada existe en el mundo
rebelde ni infecundo
bajo el poder de Dios y de la idea!"

Abstract

This work affords the preparation of mononuclear and dinuclear nitrosyl-complexes with metals of group 8, containing diverse auxiliary ligands. We focus on the different reactivity modes of the bound nitrosyl group, either as a nitrosonium (NO^+) or nitrogen monoxide (NO) species.

The new complex *trans*-$[NCRu(py)_4(CN)Ru(py)_4NO](PF_6)_3$ has been synthesized and characterized by UV-vis, IR, Raman and NMR spectroscopies. The reactivity toward nucleophiles like OH^- and cysteine were studied. The compound has an intense visible band, which was assigned as a donor acceptor charge transfer (DACT) transition from the remote Ru^{II} to the delocalized $\{Ru^{II}$-$NO^+\}$ moiety. The products of oxidation of the remote Ru and the reduction of the NO^+ were characterized through different spectroscopic techniques.

A systematic study of the addition reactions of OH^- to a large series of nitrosyl complexes was performed. A good linear correlation was found between the reactivity and the redox potential of the redox couple NO^+/NO°, which was interpreted in terms of the Marcus theory for atom-transfer reactions. In a similar way, the addition reactions of cysteine to a series of ruthenium nitrosyl complexes were studied. In a first reaction step, the fast formation of a 1:1 adduct between complex and cysteine was observed. In a subsequent step, another intermediate was produced, in principle a 1:2 adduct, which is responsible for the 2 electron reduction of most of the studied nitrosyl complexes. Although the overall reaction is complicated, the two subsequent additions of cysteine are similar to the addition of OH^-.

The one-electron reduction products for several ruthenium nitrosyl complexes were characterized through EPR and IR spectroscopies. A great constancy in the measured parameters was found, revealing a strong covalency in the RuNO moieties. IR spectroscopy showed a great decrease in the NO-stretching frequency upon reduction, of ca. 300 cm^{-1}.

Finally, the thermal decomposition of the reduced nitroprusside ion, $[Fe(CN)_5NO]^{2-}$, was studied by means of UV-vis, IR and EPR spectroscopies. A slow NO release was observed at pH > 6 (ca. 10^{-5} s^{-1}). At lower pH´s the decomposition was enhanced through CN^-- labilization. A dinitrosylated intermediate, proposed to be *trans*-$[Fe(CN)_4NO_2]^{2-}$, was detected. This compound is responsible for the disproportionation into nitroprusside and N_2O. At lower pH´s the same compound can generate another dinitrosyl complex, $[Fe(CN)_2(NO)_2]^-$.

Key words: ruthenium, nitrosyl complexes, dinuclear complex, intramolecular charge transfer, electronic coupling, electrophilic reaction, nucleophilic addition, OH^-, linear free enregy relationship, cysteine, thiols, adduct formation, nitroprusside, dinitrosyl complex, disproportionation, NO, nitrogen monoxide, nitric oxide.

Resumen

El trabajo comprende la preparación de compuestos nitrosilados mono- y dinucleares con metales del grupo 8, conteniendo diversos ligandos auxiliares, y focaliza su atención en diferentes modos de reactividad del grupo nitrosilo coordinado, sea como nitrosonio (NO^+) o como monóxido de nitrogeno (NO).

Se sintetizó el nuevo compuesto *trans*-$[NCRu(py)_4(CN)Ru(py)_4NO](PF_6)_3$, el cual se caracterizó por espectroscopías UV-vis, IR, Raman y RMN. Se estudió la reactividad frente a nucleófilos como OH^- y cisteína. El compuesto presenta una banda intensa en el espectro visible, asignada a una transición de transferencia de carga entre el Ru^{II} distante y el sistema $\{Ru^{II}\text{-}NO^+\}$. Los productos de la oxidación del Ru lejano y de reducción del NO^+ también fueron caracterizados por diversas espectroscopias, incluyendo EPR.

Se efectuó un estudio sistemático de la reacción de adición del OH^- frente a un gran número de complejos nitrosilados. Se encontró una muy buena correlación entre la reactividad y el potencial redox de la cupla NO^-/NO°, interpretada en términos de la teoría de Marcus sobre la transferencia de átomos. De forma análoga, se estudió la reacción de adición de la cisteína frente a una serie de rutenio-nitrosilos. En un primer paso de reacción se observó la rápida formación de un aducto 1:1 (complejo: cisteína). Posteriormente se forma otro aducto de estequiometría 2:1, el cual es responsable de la reducción con dos electrones de la mayoría de los complejos estudiados. A pesar de la mayor complejidad de la reacción global, las dos adiciones de cisteína son similares a la reacción con OH^-.

Una vasta serie de compuestos de rutenio conteniendo el NO^- coordinado fueron reducidos y caracterizados por EPR e IR. Se encontró una notable constancia en los parámetros medidos, revelando una apreciable covalencia en el fragmento RuNO. La espectroscopia IR revela un gran decrecimiento de la frecuencia de estiramiento N-O, del orden de 300 cm^{-1}.

Finalmente, se estudió la descomposición térmica de los productos de reducción del ion nitroprusiato, $[Fe(CN)_5NO]^{2-}$ por medio de espectroscopias UV-vis, IR y EPR. La liberación de NO a pH > 6 es un proceso lento (ca. 10^{-5} s^{-1}), el cual se hace mucho más rápido a pH´s menores por la labilización de CN^-. Se detectó un intermediario dinitrosilado, *trans*-$[Fe(CN)_4(NO)_2]^{2-}$, generado por reacción entre NO y $[Fe(CN)_4NO]^{2-}$ Este intermediario desproporciona a nitroprusiato y N_2O, o bien genera alternativamente otro compuesto dinitrosilado, $[Fe(CN)_2(NO)_2]^-$.

Palabras clave: rutenio, complejo nitrosilado, compuesto dinuclear, transferencia de carga intramolecular, acoplamiento electrónico, reacción electrofílica, adición nucleofílica, OH^-, relación lineal de energía libre, cisteina,

tiol, formación de aductos, nitroprusiato, complejo dinitrosilado, desproporcionación, NO, monóxido de nitrógeno, óxido nítrico.

Index

List of figures.

List of tables

List of schemes

1. Introduction

The present work deals with some selected topics on the coordination chemistry of nitrogen monoxide (NO). The general structural and spectroscopic properties of complexes of transition metal centers containing the nitrosyl ligand have been studied for a long time. The relevance to environmental issues associated with NO_x effluents (mixtures of NO-NO_2) was complemented in the recent years with the discovery of the biological roles of NO. An explosion of papers in the literature, related to the diverse physiological activity of NO, and the ubiquitous presence of transition metal ions in the body fluids, either free or as participating in enzyme-functions, has attracted considerable attention in order to get a deeper knowledge of the fundamental aspects of metallonitrosyl-chemistry.

One of the most studied nitrosyl complexes is the nitroprusside ion, $[Fe(CN)_5NO]^{2-}$ (NP), where the nitrosyl ligand can be formally considered as a nitrosonium, NO^+, species. Many other complexes with this electronic structure, although containing other fragments, have been described, $\{X_5MNO\}^n$, with X = aqua, amines, polypyridines, py, and other ancillary ligands. The metals span diverse groups of the Periodic Table, but a great predominance of group 8 metals can be appreciated.

In Chapter 2, we begin with a dinuclear, cyanobridged compound, which was prepared for the first time. In this way, we attempted to study the nature of the electronic communication between the metal centers, through the spectroscopic and the electrophilic reactivity changes obtained as a result of changing the redox state of both fragments.

In addition to the NO^+-redox state, the complexes can be reduced, either monoelectronically or through successive electron-additions, which can be accomplished with chemical reductants, or electrochemically. Another way of formally

reducing the nitrosonium ligand is by adding different nucleophiles. This type of reactions has been studied for a long time for different complexes, but the kinetic and mechanistic studies were limited to the OH^--additions on nitroprusside and other cyano-analogs. We afford in Chapter 3 a comprehensive study of this reaction type for a broad series of complexes, searching for significant parameters controlling the addition rates. In Chapter 4, we extend the above studies to the reactions of thiolates, selecting cysteine as a biologically relevant nucleophile adding to a set of ruthenium nitrosyl-complexes with varying redox potentials.

In Chapter 5, we address some spectroscopic studies on a series of reduced nitrosyl-complexes containing ruthenium and different coligands. By employing EPR and IR techniques, an effort is made to look for structural variations as a function of the different metal environments. Surprisingly, the differences are minor, probably associated with a strong covalency in the RuNO fragments, which interestingly do not correspond with the greater variations found for other for similar iron complexes.

Finally, Chapter 6 deals with the complex process occurring after the generation of one-electron reduced NP in solution. The $[Fe(CN)_5NO]^{3-}$ ion, which can be easily generated from NP with dithionite, affords a thermal decomposition process in a long time scale (hours). The stoichiometry and mechanism of this process is quite relevant for a better understanding of the chemistry ensuing NP injection in the body fluids for dealing with hypertensive situations. We search on the influence of pH for promoting a fast NO-release after reduction. The study is also appropriate to look for the fate of NO upon reduction of nitroprusside. Thus, dissociation from the metal, eventual redox changes occurring after dissociation, and the nature of the different products emerging at the different time scales, are crucial questions not clearly solved in the previous studies in the literature.

2. Metallonitrosyl fragment as electron acceptor: Intramolecular charge transfer, long range electronic coupling and eletrophylic reactivity in the *trans*-$[NCRu(py)_4CNRu(py)_4NO]^{3+}$ ion

2.1. Introduction

An increasing effort is nowadays directed to synthesize compounds in which relevant spectroscopic and reactivity properties can be put under precise control. Recently, in our group, an effort was focused in the study of the reactivity changes of coordinated ligands upon variations on the oxidation-state of metals located at extended distances. The chemical electrophilic reactivity of bound nitrosyl in the $[(NH_3)_5Ru^{II,III}(NC)Os(CN)_4NO]^{0,1-}$ ions was studied. A five-order of magnitude increase in the rate constant for OH^- addition was found upon oxidation of the distant ruthenium center from the II to the III state.[1] The cyano-bridge seems to play a key role in the metal-metal electronic coupling responsible of the above mentioned property.[2] Cyano-bridged polynuclear metal complexes have in fact received considerable attention over the recent years,[3] re-stimulated by studies on mixed-valent compounds, as well as on photoinduced electron- and energy-transfer processes.[4]

We considered valuable to synthesize new *trans*-cyano-bridged complexes, on the basis of recent work with the *trans*-$\{Ru(py)_4\}^{2+}$ centers (py = pyridine), which proved to be highly stable (unlike the $\{Ru^{II}(bpy)_2\}$ analogs, bpy = 2, 2′ bipyridine), and may act as nonchromophoric spacers in oligometallic structures.[5,6] The advantages of synthesizing complexes with *trans*-bridging units, instead of the more commonly found *cis*-ones, as with *cis*-$\{Ru(bpy)_2\}^{2+}$-based complexes, has been emphasized.[7] The *trans*-geometry yields structurally well defined assemblies (without potential structural isomerism), appropriate to study long-range processes.

The nitrosyl ligand appeared as a good candidate for probing the changes of reactivity when bound to the new oligomeric structures. The studies with bound

nitrosyl deserve special attention in the context of modern coordination chemistry,[8] particularly the redox interconversions, which are known to be important in fundamental processes in NO biochemistry, such as transport, uptake and delivery in the biological fluids.[9] As a typical non-innocent ligand, nitrosyl can act mainly as a diamagnetic, strongly π-acceptor[8] NO^+ or as the paramagnetic, one-electron reduced molecule, NO.[10] The presence of the two-electron reduced species, HNO, has also been demonstrated in several bound systems.[11] In the above context, the synthesis of the new dinuclear compound, *trans*-$[NCRu^{II}(py)_4(CN)Ru^{II}(py)_4NO](PF_6)_3$, was conceived as a tool for better understanding the factors that effectively control the reactivity of NO^+, particularly its behavior as an electrophile[12] and its ability to dissociate from the relevant metal centers upon changing the redox state. The possibility of variation of the adjacent coligands as well as the distant metal fragment was a part of the synthetic strategy designed for expanding the still limited set of mononuclear complexes where structure-reactivity studies have been made available. In addition, the presence of an exposed cyanide ligand in the *trans*-position to the nitrosyl sets the basis for further coordination of additional metal fragments, in order to obtain potential molecular wires.

2.2. Experimental section

Materials. Acetonitrile (AcN, Merck) was distilled under argon after refluxing for 12 h over CaH_2. Tetra-n-butylammonium hexafluorophosphate, $TBAPF_6$ (Aldrich) was recrystallized from ethanol. NaCl was p.a. grade (Merck). Decamethylferrocene (Aldrich) was used as provided. The precursor compounds $[RuCl_2(py)_4]$, *trans*-$[Ru(CN)_2(py)_4].H_2O$, *trans*-$[RuCl(NO)(py)_4](PF_6)_2$ and $[Ru(bpy)(H_2O)(tpy)](ClO_4)_2$ were prepared according to literature procedures.[5,13,15]

Water for the electrochemical experiments was deionized and distilled after refluxing for 6 hs over alkaline $KMnO_4$. All other solvents and solid reagents were

obtained commercially and used without further purification. Elemental analyses were carried out by H. Kolbe in Mülheim an der Ruhr, Germany.

Preparation of *trans*-[NC(py)$_4$Ru(CN)Ru(py)$_4$(NO)](PF$_6$)$_3$ (I). 0.30 g of *trans*-[Cl(py)$_4$Ru(NC)Ru(py)$_4$(CN)]PF$_6$ (0.28 mmols)[7] and 1.00 g of $NaNO_2$ (14.5 mmols) were suspended in 400 ml of deaerated water. The mixture was stirred in the dark for 48 hs under an Ar atmosphere. The clear solution was then concentrated to 25 ml, and *ca.* 1 ml of an NH_4PF_6 saturated water solution was added to afford a yellow solid, which was collected by filtration.

Purification was performed by ion-exchange chromatography (Dowex 50W X2, 100-200 mesh, H^- form, l = 20 cm, d = 2.5 cm) as follows: the crude product was dissolved in 50 ml of 0.1 M HCl yielding a deep violet solution, which was seeded in the column and eluted with HCl 1:4. The first major violet fraction was collected and precipitated with ca. 20 ml of the NH_4PF_6 solution. The obtained solid was repurified following the same procedure, taking special care to collect exclusively the first fraction with absorption maximum at 518 nm. Addition of saturated NH_4PF_6 solution yielded a violet solid, which was collected by filtration and dried *in vacuo* (yield 0.150 g, 40%). Scheme 2.1 summarizes the synthetic procedure. Anal. Calcd for [NCRu(py)$_4$(CN)Ru(py)$_4$NO](PF$_6$)$_3$: C, 37.32; H, 2.98; N, 11.40. Found: C, 37.16; H, 3.10; N, 11.27. δ_H (CD_3CN) 8.32 (4 H, t, H^4 x 4), 8.15 (16H, m, $H^{2,6}$, $H^{2'6'}$ x 4), 7.87 (4H, t, $H^{4'}$ x 4), 7.59 (8H, t,$H^{3'5'}$ x 4), 7.16 (8H, t, $H^{3,5}$ x 4). δ_C (CD_3CN) 158.32 (8C, $C^{3.5}$ x 4); 155.01 (8C, $C^{3',5'}$ x 4); 144.19 (4C, C^4 x 4); 138.46 (4C, C^4 x 4); 129.94 (8C, $C^{2,6}$ x 4); 126.64 (8C, $C^{2'6'}$ x 4). In spite of several attempts, we were not able to obtain single crystals suitable for X-Ray diffraction analysis.

Preparation of [(bpy)(tpy)RuNCRu(py)$_4$CNRu(py)$_4$NO](PF6)$_5$ (II). 30 mg of **I** and 28mg of [Ru(bpy)(H_2O)(tpy)](ClO_4)$_2$ (tpy = 2,2′:6′,2″-terpyridine) were suspended in 5 ml of water. 2 drops of HNO_3 (c) were added and the mixture was allowed to react in darkness for 2 days. A crystalline black solid was filtrated

out. This compound was redisolved in water. The addition of saturated NH_4PF_6 solution afforded a brown solid, which was collected by filtration and dried *in vacuo*. Yield: 20 mg (42%).

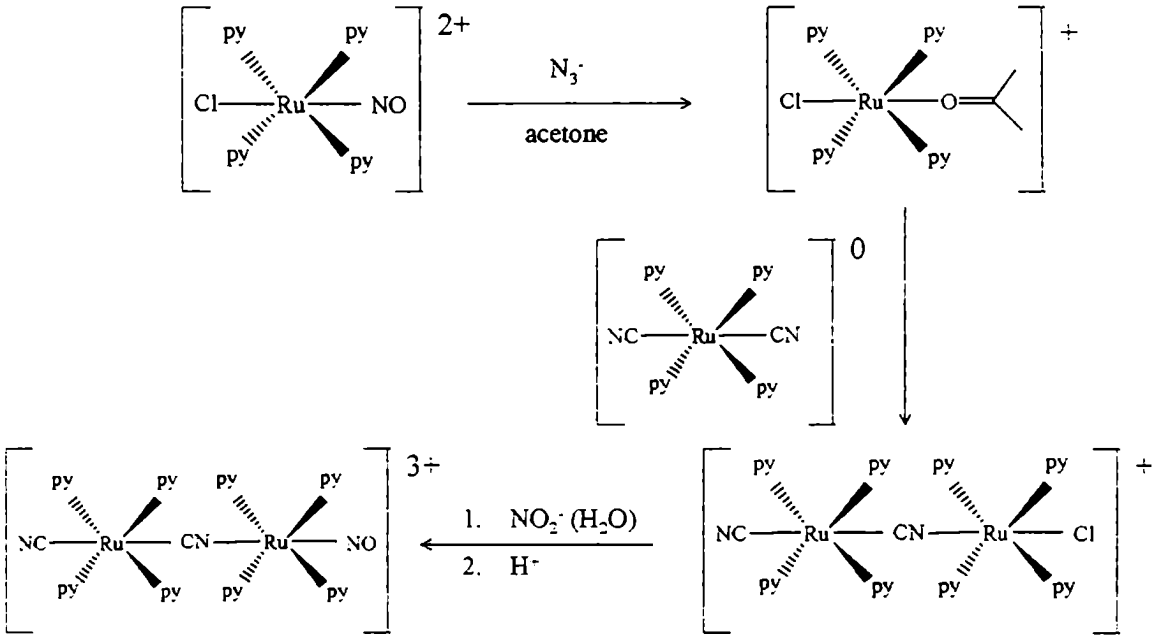

Scheme 2.1. Preparation of $[NCRu(py)_4CNRu(py)_4NO]^{3-}$

Anal. Calcd for $[(bpy)(tpy)RuNCRu(py)_4CNRu(py)_4NO](PF_6)_5$: C, 37.73; N, 10.51; H, 2.79. Found: C, 36.40; N, 9.93; H, 2.69. The NMR and IR spectra, as well as the electrochemical properties are discussed in the Results section.

Instrumentation and General Procedures. Ultraviolet-visible spectra were recorded with a diode-array instrument, HP 8453, using a RC 6 Lauda thermostat and 1-cm quartz cells. Infrared spectra were obtained using either a Nicolet 510P or a Perkin-Elmer 2000 FTIR spectrometers; solution spectra were obtained using a cell with CaF_2 windows of 3 cm ∅, and a 0.05 mm spacer. NMR spectra were measured with a Brucker AM-500 spectrometer. The Resonance Raman (RR) spectrum was measured in AcN using a rotating cell (pathlength 1-cm) to prevent photodegradation. The cell was purged with N_2 and hermetically

sealed. For excitation the 568-nm line of a cw-Kr-ion laser (Coherent 302) was used, with a power of *ca.* 40 mW at the sample. The scattered light (90°) was focused onto the entrance slit of a double monochromator (ISA, U1000) working as a spectrograph and equipped with a liquid nitrogen cooled CCD camera. The spectral bandwidth was 4 cm^{-1} and the increment per data point 0.53 cm^{-1}. The total accumulation time of the RR spectra was 20 seconds. The spectra are the average of at least 3 independent measurements. Background was removed by polynomial subtraction. Electrochemical measurements were made using a PAR Model 273A potentiostat, in aqueous and AcN solutions, with 0.1 M NaCl or $TBAPF_6$ as supporting electrolytes, respectively. A glassy carbon disc (d = 3 mm) was used as the working electrode, with Pt and Ag/AgCl, 3 M KCl as counter- and reference electrodes, respectively. In AcN, a silver wire was used, with decamethylferrocene as an internal reference. The presently reported potentials refer to the Ag/AgCl, 3 M KCl reference electrode (0.21 V *vs* NHE). The spectroelectrochemical and coulometric experiments were done under argon in 0.1 M $TBAPF_6$ AcN solutions. The *trans*-$[NCRu^{II}(py)_4(CN)Ru^{II}(py)_4NO]^{3-}$ complex was alternatively reduced and oxidized at –20 °C under controlled potential conditions. These procedures were repeated several times without decomposition, as proved by UV-Vis and IR spectroscopies. Samples prepared in this way were transfered via syringe for EPR analysis. The infrared spectroelectrochemical experiments were performed using a three-electrode OTTLE Cell. For the UV-Vis spectroelectrochemistry, a specially modified 1-cm pathlength quartz cuvette attached to a 5-ml glass container was used. The whole setup was purged with Ar and thermostatised (Lauda RL6 CP cryostat). Electrolysis was performed over a platinum-net. A second platinum-net separated by a frit glass was used as a counter electrode, and $Ag/AgNO_3$ (AcN) was used as a reference. X-band EPR spectra were determined with a Bruker ESP 300E spectrometer equipped with a helium flow cryostat (Oxford Instruments ESR 910). The spectra were recorded at 9.45 GHz, 10 μW power, 100 KHz modulation

frequency and 10.0 G modulation amplitude. The one-electron oxidized product of *trans*-$[Ru(CN)_2(py)_4]$ and the one-electron reduced product of *trans*-$[RuCl(py)_4(NO)]^{2-}$ were prepared and characterized in a similar way, providing valuable information for the spectral assignments in the diruthenium compounds.

Spectroelectrochemical experiments with **I** in the UV-visible region (reduction and oxidation) were also done in aqueous solutions (see Table 2.1 for details).

Nucleophilic Addition to Bound Nitrosyl. We performed equilibrium and kinetic studies of OH^- addition into **I**. The solutions for the equilibrium measurements were prepared in the pH range 4.50-6.62, by mixing 1.00 ml of a 4.0 x 10^{-4} M solution of **I** with 4.00 ml of a buffer solution (acetate or phosphate, final I = 1 M, NaCl). All the solutions were equilibrated in the dark at 25.0 ± 0.1 °C for at least 12 hs before recording the spectra. A multiwavelength global analysis of the absorbance *vs* pH data[14] accounted for only two colored species. Application of the chemical model described by eq 2.1 afforded the equilibrium constant and the spectra of the species present in solution.

$$[NCRu(py)_4CNRu(py)_4NO]^{3-} + 2\ OH^- \rightleftarrows [NCRu(py)_4CNRu(py)_4NO_2]^- + H_2O \quad (2.1)$$

The temporal evolution of the above reaction was monitored spectrophotometrically following the disappearance of **I** at 518 nm. Solutions in the pH range 6.75 – 8.15 were prepared by mixing 1 ml of a ca. 5 x 10^{-5} M solution of **I** with 2 ml of a phosphate buffer solution (final I = 1 M, NaCl). Temperature variation in the range 20.0–40.0 ± 0.1°C afforded the activation parameters.

The reaction of **I** with *L*-cysteine was studied with a Hi Tech PQ/SF-53 stopped flow and a Hi Tech SU-40 spectrophotometric unit. The data was acquired by a Hewlett Packard 54600A osciloscope. This last instrument was interfaced to a

computer. With the first instrument a solution 6 x 10^{-5} - 1.2 x 10^{-4} M in **I** was mixed with another solution 6.0 x 10^{-4} – 1.4 x 10^{-2} M in *L*-cysteine. The other conditions were: pH 4.0 (0.1 M acetic buffet), I = I M (NaCl), T = 25.0 °C. Kinetic traces were obtained at 461 nm, where the product of the primary interaction shows an absorption maximum, and were fitted to a single exponential 4 half lives.

Photolysis of *trans*-[NCRu(py)$_4$(CN)Ru(py)$_4$NO]$^{3+}$. Aqueous and AcN solutions of **I** were irradiated with a UV filtered halogen lamp (150 w). The products were tested through UV-vis, IR and electrochemical measurements. In aqueous solution, the release of NO was detected with a specific amiNO-100 electrode (Innovative Instruments, Inc.). Fast decomposition of **I** was achieved by using unfiltered radiation.

2.3. Results

Electrochemistry. Figure 2.1 shows a typical cyclic voltammogram (CV) of **I** in AcN. Two reversible processes at $E_{1/2}$ = 0.50 and 1.40 V are observed, which correspond to a one-electron reduction and one-electron oxidation of **I**, as indicated by controlled potential coulometry. A third irreversible wave at ca. –0.4 V (see Table 2.1) was also observed when extending the potential sweep range. It is most probably related to an additional one-electron reduction with further ligand labilization.[8,9] Table 2.1 collects the half-wave potentials, including values in aqueous solution. In this case, both waves are shifted to more negative potentials ($E_{1/2}$ = 0.22 and 1.18 V, respectively). The waves are fully reversible in the pH range 0 – 2. In the pH range 2-6 an anodic scan (square wave voltammetry, SWV) reveals the same waves, but a reductive scan (starting at 1.3 V, with 5 seconds of equilibration time), triggers the appearance of new waves, revealing the onset of irreversible chemical reactions following one electron oxidation. Above pH 9, both redox waves are replaced by new ones at $E_{1/2}$ = 0.83 and 1.20 V. These results

suggest that not only **I** but also its oxidized form, I_{ox}, might be reactive toward OH^- We describe this in more detail in the Section devoted to Electrophilic Reactivity.

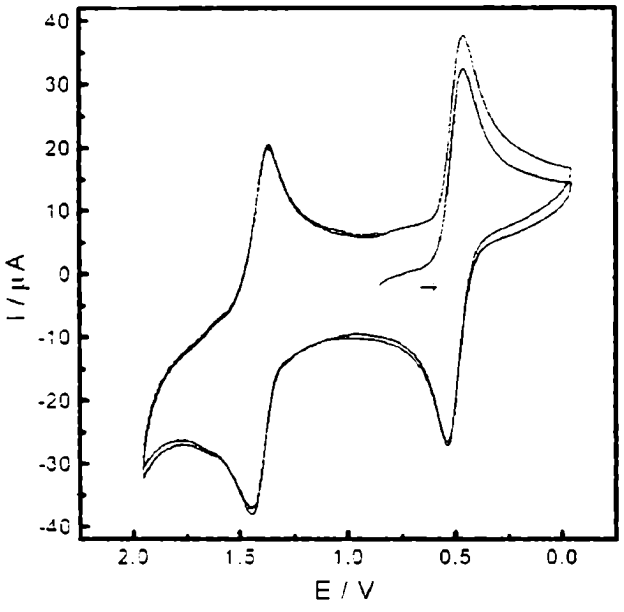

Figure 2.1. Cyclic voltammogram of $[NCRu(py)_4CNRu(py)_4NO](PF6)_3$ in acetonitrile solution, 0.1 M $TBAPF_6$, scan rate 20 mV/s, T = 25 °C.

Electronic Spectra. The visible region of the spectrum of **I** in AcN is dominated by an intense absorption centered at 555 nm (ε = 5800 $M^{-1}cm^{-1}$). Figure 2.2 displays the changes observed in the electronic spectra upon controlled potential conversion to the one electron reduced ($\mathbf{I_{red}}$) and the one electron oxidized ($\mathbf{I_{ox}}$) species in the same solvent. Table 2.1 includes the absorption maxima and molar absorbances for the three redox-linked species. Data for related mononuclear complexes are also included for comparison. The reduction process induces the decay of the 555 nm band and the growth of new bands in the UV region, red-shifted with respect to those of **I** (Figure 2.2, top). The existence of several isosbestic points indicates that side reactions are absent. The total charge related to this conversion accounts for one electron. Chemical reduction under mild conditions using one equivalent of decamethylferrocene yields the same spectral

changes. $\mathbf{I_{red}}$ showed to be stable for hours under anaerobic conditions, and can be reoxidized electrochemically or exposing the solution to air, with total recovery of the characteristic spectrum of **I.** The same holds true for the behavior of the reduced species obtained from $[Ru^{II}Cl(py)_4NO]^{2+}$.

Figure 2.2 (bottom) shows the electrooxidation experiment. A decay of the UV-visible bands of **I** is also observed, with new bands for $\mathbf{I_{ox}}$ appearing at 440, 401, 329, 295 and 260 nm. The same considerations about isosbestic points and total charge hold true in this case. $\mathbf{I_{ox}}$ was stable in AcN solution and **I** was recovered quantitatively by electrochemical reduction. Remarkably, $\mathbf{I_{ox}}$ proved to be very reactive toward traces of water in the solvent. This last observation is related to the complications already described in the electrochemical experiments.

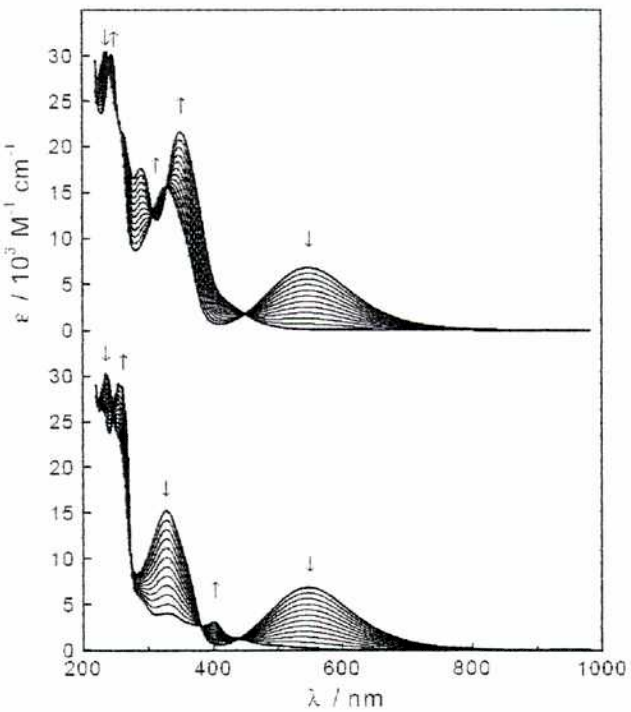

Figure 2.2. UV-vis spectroelectrochemistry of $[NCRu(py)_4CNRu(py)_4NO](PF_6)_3$ in acetonitrile solution 0.1M $TBAPF_6$, T = -20°C. Top: one electron-reduction. Bottom: one-electron oxidation.

For these reasons, the characterization of the three redox-related species in aqueous solution was performed in 1 M or 0.01 M HNO_3 solutions, keeping in mind the onset of electrophilic reactivity. Under these conditions, the redox processes showed an equivalent picture as for AcN. Electrochemical reduction of **I** triggers the complete decay of the band at 518 nm and appearance of several new bands in the UV region. The electrooxidation experiments, if done at pH's lower than 2, show that $\mathbf{I_{ox}}$ is also obtained, without attack at the NO^+ site. This is shown by its CV response (identical to the one displayed by **I**) and the replacement of the UV absorptions characteristic of the Ru^{II}-py chromophores by new absorptions in the near UV-vis region, which we assign as before for the case of AcN solutions. Chemical oxidation of **I** with one equivalent of Ce(IV) induces similar spectral changes. In both cases **I** can be recovered electrochemically at E_{app} = 0.6 V. In general terms, the energies of the near-UV-visible bands for all the dinuclear species shift to greater energies in water compared to AcN, by ca. 1300 cm^{-1} (see Table 2.1, including values for the absorption maxima below 300 nm, which are unshifted in both solvents).

Infrared Spectroscopy. The cyanide and nitrosyl stretching vibrations, ν_{CN} and ν_{NO}, are very sensitive to the redox changes. Figure 2.3 shows the IR spectrum of **I** in AcN, with signals at 2001 and 1976 cm^{-1} (assigned as ν_{CN}, see below) and 1917 cm^{-1}, corresponding to ν_{NO}. A very weak absorption can also be appreciated at *ca.* 2050 cm^{-1}. Upon electrochemical one-electron reduction, ν_{CN} and ν_{NO} shift in opposite directions: the former to 2056 cm^{-1} and the latter to 1626 cm^{-1}. A slight shift of the band at 1612 cm^{-1} (probably associated to pyridine vibrations) to 1609 cm^{-1} is also observed. Chemical reduction using decamethylferrocene or $[RuCl_2(py)_4]$ affords the same spectral features.

In the one electron oxidized product $\mathbf{I_{ox}}$, new ν_{CN} and ν_{NO} bands develop at 2137, 2120 and 1952 cm^{-1}, respectively. Table 2.1 collects the vibrational

information and includes stretching frequencies obtained in aqueous solution, where all the signals are blue-shifted compared to AcN.

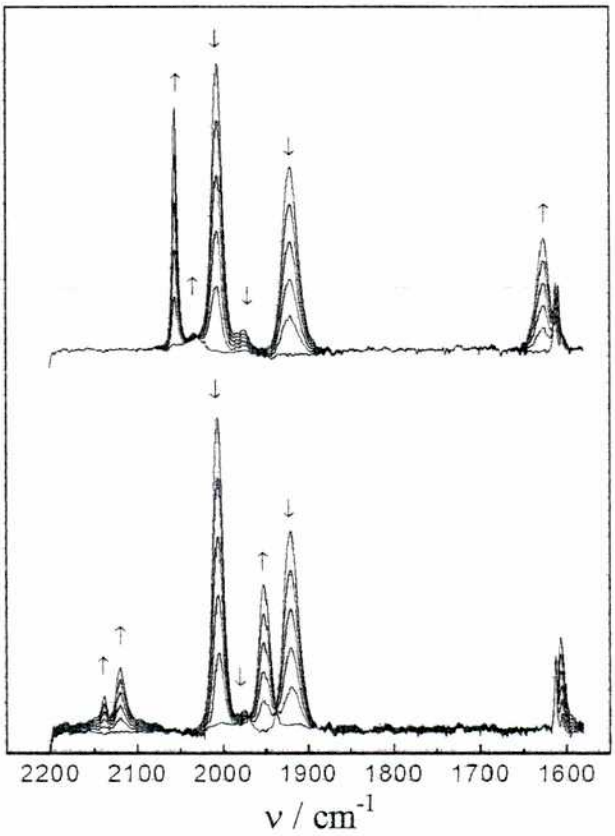

Figure 2.3. Infrared spectroelecytrochemistry of $[NCRu(py)_4CNRu(py)_4NO](PF)_6$ in acetonitrile solution, 0.1 M $TBAPF_6$, T = -20°C. Top: one electron reduction. Bottom: one electron oxidation.

Raman Spectrum of I. A preliminary experiment was performed by irradiating near the maximum of the intense visible band, under resonance conditions. A strong signal appeared at 2000 cm^{-1}, together with a medium-intensity one at 1920 cm^{-1}.

Table 2.1. UV-Visible, IR and Electrochemical Results (Acetonitrile and Aqueous Solutions) for the $[NCRu^{II}(py)_4(CN)Ru^{II}(py)_4NO]^{3+}$ Ion (**I**), and its Reduced $[NCRu^{II}(py)_4(CN)Ru^{II}(py)_4NO]^{2+}$ ($\mathbf{I_{red}}$), and Oxidized Forms $[NCRu^{III}(py)_4(CN)Ru^{II}(py)_4NO]^{4+}$ ($\mathbf{I_{ox}}$).

Complex	$\lambda_{max}(\varepsilon)$,[a] nm ($M^{-1}cm^{-1}$)		Assignment	ν, cm^{-1}		$E_{½}(\Delta E_p)$, V[b]	
	AcN[c]	H_2O[d]		AcN[c]	H_2O[d]	AcN	H_2O
I	555 (5800)	518[e] (6100)	$d_\pi \rightarrow \pi^*_{NO}$	2050 vw	2032 vw	1.40[f] (90)	1.18[g]
	330 (14300)	317 (14500)	$d_\pi \rightarrow \pi^*_{py}$[h]	2001 s	2014[i] s	0.50[f] (95)	0.22[g]
	256sh (20000)	260sh (20000)	$\pi_{py} \rightarrow \pi^*_{py}$[h]	1976 w		-0.45[f,j]	-0.39[j,k]
	237 (27600)	233 (32000)	$d_\pi \rightarrow \pi^*_{py}$[l]	1917 s	1923[m] s		
$\mathbf{I_{red}}$	350 (18500)	333 20200)	$d_\pi \rightarrow \pi^*_{py}$[h]	2056[n] s			
	290 (15000)	294 (20300)	$d_\pi \rightarrow \pi^*_{py}$[l]	2033 sh			
	262 (25000)	262sh (23600)	$\pi_{py} \rightarrow \pi^*_{py}$[l]				
	245 (25700)	239sh (32100)	$\pi_{py} \rightarrow \pi^*_{py}$[h]	1626 s			
$\mathbf{I_{ox}}$	440 (1020)	532sh (500)	$CN^- \rightarrow d_\pi$	2137[o] m			
	401 (2600)	440sh (1670)	$CN^- \rightarrow d_\pi$	2120 s			
	329 (3420)	400 (3500)	$CN^- \rightarrow d_\pi$	1952 s			
	295 (4320)	299 (9200)	$CN^- \rightarrow d_\pi$				
	260 (24600)	266sh (25300) 260 (28800)	$\pi_{py} \rightarrow \pi^*_{py}$[h]				
$[Ru(CN)_2(py)_4]$[p]	374 (22500)		$d_\pi \rightarrow \pi^*_{py}$	2062 s		0.80	
	248 (15500)		$\pi_{py} \rightarrow \pi^*_{py}$				

$[Ru(CN)_2(py)_4]^+$	475 (650)	$CN^- \rightarrow d_\pi$	2108 s		
	377 (1900)	$CN^- \rightarrow d_\pi$			
	258 (21000)	$\pi_{py} \rightarrow \pi^*_{py}$			
$[RuCl(py)_4NO]^{2+}$ [p,q]	450 (150)	d-d; $d_\pi \rightarrow \pi^*_{NO}$	1910 s	0.31 (100)	0.10
	258 (15100)	$\pi_{py} \rightarrow \pi^*_{py}$			-0.24
	232 (20000)	$d_\pi \rightarrow \pi^*_{py}$		-0.62	-0.45
$[RuCl(py)_4NO]^+$	377 (730)	$d_\pi \rightarrow \pi^*_{NO}$	1610 s		
	290 (11500)	$d_\pi \rightarrow \pi^*_{py}$			
	261 (14500)	$\pi_{py} \rightarrow \pi^*_{py}$			

[a] Bands below 230 nm are not reported. [b] Against Ag/AgCl, 3M KCl. [c] See text for experimental details in AcN. [d] The electroreduction in aqueous solution was performed at E_{appl} = 0 V *vs* Ag/AgCl, over a platinum net, I = 0.1 M, HCl. The electrooxidation was performed at E_{appl} 1.4 V, in 1M HNO_3 for the absorptions above 300 nm, and 0.01 M for those below 300 nm. [e] 1 M HCl. [f] CV, 0.02 V/s, in 0.1 M $TBAPF_6$. [g] SWV, 60 Hz, 1 M HNO_3. [h] Corresponding to the dicyano-chromophore. [i] In KBr disk, 2011 cm^{-1}. [j] Irreversible wave. [k] SWV, 60 Hz, 0.01 M HCl, 1 M NaCl. [l] Corresponding to the NO-containing chromophore. [m] In KBr disk, 1917 cm^{-1}. [n] Spectroelectrochemical reduction. [o] Spectroelectrochemical oxidation. [p] Reference 5. [q] The bands at 258 and 232 nm were assigned to $d_\pi \rightarrow \pi^*_{py}$ and $\pi_{py} \rightarrow \pi^*_{py}$, respectively, in reference 5.

EPR. Figure 2.4 shows the spectra of $\mathbf{I_{red}}$ and *trans*-$[RuCl(py)_4NO]^+$ at 10 K. The samples were electrogenerated and rapidly frozen in liquid N_2. Also shown are the results of the powder-simulation,[16] obtained including hyperfine coupling with one nitrogen nucleus (^{14}N, 99.64 % natural abundance, I = 1), and using the spin-hamiltonian parameters $\bar{g}$ = (1.990, 2.024, 1.865), and $\bar{A}/10^{-4}$ cm^{-1} = (31.7, 14.5, 9.1) for $\mathbf{I_{red}}$ and $\bar{g}$ = (1.989, 2.033, 1.874), and $\bar{A}/10^{-4}$ cm^{-1} = (29.7, 14.1, 10.0) for *trans*-$[RuCl(py)_4NO]^+$. As will be discussed later (see Chapter 5), these features agree with other reports on coordinated $NO^{\bullet}$, including ruthenium complexes.[17,18]

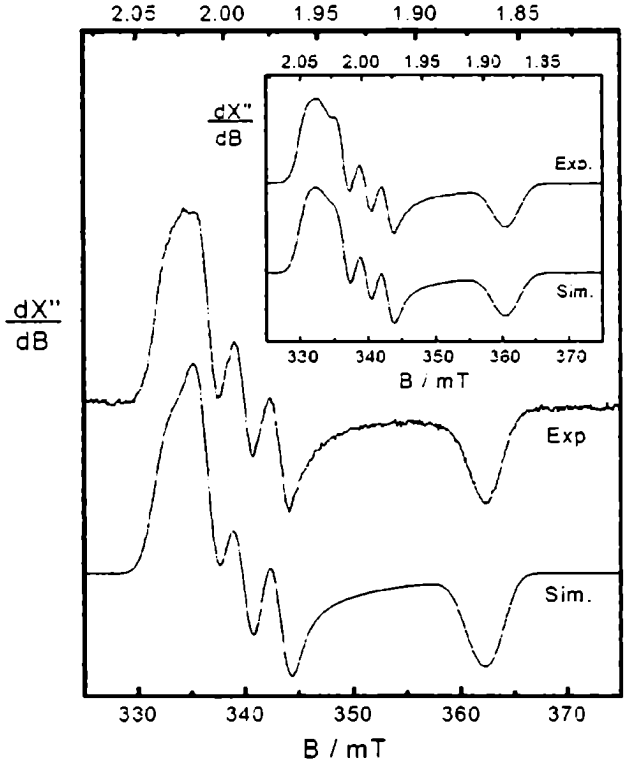

Figure 2.4. Top: EPR spectrum of electrogenerated $[NCRu(py)_4CNRu(py)_4NO]^{2+}$ in acetonitrile, 0.1 M $TBAPF_6$, at 10 K. Bottom: computer simulated spectrum with the parameters detailed in the text (see results section). Inset: same but for the $[RuCl(py)_4NO]^+$ ion.

Electrophilic Reactivity. Figure 2.5 shows the consecutive spectra obtained for the reaction of **I** with OH^-, according to eq 2.1. The consumption of **I** is revealed by the decrease in intensity of the characteristic bands at 233, 255 and 518 nm. The original band at 317 nm shifts to 345 nm, with an increase in intensity. The conversion comprises well-defined isosbestic points in the complete UV-visible region, and the product is stable in the time scale of hours. The equilibrium constant is $K_1 = 3.2 \pm 1.4 \times 10^{15}$ M^{-2} (25 °C, I = 1 M). Equal amounts of the nitrosyl and nitro-species are present at pH 6.3. Acidification down to pH 4 quantitatively recovers **I**

The rate-law for reaction 2.1 shows a first-order behavior with respect to the concentrations of OH^- and **I**, with $k_1 = 9.2 \pm 0.2 \times 10^3$ M^{-1} s^{-1} (25 °C, I = 1 M). The activation parameters are $\Delta H^{\neq} = 90.7 \pm 3.8$ kJ mol^{-1} and $\Delta S^{\neq} = 135 \pm 13$ J K^{-1} mol^{-1}.

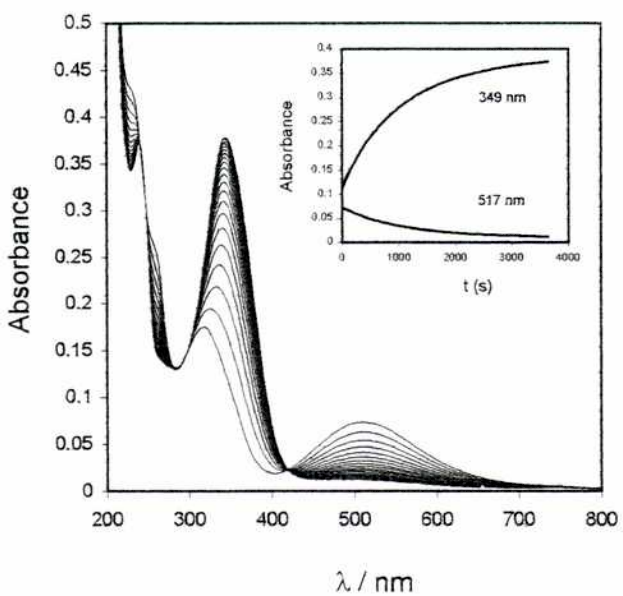

Figure 2.5. Time evolution of the UV-Vis spectra for an aqueous solution of $[NCRu(py)_4CNRu(py)_4NO](PF_6)_3$ (pH 6.77; I = 1 M, NaCl; T = 30 °C, cycle time = 180 s). Inset: kinetic traces at 349 and 517 nm, $k_{obs} = 1.01 \times 10^{-3}$ s^{-1}.

Upon reaction of **I** with excess of cysteine, a new band at 461 nm is observed (see Figure 2.6). The formation of this new compound shows a first order behavior in both reactants. The plot of k_{obs} *vs* cysteine-concentration shows a linear distribution with a slope equal to7.00 ± 0.09 x 10^3 $M^{-1}s^{-1}$ and an intercept of 1.5 ± 0.3 s^{-1} (pH 4.0, I = 1 M, T = 25.0 °C). The last compound reacts further with cysteine in excess. Analogously, the plot of k_{obs} *vs* cysteine-concentration for this second reaction shows a linear distribution, the slope is 35 ± 1 $M^{-1}s^{-1}$ and the intercept is 1.9 ± 0.5 x 10^{-2} s^{-1} (under the same conditions).

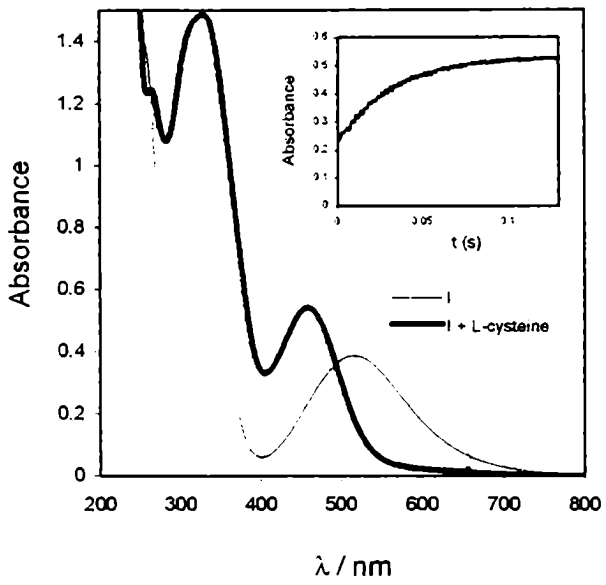

Figure 2.6. Spectrum of **I**, and spectrum of **I** in the presence of *L*-cysteine (pH 4.0, I = 1 M, T = 25.0 °C, cysteine concentration 3 x 10^{-3} M, complex concentration 6 x 10^{-5} M). Inset: kinetic trace at 461 nm, k_{obs} = 23.7 s^{-1}.

The electrochemistry above pH 2 provides some insight on the electrophilic reactivity of $\mathbf{I_{ox}}$. For example, at pH 4.0, after setting the potential at 1.3 V for 15 seconds, new waves appear at 0.41, 0.49, 0.62 and 1.07 V (Figure 2.7). Longer oxidation periods increase the intensity of the new waves, while the waves assigned to **I** (0.22 and 1.2 V) decrease. Following exhaustive electrolysis at 1.3 V the SWV

reveals the complete disappearance of **I** and the formation of a new product with waves at 0.47 and 1.07 V, together with minor quantities of other species. Exhaustive reduction at 0.7 V or at 0.3 V did not recover **I**. The solution reduced at 0.7 V was precipitated with NH_4PF_6, and the solid obtained did not show bands associated with the nitrosyl stretching. The nature of this product is still uncertain, but the evidence clearly suggests that above pH 2 the electrogenerated $\mathbf{I}_{ox}$ is reactive toward nucleophilic attack by OH^-

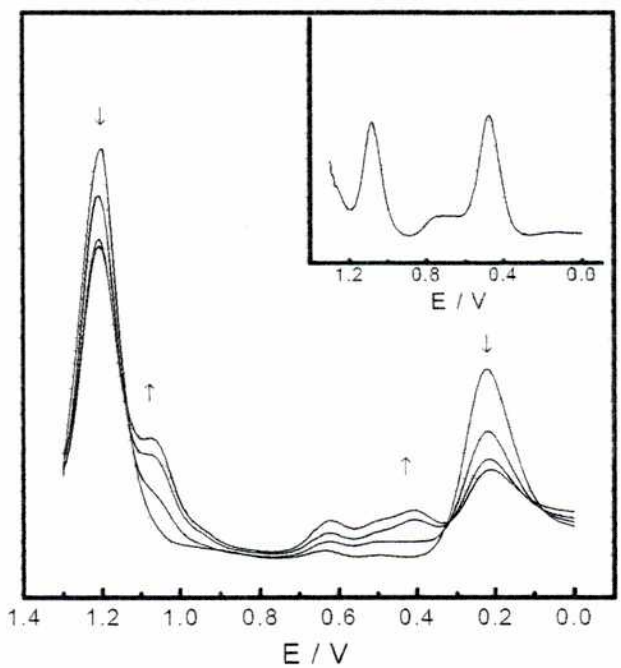

Figure 2.7. Consecutive SWV scans for the electrooxidation of an aqueous solution of $[NCRu(py)_4(CN)Ru(py)_4NO](PF_6)_3$ at 1.3 V (pH 4.0; I = 1 M, NaCl; T = 25 °C). Each scan was obtained subsequent to 15 sec of electrolysis. Inset: scan after exhaustive oxidation at the same potential.

Photoreactivity. The complex **I** was photolyzed in aqueous and AcN solutions, the decomposition being faster in the latter case. The UV-visible bands of **I** disappear, and the IR absorptions of the product suggest the presence of

Ru(III). In water, at pH 4, the presence of free NO was detected, subsequently to light flashing.

Properties of the trinuclear complex (II). The IR spectrum shows, between 1700 cm^{-1} and 2200 cm^{-1}, only two signals at 2012 and 1913 cm^{-1}, which correspond to the ν_{CN} and ν_{NO} respectively. Through cyclic voltammetry in acetonitrile only two waves in the range 0.2 – 1.8 v vs Ag/AgCl are observed, the first one at 0.55 v *vs* Ag/AgCl and the second one at 1.26 v vs Ag/AgCl. These values are similar to those found for complex **I**. The first wave can be assigned to the reduction of the nitrosyl and the second to the oxidation of one of the Ru uncoordinated to the nitrosyl. The oxidation of the other Ru may be at a too high potential to be observed.

Complex **II** was studied by several NMR techniques: ^{1}H-NMR, ^{13}C-NMR, ^{1}H-^{1}H COSY and ^{1}H-^{13}C HMQC (see Figures 2.8 and 2.9). The data from these spectra is summarized in Table 2.2. The assignations of the positions for the [Ru(bpy)(tpy)] fragment are shown in Figure 2.10. There are two types of pyridines, 1 and 2. Pyridines of type 1 are, in principle, closer to the nitrosyl. The signals corresponding to the bpy ligand were assigned in base to similar complexes reported in literature.[27]

All the spectroscopic and electrochemical data obtained for complex **II** are consistent with a structure *trans*-$[(bpy)(tpy)Ru(NC)Ru(py)_4(CN)Ru(py)_4NO]^{5-}$

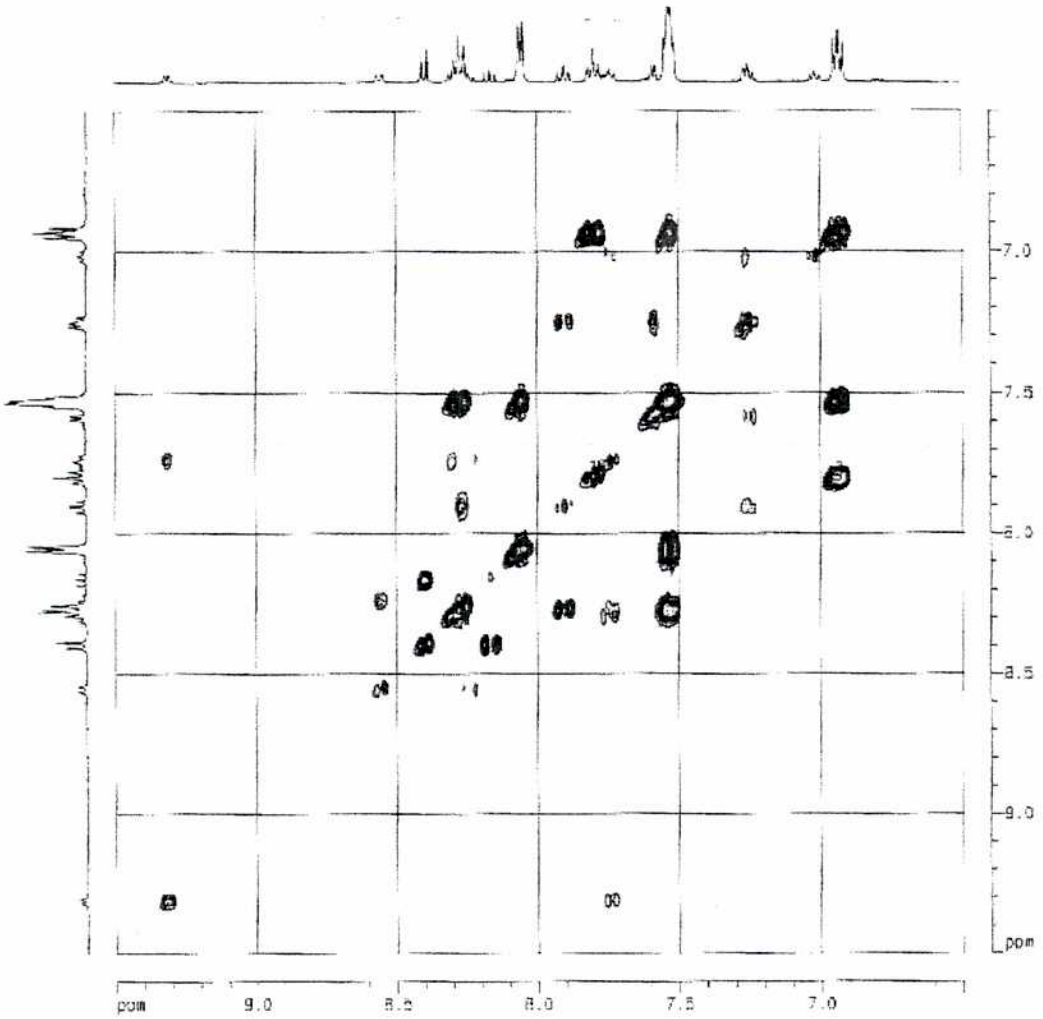

Figure 2.8. ^{1}H-^{1}H COSY spectrum of **II** in acetonitrile.

2.4. Discussion

Previous work on dinuclear, cyano-bridged complexes containing the nitrosyl ligand, $[(NH_3)_5Ru^{II,III}(NC)M(CN)_4NO]^{0,1+}$ (M = Fe, Ru, Os)[1] suggested a significant electronic interaction between the metal centers, mediated by cyanide, as revealed by an intense band (ε = ca. 4000 M^{-1} cm^{-1}) in the visible region and significant effects on the electronic structure and electrophilic reactivity of the

(formally) NO^+ ligand upon changing the redox state of the *distant* $[Ru(NH_3)_5]$ fragment. This work showed for the first time that the strongly coupled $\{M\text{-}NO\}^6$ moiety (usually considered to contain $M^{II}\text{-}NO^+)^8$ might behave as the acceptor component of the overall charge transfer (CT) process promoted by the $[Ru^{II}(NH_3)_5]$ donor fragment. We now succeeded in preparing complex **I**, a system where the geometry of the bridge is clearly defined as *trans* to the nitrosyl ligand. In this way, both rutheniums, the cyano-bridge, and the NO^+ ligand lay on the same axis. Two sets of four equivalent pyridines (as revealed by the ^1H- and ^{13}C-NMR) and a distant exposed cyanide complete the coordination spheres.

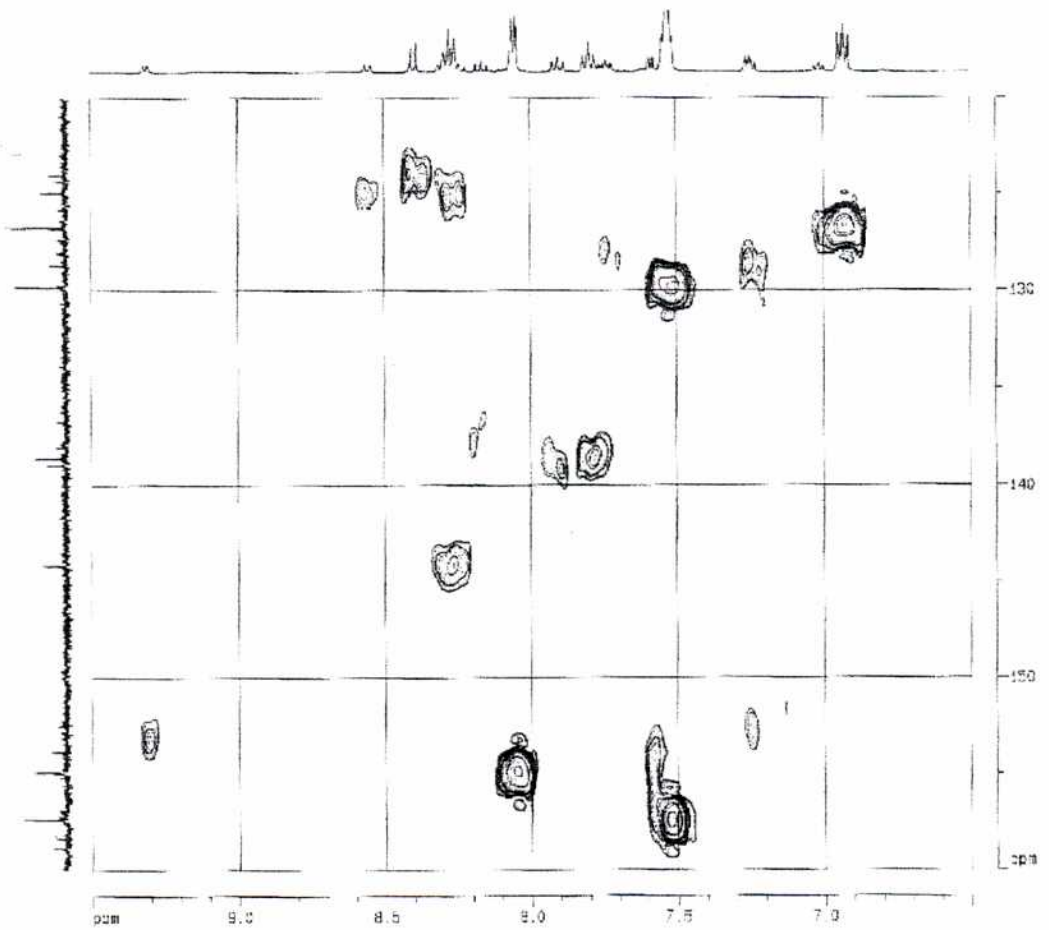

Figure 2.9. $^1H - ^{13}C$ HMQC spectrum of **II** in acetonitrile.

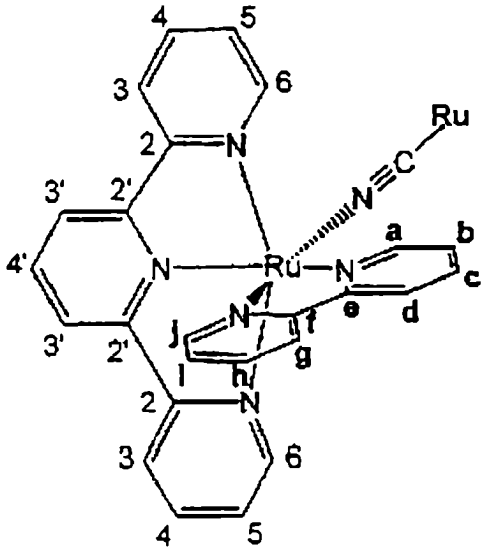

Figure 2.10. Assignations of the positions for the [Ru(bpy)(tpy)] fragment in complex **II**.

Table 2.2. NMR spectroscopic data for complex **II**.

δ_H (ppm)	Integration	H-C coupling, δ_C (ppm)	H-H coupling, δ_H (ppm)	Assignation [a]
9,31	1	152	7,74	a
8,56	1	124,9	8,29	d
8,40	2	124,0	8,16	3´
8,29	8	124,4; 144,2; [c]	7,53; 7,74; 7,90; 8,56	3, 4(py_1), c, g
8,16	1	138,0	8,40	4´
8,05	8	154,9	7,53	2(py_1)
7,90	2	138,9	7,26; 8,29	4
7,80	4	138,6	6,91	4(py_2)
7,74	2	127,7; [b]	6,95; 8,29; 9,31	b, h
7,59	2	153,9	7,26	6
7,53	16	129,8; 157,3; [b]	6,91; 8,05; 8,29	2(py_2), 3(py_1)
7,26	3	128,7	6,95; 7,59; 7,90	5, j
6,95	1	126	7,74; 7,26	i
6,91	8	126,7	7,53; 7,80	3(py_2)

[a] see Figure 2.10. [b, c] two and three signals not observed, respect. Signals corresponding to quaternary carbons were not observed.

Figure 2.1 shows that complex **I** can undergo reversible one-electron reduction in AcN, leading to the formation of $\mathbf{I_{red}}$. The EPR X-band spectrum of

$\mathbf{I_{red}}$ in frozen AcN displayed in Figure 2.4 is comparable to the one obtained from *trans*-$[RuCl(py)_4NO]^+$ In both cases, the *g* and nitrogen hyperfine-coupling tensors are consistent with an unpaired electron in a NO π^* orbital. Although the free $NO^\bullet$ radical does not exhibit an EPR spectrum under normal conditions, coordination to metal centers provides EPR signals which allow for an analysis of the electronic structure. Following previous work,[17,18] we conclude that the EPR signals arise from bound $NO^\bullet$ radicals in which the axial symmetry is removed by coordination. The largest ^{14}N-hyperfine component lays along the x axis of the *g* tensor, indicating that the unpaired electron is in the π_x orbital of $NO^\bullet$.[18] The large anisotropy in the *g* tensor suggests a bent Ru(II)-$NO^\bullet$ motif.

The IR spectrum of $\mathbf{I_{red}}$ (Figure 2.3 top) also agrees with a nitrosyl-centered reduction: ν_{NO} shifts significantly from 1917 to 1626 cm^{-1}, as found with several reduced nitrosyl-complexes,[19,20] and consistent with a decrease in bond order upon reduction. The ν_{CN} values of $\mathbf{I_{red}}$ are around 2050 cm^{-1}, typical of cyanide coordinated to Ru(II) centers.[21] The spectroscopic evidence thus suggests that $\mathbf{I_{red}}$ is best described as $[NC Ru^{II}(py)_4(CN)Ru^{II}(py)_4(NO^\bullet)]^{2+}$ The inertness of the latter species toward $NO^\bullet$ dissociation is remarkable. We also observed the same behavior for the $[RuCl(py)_4NO^\bullet]^+$ ion, consistently with the reported result for the $[Ru(bpy)_2ClNO^\bullet]^+$ ion.[19a] In contrast, cyanide or NO are more rapidly released from $[Fe(CN)_5NO^\bullet]^{3-}$ [10] or from some members of the *trans*-$[Ru(NH_3)_4LNO]^{n+}$ series ensuing nitrosyl reduction (L = *N*-heterocyclic ligands, imidazole, H_2O, etc), respectively.[22,25]

One-electron oxidation of **I** in AcN leads to $\mathbf{I_{ox}}$, whose IR spectrum in solution (Figure 2.3 bottom) displays ν_{CN} stretching frequencies (see Table 2.1) characteristic of coordination to Ru(III).[22] The strong signal at 1952 cm^{-1}, ascribed to ν_{NO}, suggests that the Ru^{II}-NO^+ fragment is preserved upon oxidation, and that $\mathbf{I_{ox}}$ should be formulated as $[NC Ru^{III}(py)_4(CN)Ru^{II}(py)_4(NO)]^{4+}$ The increase of

ν_{NO} if compared to **I** probably reflects the electron-withdrawing influence of the distant Ru(III) center (see later).

The three redox-related species display a rich UV-Vis spectroscopy (Figure 2.2, Table 2.1). Most of the features can be explained as a superposition of the electronic transitions of the two constituent {$Ru(py)_4$} fragments, slightly perturbed by their mutual presence. Thus, **I** displays an intense band at 330 nm and a shoulder at 256 nm in AcN solution, which can be assigned to $d_\pi \rightarrow \pi^*_{py}$ and $\pi_{py} \rightarrow \pi^*_{py}$ transitions, respectively, within the dicyano-chromophore. The intense peak at 237 nm can be assigned to the $d_\pi \rightarrow \pi^*_{py}$ transition in the $[Ru(py)_4NO]$ chromophore (see Table 2.1 for comparisons with the $[RuCl(py)_4NO]^{2+}$ complex). The fast decomposition of **I** upon irradiation in the 300-350 nm region is consistent with the absorption at the Ru^{II}-py chromophores, which could be followed by fast population of lower-lying d-d states and consequent labilization of pyridines. In the same spectral region $\mathbf{I_{red}}$ displays two absorptions at 350 and 290 nm, probably also $d_\pi \rightarrow \pi^*_{py}$ in origin, corresponding to the dicyano- and NO-containing chromophores, respectively. Both absorptions are red-shifted compared to the similar transitions in **I**, as expected from the strong stabilization of the metal orbitals in **I** associated to the presence of the NO^- ligand. Conversely, $\mathbf{I_{ox}}$ displays a series of characteristic LMCT transitions from cyanide to Ru(III),[23] in addition to the $\pi_{py} \rightarrow \pi^*_{py}$ transition appearing at greater wavelengths.

Strikingly, solutions of **I** are *deeply* violet colored because of a broad, intense band centered at 555 nm (Figure 2.2). This is remarkable, because the $[RuCl(py)_4NO]^{2-}$ ion[5] (and many other mononuclear $[X_5M^{II}\text{-}(NO^-)]$ complexes (M = Fe, Ru, Os; X = cyanides, ammines, polypyridines) show *weak* bands in the visible region, which in spite of the low intensity have been assigned as Ru(II) $\rightarrow$ NO^- charge transfer (CT) transitions.[24] Under C_4 symmetry the d_π orbitals of both metal centers transform as b and e. Only the latter have the appropriate symmetry to interact with the empty π^* orbitals in the isoelectronic CN^- and NO^+ fragments.

The orbital interaction might result in extended MO's that provide the pathway for long-range electronic communication. Following this idea, we assign the intense visible band to a symmetry allowed transition between orbitals of e symmetry,* which involves a $d_{\pi(Ru^{II}\ distant)} \rightarrow \pi^*_{(\{Ru\text{-}NO\}^6)}$ charge transfer.

The following additional evidence supports our interpretation: (1) The visible band disappears upon reduction of NO^+ or oxidation of the distant Ru(II), as shown in Figure 2.2. (2) The solvatochromic behavior is compatible with the terminal cyanide on the donor fragment behaving as an electron donor toward the solvent.[26] The interaction with acceptor solvents contributes to stabilize the $e(d_\pi)$ orbitals in the donor fragment. The $\{Ru\text{-}NO\}^6$ moiety is less sensitive to the solvent; consequently, the CT band shifts to higher energy in high acceptor number solvents. Actually, the magnitude of the shift is comparable to that observed in the CT transitions of related compounds containing *one* cyanide.[26] (3) The RR experiment shows enhancement of ν_{CN} and ν_{NO} Although both terminal and bridging cyanides (ν_{CNt} and ν_{CNbr}, respectively) could be coupled to the electronic transition,[3d,28] we propose that the great raman intensity at 2000 cm^{-1} arises from ν_{CNbr}, in agreement with RR results in cyano-bridged mixed-valent complexes (see also below on the IR "red-shift" of ν_{CNbr} compared to ν_{CNt} in the latter systems).[2b] 4) Preliminary experiments show that selective irradiation of the visible band induces the release of NO. A detailed photochemical study has not been performed, but similar results have been reported for $[Fe(CN)_5NO]^{2-}$,[29] *cis*-$[Ru^{II}(bpy)_2Cl(NO)]^{2+}$,[19a] and *trans*-$[Ru^{II}(NH_3)_4L(NO)]^{3+}$ complexes (L = py, pz and derivatives).[22,25] The proposed mechanism relies on the CT assignment of the absorption bands. **I** is quite stable under exposure to diffuse day-light (in contrast

---

* Though b → e transitions are not symmetry-forbidden, they are expected to contribute with very low intensity to the spectrum because of poor overlap between the orbitals involved.

to other nitrosyl containing substances like $[Fe(CN)_5NO]^{2-}$), suggesting that the quantum efficiency of the photo-process is low.

Remarkably, both ν_{CN} and ν_{NO} in **I** are solvent dependent. The greater values of ν_{CN} and ν_{NO} in water compared to AcN are consistent with the decrease in electronic density in the donor fragment due to a greater interaction of the exposed cyanide with water (see previous discussion).

The Role of Donor-Acceptor (D/A) Coupling. Long-range CT bands may arise from Donor/Acceptor (D/A) interactions between (covalently-) linked fragments. In this context, the low energy band in **I** can be viewed as a D → A transition between the distant Ru(II) donor and the $\{Ru\text{-}NO\}^6$ acceptor (DACT).

The *energy* of the DACT is related to the redox potentials at the donor and acceptor sites, according to:

$$h\nu = \Delta E_{redox} + \chi_i + \chi_o + C \qquad (2.2)$$

In eq 2.2, $h\nu$ is the energy of the optical transition in **I** (2.23 eV), ΔE_{redox} is the difference of redox potentials at the donor and acceptor sites (0.90 V), χ_i and χ_o are the reorganization energy parameters for the CT process, and C includes solvational energy contributions.[30,*] The difference between hν and ΔE_{redox} is in our case 1.33 eV, a large value if compared to other D/A systems, as the related mixed-valent ion, $[Cl(py)_4Ru^{III}(NC)Ru^{II}(py)_4CN]^{2+}$ (ΔE_{redox} = 0.67 V; hν = 1.38 eV and

---

* Equation 2.2 allows us to correlate spectroscopic and electrochemical data, provided that several conditions are met, namely that the CT bands have a gaussian shape, and that the donor and acceptor orbitals associated to the electronic transition are the same as those involved in the electrochemical processes. Configurational interactions mixing the ground and excited states are neglected. Solvational contributions to the C values could be around 0.1-0.3 eV (see ref. 30 for details)

($h\nu$- ΔE_{redox}) = 0.71 eV).* This could be traced to the changes in reorganization energies provided that the Ru-N and N-O distances are known to change upon reduction, while the Ru-N-O fragment bends,[18] in contrast to the small distance changes expected to occur within the $Ru^{II,III}$ redox centers. **

The *oscillator strength* of the DACT is a function of the D/A coupling. The high intensity observed for **I** is indicative of efficient long-range electronic communication along the axial π-backbone. Estimation of the electronic coupling can be achieved using the Born-Oppenheimer approximation and first order perturbation theory arguments (Marcus-Hush formalism).[32] The D/A interaction is then described in terms of H_{DA}, the off-diagonal electronic coupling matrix element, which can be estimated from the experimental absorption band as:

$$H_{DA} = (0.0205/r_{DA})[\varepsilon_{max}\, \Delta\nu_{1/2}\, \nu_{max}]^{1/2} \qquad (2.3)$$

In eq 2.3, ε_{max}, $\Delta\nu_{1/2}$, and ν_{max} are the extinction coefficient, the full width at half-height, and the wavenumber of the DACT at its absorption maximum, respectively. r_{DA} is the transition dipole length, i.e. the effective one-electron transfer distance, and the DACT band shape is assumed to be Gaussian. The values for the above mentioned band properties of **I** are: 5.8 x 10^3, 5.6 x 10^3 and 1.8 x 10^4 cm^{-1}, respectively. If r_{DA} is approximated to the distance between the Ru bound to

---

* Our experiments show that the $[Cl(py)_4Ru^{II}(NC)Ru^{II}(py)_4CN]^-$ ion[7] can be oxidized to $[ClRu^{III}(py)_4(NC)Ru^{II}(py)_4CN]^{2+}$ The latter compound shows a band at *ca.* 900 nm, which may be assigned to the intervalence CT transition. Similar results were calculated by using data for the $[NCRu^{II}(py)_4(CN)Ru^{III}(NH_3)_5]^{3+}$ ion:[2c] ΔE_{redox} = 1.0 V; hν = 1.66 eV and (hν - ΔE_{redox}) = 0.66 eV.

** The orbitals involved in the CT process could be different from those involved in the redox processes. This factor could contribute to the observed (hν - ΔE_{redox}), but it is not probably the origin of the large difference observed upon variation of the acceptor site.

the C of the cyano-bridge and the N of nitrosyl (r_{DA} = 6.98 Å),* H_{DA} is ca. 2200 cm^{-1}. This is in very good agreement with reported values for dinuclear cyano-bridged mixed-valent compounds.[33] On the other hand, assuming that the charge is transferred between the two ruthenium sites (r_{DA} = 5.21 A), we calculate an anomalous great value for H_{DA}, ca. 3000 cm^{-1}. Eventually, a more precise value of the D/A distance is required to fully understand the electronic properties of this complex. In spite of these uncertainties, the intensity of the DACT suggests a moderate to strong D/A coupling.

The IR spectral data for **I** (Table 2.1) show unusual low numbers for ν_{CN}. We assign the band at 2001 cm^{-1} (in AcN) to the stretching mode of the bridging cyanide, ν_{CNbr}, and the very weak absorption at 2050 cm^{-1} to the terminal mode, ν_{CNt}, in consistency with the RR assignment. The weak band at 1976 cm^{-1} is probably related to a ^{13}C-N stretching. In $[Ru^{II}(CN)_2(py)_4]$, ν_{CN} was found at 2062 cm^{-1}.[5] A single value at 2064 cm^{-1} was also found in the *trans*-$[Cl(py)_4Ru^{II}(NC)Ru^{II}(py)_4CN]PF_6$ complex, and was assigned to ν_{CNt} (ν_{CNbr} was claimed to be obscured by its low intensity, associated to a small dipolar change).[7] Although an increase was observed for ν_{CNbr} compared to ν_{CNt},[34] it has been suggested that back-bonding effects may contribute to a decrease in ν_{CNbr}.[28] Besides, in some mixed-valent systems such as $[NCRu^{II}(py)_4(CN)Ru^{III}(NH_3)_5]^{3-}$, the combination of a low value for ν_{CNbr} (2006 cm^{-1}) and a high intensity of the intervalence CT transition has been traced to electronic coupling between the metal centers.[2b,c]

Electrophilic Reactivity of I. The spectral changes shown in Figure 2.5 are consistent with reaction 2.1 (see Results). The decay of the CT band of **I** is

---

* The value or r_{DA} = 6.98 Å was estimated from data for the trinuclear *trans*-$[Cl(py)_4Ru(NC)Ru(py)_4(CN)Ru(py)_4Cl]^{2+}$ ion,[7] (Ru-C: 2.04 Å; C-N: 1.16 Å; Ru-N(nitrile): 2.01 Å) and for the $[RuCl(py)_4NO]^{2+}$ ion (Ru-N (nitrosyl): 1.77 Å).[6b]

accompanied by a shift to lower energy and an increase of the absorption intensity of the bands associated to the Ru^{II}-py chromophores (which probably include the new MLCT absorption to the nitro-ligand). The SWV results at pH 9.4 show the expected two waves corresponding to the ruthenium centers; the wave at lower potential, 0.82 V, corresponds to oxidation at the fragment containing the nitro-ligand (no reduction wave of the nitrosyl ligand is observed). On the other hand, the band at 1.2 V is still at a greater potential than for $[Ru(CN)_2(py)_4]$, although smaller than for **I**, consistent with the weaker acceptor ability of the nitro-ligand compared to NO^+ The value of K_1, 3.1 x 10^{15} M^{-2}, is smaller than the value measured for the similar reaction with $[Ru(bpy)NO(tpy)]^{3-}$, 2.1 x 10^{23} M^{-2}.[19b] Although the charges are the same, this is probably to the greater E value for nitrosyl reduction in the latter complex, 0.25 V (see Chapter 3).

The rate-law can be interpreted on the basis of a generally accepted mechanism for the OH^- additions to nitrosyl complexes,[12] involving a slow equilibrium reaction of OH^- to form the NO_2H ligand, and subsequent fast deprotonation. The rate constants, k_1 (M^{-1} s^{-1}), are the appropriate indicators of nucleophilic reactivity, rather than the frequently used equilibrium constants K_1 corresponding to the overall reaction.[12]. The only values of k_1 available in the literature for the addition of OH^- correspond to the reactions of the pentacyanonitrosyl complexes. These are always lower than 1 M^{-1} s^{-1} at 25 °C.[35] The presently reported value, k_1 = 9.2 x 10^3 M^{-1} s^{-1}, is the first one for a positively charged electrophile. The significant increase in k_1 can be traced to charge effects, or, more probably, to an increase in the redox potential for nitrosyl reduction; for instance, the potential for NO^+ reduction in the $[Ru(CN)_5NO]^{2-}$ ion is -0.39 V in aqueous solution,[36] compared to 0.22 V for complex **I**. In contrast, the values of ν_{NO} are strikingly similar for the above compounds (1926[35] and 1917 cm^{-1}, respectively, in KBr disk), and behave in the opposite sense as expected.[12b] Therefore, the increase in electrophilicity associated to an increase in ν_{NO} must be

considered with caution when comparing values for a limited set of data. In Chapter 3 additional measurements of k_1 values with a broader set of complexes are described and these data are analyzed considering all the three potentially significant variables, namely the charges of the reactants, ν_{NO} and the redox potentials at the nitrosyl site.

Activation parameters for reaction 2.1 show that $\Delta H^{\neq}$ is in the range usually obtained for other nitrosyl complexes (50-90 kJ mol^{-1}).[35] However, the high positive value of $\Delta S^{\neq}$, 135 J K^{-1} mol^{-1}, appears as remarkable, probably reflecting a strong desolvation when going to the transition state (adduct formation). This is in expected contrast with the negative entropies found for the reaction of OH^- with negatively charged electrophiles, such as the $[M(CN)_5NO]^{2-}$ ions (M = Fe, Ru, Os).[35]

The reaction of **I** with cysteine was also studied. Considering the previous work with $[Fe(CN)_5NO]^{2-}$,[38] we propose that the new compound with maximum absorption at 461 nm is an adduct with cysteine. Equation 2.4 describes de formation of this compound. We interpret the slope and intercept in the plot k_{obs} *vs.* cysteine as k_4 and k_{-4}, respect. in equation 2.4. The only available data for this type of reactions corresponds to the $[Fe(CN)_5NO]^{2-}$ complex, for which a formation rate constant of 2.2 x 10^4 $M^{-1}s^{-1}$ was reported at pH 10[38] In the comparison of these values we must consider that at pH 4, where the reaction with **I** was measured, the thiolate is protonated. An estimation of this rate constant at pH 10, considering a pK_a for the dissociation of cysteine of 8.3, would give a value 1.4 x 10^8 $M^{-1}s^{-1}$. This is a much higher number than the one of the $[Fe(CN)_5NO]^{2-}$ complex. A systematic study of a series of Ruthenium complexes with cysteine is presented in Chapter 4.

$$[NCRu(py)_4(CN)Ru(py)_4NO]^{3-} + RS^- \rightleftarrows [NCRu(py)_4(CN)Ru(py)_4N(O)SR]^{2-} \quad k_4,\ k_{-4} \quad (2.4)$$

The results in Figure 2.7 show that $\mathbf{I_{ox}}$ is unstable above pH 2. We suggest that $\mathbf{I_{ox}}$ is susceptible of nucleophilic attack, eq 2.5:

$$[NCRu^{III}(py)_4(CN)Ru^{II}(py)_4NO]^{4+} + 2OH^- \rightleftarrows [NCRu^{III}(py)_4(CN)Ru^{II}(py)_4NO_2]^{2+} + H_2O \quad (2.5)$$

Reaction 2.5 is followed by a complex set of irreversible reactions. It is feasible that $[NCRu^{III}(py)_4(CN)Ru^{II}(py)_4NO_2]^{2+}$ isomerizes to the stable form $[NCRu^{II}(py)_4(CN)Ru^{III}(py)_4NO_2]^{2+}$ and reacts further at the electrode producing $[NCRu^{III}(py)_4(CN)Ru^{III}(py)_4NO_2]^{3+}$ Given the known reactivity of the Ru(III)-NO_2^- complexes,[37] the latter product should be unstable toward the disproportionation of NO_2^-, explaining the irreversible character of the oxidation.

The analysis of the electrochemical results at different pHs suggests that reaction 2.5 should attain 50% conversion around pH 3.0. Thus, we estimate that the equilibrium constant, K_5, is around 10^{22} M^{-2}, which is significantly greater than K_1. This suggests that an increase of electrophilicity at the nitrosyl ligand is also operative upon oxidation of the distant ruthenium center, which is consistent with the previously discussed spectroscopic changes upon formation of $\mathbf{I_{ox}}$.

2.5. Conclusions

A new cyano-bridged complex with *trans* geometry, $[NC(py)_4Ru(CN)Ru(py)_4NO](PF_6)_3$ has been prepared, containing the nitrosyl (NO^+) ligand bound to one of the ruthenium(II) metal centers. A strong donor-acceptor interaction is established between both metal sites, as shown by an intense electronic band in the visible region, which can be analysed in terms of the Hush model, as with related mixed-valent systems. The coupled $\{Ru^{II}$-$NO^+\}$ site is the acceptor component of the charge transfer originated in the remote Ru(II)-donor fragment, with a significant participation of the π^* nitrosyl orbital as acceptor. The

latter is also the site of electrophilic reactivity, as well as of chemical, electrochemical or photoinduced reduction. The complex can be also oxidized at the $[NCRu(py)_4CN]$ fragment, thus increasing significantly the reactivity at the distant nitrosyl site. Specific interactions of the exposed cyanide with solvents of different acceptor number (water, AcN) show up in measurable spectroscopic changes. Thus, a controlled tuning of the reactivity at the nitrosyl site can be envisaged, which could also be achieved by the introduction of appropiate substituents at the pyridine ligands. Finally, a new trinuclear complex was also synthetized through the coordination of the [Ru(tpy)(bpy)] fragment to the exposed cyanide. Studies on the reactivity of complex **II** together with other new trinuclear complexes will be done in the future within other project.

Acknowledgment. I thank Prof. Leonardo D. Slep for valuable measurements of EPR and spectroelectrochemistry, Prof. Luis M. Baraldo for co-direction in this project, Prof. K. Wieghardt (Max-Planck-Institut für Strahlenchemie) for providing access to his laboratory equipment, and Daniel Murgida for the Raman measurements.

2.6 References

1. Forlano, P.; Parise, A. R.; Olabe, J. A. *Inorg. Chem.* **1998**, *37*, 6406.
2. Scandola, F.; Argazzi, R.; Bignozzi, C. A.; Chiorboli, C.; Indelli, M. T.; Rampi, M. A. *Coord. Chem. Rev.* **1993**, *125*, 283. (b) Watzy, M. A.; Endicott, J. F.; Song, Z.; Lei, Y.; Macatangay, A. V. *Inorg. Chem.* **1996**, *35*, 3463. (c) Macatangay, A. V.; Endicott, J, F. *Inorg. Chem.* **2000**, *39*, 437. (d) Watson, D. F.; Bocarsly, A. B. *Coord. Chem. Rev.* **2001**, *211*, 177. (e) Pfennig, B. W.; Fritchman, V. A.; Hayman, K. A. *Inorg. Chem.* **2001**,

40, 255. (f) Wang, C.; Mohney, B. K.; Williams, R. D.; Petrov, V.; Hupp, J. T.; Walker, G. C. *J. Am. Chem. Soc.* **1998**, *120*, 5848. (g) Karki, L.; Hupp, J. T. *J. Am. Chem. Soc.* **1997**, *119*, 4070. (h) Vance, F. W.; Karki, L.; Reigle, J. K.; Hupp, J. T.; Ratner, M. A. J. Phys. *Chem. A* **1998**, *102*, 8320. (i) Bublitz, G. U.; Laidlaw, W. M.; Denning, R. G.; Boxer, S. G. *J. Am. Chem. Soc.* **1998**, *120*, 6068.

3. Dunbar, K. R.; Heintz, R. A. *Prog. Inorg. Chem.* **1997**, *45*, 283. (b) Vahrenkamp, H.; Geiß, A.; Richardson, G. N. *J. Chem. Soc. Dalton Trans.* **1997**, 3643. (c) Wu, Y.; Pfennig, B. W.; Sharp, S. L.; Ludwig, D. R.; Warren, C. J.; Vicenzi, E. P.; Bocarsly, A. B. *Coord. Chem. Rev.* **1997**, 159, 245. (d) Doorn, S. K.; Blackbourn, R. L.; Johnson, C. S.; Hupp, J. T. *Electrochim. Acta* **1991**, *36*, 1775.

4. Pfennig, B. W.; Lockard, J. V.; Bocarsly, A. B. *Inorg. Chem.* **1999**, *38*, 2941. (b) Pfennig, B. W.; Cohen, J. L; Sosnowski, I.; Novotny, N. M.; Ho, D. M. *Inorg. Chem.* **1999**, *38*, 606. (c) Pfennig, B. W.; Goertz, J. K.; Wolff, D. W.; Cohen, J. L. *Inorg. Chem.* **1998**, *37*, 2608. (d) Wang, C.; Mohney, B. K.; Akhremitchev, B. B.; Walker, G. C. *J. Phys. Chem. A* **2000**, *104*, 4314. (e) Richardson, G. N.; Brand, U.; Vahrenkamp, H. *Inorg. Chem.* **1999**, *38*, 3070. (f) Zhu, N.; Vahrenkamp, H. *Chem. Ber./Recueil* **1997**, *130*, 1241. (g) Kunkely, H.; Vogler, A. *Inorg. Chim. Acta* **1997**, *254*, 195. (h) Argazzi, R.; Bignozzi, C. A.; Heimer, T. A.; Meyer, G. J. *Inorg. Chem.* **1997**, *36*, 2. (i) Thompson, D. W.; Schoonover, J. R.; Meyer, T. J.; Argazzi, R.; Bignozzi, C. A. *J. Chem. Soc. Dalton Trans.* **1999**, 3729. (j) Forlano, P.; Parise, A. R.; Videla, M.; Olabe, J. A. *Inorg. Chem.* **1997**, *36*, 5642. (k) Bernhardt, P. V.; Macpherson, B. P.; Martínez, M. *Inorg. Chem.* **2000**, *39*, 5203.

5. Coe, B. J.; Meyer, T. J.; White, P. S. *Inorg. Chem.* **1995**, *34*, 593.

6. Bottomley, F.; Mukaida, M. *J. Chem. Soc. Dalton Trans.* **1982**, 1933. (b) Kimura, T.; Sakurai, T.; Shima, M.; Togano, T.; Mukaida, M.; Nomura, T. *Inorg. Chim. Acta* **1983**, *69*, 135.
7. Coe, B. J.; Meyer, T. J.; White, P. S. *Inorg. Chem.* **1995**, *34*, 3600.
8. Richter-Addo, G. B.; Legzdins, P. *Metal Nitrosyls*; Oxford University Press: New York, 1992.
9. Feelisch, M.; Stamler J. S., Eds.; *Methods in Nitric Oxide Research*, J. Wiley & Sons, Chichester, 1996. (b) Butler, A. R.; Glidewell, C. *Chem. Soc. Rev.* **1987**, *16*, 61. (c) Clarke, M. J.; Gaul, J. B. *Struct. Bonding (Berlin)* **1993**, *81*, 147.
10. Cheney, R. P.; Simic, M. G.; Hoffman, M. Z.; Taub, I. A.; Asmus, K. D. *Inorg. Chem.* **1977**, *16*, 2187. (b) van Voorst, J. D. W.; Hemmerich, P. *J. Chem. Phys.* **1966**, *45*, 3914. (c) Nast, R.; Schmidt, J. *Angew. Chem., Int. Ed. Engl.* **1969**, *8*, 383. (d) Butler, A. R.; Calsy-Harrison, A. M.; Glidewell, C. *Polyhedron*, **1988**, *7*, 1197.
11. Southern, J. S.; Hillhouse, G. L. *J. Am. Chem. Soc.* **1997**, *119*, 12406. (b) Wilson, R. D.; Ibers, J. A. *Inorg. Chem.* **1979**, *18*, 336. (c) Lin, R.; Farmer, P. J. *J. Am. Chem. Soc.* **2000**, *122*, 2393.
12. Bottomley, F., in Braterman P. S., Ed., *Reactions of Coordinated Ligands*, Vol.2, Plenum, New York, 1985, p. 115. (b) Bottomley, F. *Acc. Chem. Res.* **1978**, *11*, 158.
13. Evans, I. P.; Spencer, A.; Wilkinson, G. *J. Chem. Soc. Dalton Trans.* **1973**, 204.
14. Slep, L. D.; Pollak, S.; Olabe, J. A. *Inorg. Chem.* **1999**, *38*, 4369.
15. Thompson, M. S.; PhD Dissertation, University of North Carolina at Chapel Hill.
16. Frank Neese, Diploma Thesis, University of Konstanz, 1993.

17. Mc Garvey, B.; Ferro, A. A.; Tfouni, E.; Bezerra, C. W. B.; Bagatin, I.; Franco, F. F. *Inorg. Chem.* **2000**, *39*, 3577. (b) Lantg, D. R.; Davis, J. A.; Lopes, L. G. F.; Ferro, A. A.; Vasconcellos, L. C. G.; Franco, D. W.; Tfouni, E.; Wieraszko, A.; Clarke, M. J. *Inorg. Chem.* **2000**, *39*, 2294.

18. Wanner, M.; Scheiring, T; Kaim, W.; Slep, L. D.; Baraldo, L. M.; Olabe, J. A.; Zális, S.; Baerends, E. J., *Inorg. Chem.*, **2001**, *40*, 5704.

19. Callahan, R. W.; Meyer, T. J. *Inorg. Chem.* **1977**, *16*, 574. (b) Abruña, H. D.; Walsh, J. L.; Meyer, T. J.; Murray, R. W. *J. Am. Chem. Soc.* **1980**, *102*, 3272.

20. Baumann, F.; Kaim, W.; Baraldo, L. M.; Slep, L. D.; Olabe, J. A.; Fiedler, J. *Inorg. Chim. Acta* **1999**, *285*, 129.

21. Nakamoto, K. *Infrared and Raman Spectra of Inorganic and Coordination Compounds*, 4th ed.; Wiley: New York, 1986.

22. Gomes, M. G.; Davanzo, C. U.; Silva, S. C.; Lopes, L. G. F.; Santos, P. S.; Franco, D. W. *J. Chem. Soc. Dalton Trans.* **1998**, 601.

23. Kang, H. W.; Moran, G.; Krausz, E. *Inorg. Chim. Acta* **1996**, *249*, 231.

24. Gorelsky, S. I.; da Silva, S. C.; Lever, A. B. P.; Franco, D. W. *Inorg. Chim. Acta* **2000**, *300-302*, 698, and references therein.

25. Borges, S.da S.S.; Davanzo, C. U.; Castellano, E. E.; Z-Schpector, J.; Silva, S. S.; Franco, D. W. *Inorg. Chem.* **1998**, *37*, 2670.

26. Timpson, C. J.; Bignozzi, C. A.; Sullivan, B. P.; Kober, E. M.; Meyer, T. J. *J. Phys. Chem.* **1996**, *100*, 2915.

27. Sondaz, E.; Gourdon, A.; Launay, J. P.; Bonvoisin, J. Inorg. Chim. Acta **2001**, 316, 79.

28. Bignozzi, C. A.; Argazzi, R.; Schoonover, J. R.; Gordon, K. C.; Dyer, R. B.; Scandola, F. *Inorg. Chem.* **1992**, *31*, 5260. (b) Forlano, P.; Baraldo, L. M.; Olabe, J. A.; Della Védova, C. O. *Inorg. Chim. Acta* **1994**, *223*, 37.

29. Wolfe, S. K.; Swinehart, J. H. *Inorg. Chem.* **1975**, *14*, 1049.

30. Lever, A. B. P.; Dodsworth, E. S., in Solomon, E. I. and Lever A. B. P., Eds., *Inorganic Electronic Structure and Spectroscopy,* Vol.II, Wiley, 1999, p. 227.

31. Creutz, C. *Prog. Inorg. Chem.* **1983**, *30*, 1.

32. (a) Hush, N. S. *Prog. Inorg. Chem.* **1967**, *8*, 391. (b) Marcus, R. A.; Sutin, N. *Biochimica et Biophysica Acta* **1985**, *811*, 265.

33. (a) Burewicz, A.; Haim, A. *Inorg. Chem.* **1988**, *27*, 1611. (b) Díaz, C.; Arancibia, A. *Inorg. Chim. Acta* **1998**, *269*, 246.

34. Dows, D. A.; Haim, A.; Wilmarth, W. K. *J. Inorg. Nucl. Chem.* **1961**, *21*, 33.

35. Baraldo, L. M.; Bessega, M. S.; Rigotti, G. E.; Olabe, J. A. *Inorg. Chem.* **1994**, *33*, 5890.

36. Fiedler, J. *Collect. Czech. Chem. Commun.* **1993**, *58*, 461.

37. Keene, R.; Salmon, D. J.; Walsh, J. L.; Abruña, H. D.; Meyer, T. J. *Inorg. Chem.* **1980**, *19*, 1896

38. Johnson, M. D.; Wilkins, R. G. *Inorg. Chem.* **1984**, 2, .231

3. Kinetic and mechanistic study of the electrophilic reactions of nitrosyl complexes with hydroxide

3.1 Introduction

The electrophilic reactions of the nitrosyl ligand bonded to transition metal centers have been known for a long time and constitute one of its most important reactivity modes.[1] Early use of the reactions of the pentacyanonitrosylferrate(II) ion, $[Fe(CN)_5NO]^{2-}$, (NP) as color tests for identifying SH^- or SO_3^{2-},[2] have been followed by some mechanistic studies in the 1970s.[3] The work has been extended to other $\{MX_5NO\}^n$ complexes (mainly ruthenium with ancillary coligands: amines, polypyridines, etc.).[4] These systems generally have the $\{MNO\}^6$ configuration, according to the Enemark-Feltham notation,[5] the superscript meaning the number of electrons associated with the metal d and π^*(NO) orbitals.

Several nucleophiles have been used in these studies. Most important are the N-binding and S-binding species: ammonia, amines, hydroxylamine, hydrazine, azide, SH^-, SR^-, SO_3^{2-}, and so forth. Their reactions with the $\{MX_5NO\}^n$ fragments are assumed to proceed through initial reversible adduct formation, and are followed by redox processes associated with the reduction of nitrosyl and oxidation of the nucleophile.[3,4] These reactions are most relevant in the redox interconversions of nitrite to ammonia in the natural media, which still show mechanistic uncertainties due to the lack of characterization of several intermediates, sometimes even ill-defined.[3,4,6] On the other hand, the electrophilicity of nitrosyl, particularly toward thiolates, is proposed to be important in the process of NO uptake, release and transportation by transition metal centers in the biological fluids, given the presence of iron-containing enzymes which attain a pseudo-octahedral, low-spin d^6 configuration upon NO binding.[7]

The simplest electrophilic reactions of bound nitrosyl are those involving OH^- as the nucleophile (eq 3.1), because no subsequent redox processes occur after addition. The stoichiometry is characteristic of several complexes with different MX_5 fragments (M = Fe(II), Ru(II), Os(II), Ir(III); X = NH_3, CN^-, halides, OH^-, polypyridines, etc):[3,4]

$$[MX_5NO]^n + 2OH^- \rightleftarrows [MX_5NO_2]^{(n-2)} + H_2O \qquad K_{eq} \qquad (3.1)$$

In eq 3.1, a reversible acid-base reaction occurs. Although values of K_{eq} have been measured for a variety of MX_5 fragments, kinetic and mechanistic results are scarce, limited to reactions of the pentacyanonitrosylmetallates (Fe, Ru, Os).[2,8] It is generally accepted that slow OH^- addition to the {MNO} fragment is followed by a fast deprotonation of the $\{MX_5NO_2H\}^{(n-1)}$ intermediates to give the corresponding nitro-complexes. However, no direct evidence of these intermediates is available.

The electrophilic reactivity of bound nitrosyl has been early associated with the value of the IR stretching frequency, ν_{NO}. It has been proposed that complexes with ν_{NO} = *ca.* 1860 cm^{-1} or greater will be reactive.[9] This is a useful guide with some rationale in that ν_{NO} should reflect the electron density at the *N*-atom of the nitrosyl, which is the site of attack by nucleophiles.[3,4] It has also been recognized that larger values of K_{eq} are obtained with complexes having the more positive values of ν_{NO}.[10] However, these correlations are still unable to present a satisfactory account of the factors determining the reactivity of bound nitrosyl, given the variety of metal centers, ancillary X ligands, and overall charge of the complexes. Remarkably, electrophilic reactivity is currently discussed in terms of the above mentioned parameters, but the key ones are lacking, namely the values of the *rate constants* for the elementary steps comprising nucleophilic addition.[3,4]

We present a systematic kinetic and mechanistic study of the reactions of $\{MX_5NO\}^n$ complexes with OH^- (mainly ruthenium metal centers). Included are the members of well characterized series of nitrosyl-complexes, containing a variety of ancillary ligands, for which some type of information already exists, such as K_{eq}, ν_{NO} and $E_{NO^+/NO}$ values.

3.2. Experimental section

Preparation of complexes. The complexes of the *cis*-$[Ru(bpy)_2(NO)(X)]^{n+}$ series were prepared as previously described, for X = CH_3CN, NO_2^-, Cl^-,[10ab] as was also the case with *cis*-$[Ru(bpy)(NO)(tpy)]^{3+}$.[10c] The complexes of the *trans*-$[Ru(NO)(py)_4X)]^{2+}$ series (X = Cl^-, OH^-) were obtained as reported previously.[11] The synthesis of *trans*-$[NCRu(py)_4CNRu(py)_4NO]^{3+}$ has been described in Chapter 2. The members of the *trans*-$[Ru(NH_3)_4(NO)(X)]^{n+}$ series (X = pyrazine, nicotinamide, chloropyridine, pyridine, 4-methylpyridine and histidine) were prepared as described in the literature.[13-14] This was also the case for the [Ru(Hedta)NO] complex (edta = ethylenediaminetetraacetate).[12] The purity was checked by ^{1}H-NMR, IR and UV-Vis spectroscopies. All chemicals used for buffer solutions were analytical grade and were used without further purification.

[Ru(bpz)(NO)(tpy)](PF$_6$)$_3$: $Ru(tpy)Cl_3$[20] (100 mg) and bpz (2,2'-bipyrazine, 60 mg) were heated to reflux during 3 h in 50 ml of EtOH/H_2O 1:1. An amount of 150 mg of $NaNO_2$ was added to the red-brown solution and refluxing was continued for 2 h. The red solution was then filtered and a concentrated solution of NH_4PF_6 was added until complete precipitation of the product was ensured. The red solid was suspended in 3M HCl and NH_4PF_6 was added in the same way as before to afford a brown solid. The product was further purified by recrystallization from acetonitrile-diethyl ether. IR: ν(NO): 1957 cm^{-1}, $E_{1/2}$ = 0.46

V vs. Ag/AgCl. Anal. Calc. for $[(terpy)(bpz)Ru(NO)](PF_6)_3$: C, 28.85, H, 1.79, N, 11.71%. Found: C, 27.66, H, 1.74, N, 11.04%. ^{1}H-NMR (CD_3CN): 10.12 (s, 1H), 9.96 (s, 1H), 9.51 (d,1H), 9.38 (d, 1H), 8.99 (t, 1 H), 8.87 (d, 2H), 8.82 (d, 1H), 8.71 (d, 2H), 8.47 (t, 2H), 8.06 (d, 2H), 7.73 (t, 2H), 7.22 (t, 1H) ppm.

***trans*-[Ru(NO)(py)$_4$(SCN)](PF$_6$)$_2$**: 100 mg of *trans*-$[Ru(NO_2)_2(py)_4]$[11] and 300 mg of NaSCN were suspended in 20 ml of acetonitrile, and 0.5 ml of concentrated HPF_6 were added. After mixing, the sample was evaporated to dryness. The solid residue was suspended in water and filtered. To the solution NH_4PF_6 was added and a yellow solid was obtained. This compound was further purified by loading onto a DOWEX 50 WX2 cation exchanger (100 – 200 mesh) in acid form and by eluting with 1M HCl. The main orange fraction was collected and precipitated with NH_4PF_6. Anal.: Calc. for *trans*-$[Ru(NO)(py)_4(SCN)](PF_6)_2$: C, 31.69; H, 2.01; N, 10.56; S, 4.03%. Found: C, 31.90; H, 2.27; N, 10.12; S, 3.63%.. IR: ν(NO): 1902 cm^{-1}. $E_{1/2}$: 0.12 V and –0.35 V vs. Ag/AgCl. ^{1}H-NMR (CD_3CN): 8.29 (t, 4H, H^4), 8.26 (d, 8H, $H^{2,6}$), 7.70 (t, 8H, $H^{3,5}$) ppm.

Spectroscopic and electrochemical measurements. IR spectra were taken in KBr pellets on a Thermo Nicolet, mod. Avatar 320 FT-IR instrument.^{1}H-NMR spectra were obtained on a Bruker 500 MHz spectrometer. Electrochemical studies were done with all the complexes, with exception of the pentacyanonitrosyl-metallates (data taken from the literature),[15] on a Princeton Applied Research Potentiostat 273A, using square wave voltammetry (SWV) at 60 Hz, vitreous carbon as working electrode and Ag/AgCl (3 M KCl) as a reference. The electrolyte was a HCl solution, pH 2.0 at I = 1 M (NaCl). Elemental analyses were done on a Carlo Erba elemental analyser, model 1106.

Kinetic measurements. All the kinetic experiments were done at I = 1 M (NaCl), with final complex concentration 2-10 mg/100ml and under pseudo first order conditions. Buffer solutions (0.05 M) were employed to control the pH of the system (acetate buffer for pH 3.5-6.0; phosphate buffer for pH 6.0-8.0 and

carbonate buffer for pH 8.0-10.0). At pH values higher than 11, NaOH solutions were used. Distilled water was boiled plenty of time to eliminate carbon dioxide and then was used to prepare NaOH solutions, which were handled under nitrogen. The concentration of OH^- was determined by titration of potassium biphtalate. The pH measurements were done with a Metrohm 744 pH meter, using Merck buffers for calibration.

The complex solution and the buffer or the NaOH solution were maintained at the desired temperature ($\pm$ 0.1 °C) with a RC 6 Lauda thermostat for 15 minutes, and then were mixed by means of a RX1000 Applied Photophysics rapid kinetics accessory, attached to a 1-cm quartz flow cell. Spectral changes in the range 200-800 nm were recorded with a Hewlett Packard 8453 diode array spectrophotometer. Six wavelengths that showed the biggest changes were selected, and kinetic traces were obtained from them. Each experiment was repeated at least three times. All traces were fitted to one exponential until at least five half lives, unless otherwise stated. This afforded at least 18 values for the observed rate constant (k_{obs}). Values, which differed less than 10 % (usually less than 5%), were averaged. Complexes 2, 7, 9, 15 did not show a first order process during the reaction and the whole spectral changes were analyzed by the SPECFIT program.[16] A two exponential model was employed, and the rate constant corresponding to the first process was considered as the observed rate constant (k_{obs}). Complex 9 was studied at [OH^-] lower than 1.7×10^{-2} M, because at higher concentrations the initial spectrum was different from the reagent spectrum, the process was a first order one and the observed rate constant was much lower.

For the [Ru(Hedta)NO] complex, equal volumes of each solution were mixed in a Hi-tech PQ/SF 53A stopped flow equipment. Absorption-changes at 370 nm, corresponding to the build-up of product, were measured by a SU 40 Hi Tech Spectrophotometric unit. The signal was registered by Hewllett Packard

54600A oscilloscope, which was interfaced to a computer and kinetic traces were fittet to a single exponential by a home made program.

The concentration of OH^- was varied at least one order of magnitude to get the second order rate constant (k_{OH^-}). Plots of $k_{obs}[OH^-]$ *vs* $[OH^-]^2$ were built for all the complexes. In all the cases a linear distribution was observed. The slope was equal to the second order rate constant, k_{OH^-}. Plots of k_{obs} *vs* $[OH^-]$ showed linear distributions in most cases and the slope did not differ significantly from the one obtained by the previous method. This procedure was repeated for selected systems at different temperatures (range 10-40 °C), and Eyring plots allowed for the activation parameters.

Linear fits were obtained using a least-squares method (statistical function of Microsoft Excel), which afforded the errors in slopes and intercepts. Non-linear fits were obtained using a Microsoft Excel Solver.

For the estimation of K_{ip} (eq 3.5), the Fuoss-Eigen equation was employed.[17] At 25.0 °C, in water, this equation takes the expression described in eq 3.2.

$$K_{IP} = 2.523\times10^{21}(r + r_{OH^-})^3 e^{\frac{-7.131\times10^{-8} Z_- Z_-}{(r+r_{OH^-})[1+3.285\times10^{7}\sqrt{I}(r+r_{OH^-})]}} \quad (3.2)$$

Where r is the radium of the complex expressed in cm, r_{OH^-} is the radium of OH^- taken as 2.29 x 10^{-8} cm,[19] I is the ionic strength, and Z_- and Z_- are the charges of the complex and OH^- respect.

r values were estimated from crystalline structures of related compounds published in the Cambridge Structural Database.[18]

Attempts to determine K_{eq} were done for the [Ru(Hedta)NO] complex. As the reaction product was unstable under our experimental conditions, a direct measurement of K_{eq} was not possible. A complementary estimation of this number

was obtained by extrapolation of the absorbance at $t = \infty$, by using the same exponential function employed to fit the trace. This value was A_∞. To compensate for the instabilities in the base line for different data, we calculated the difference of absorbance during the reaction (ΔA) as $A_\infty - A_o$ (where A_o is the absorbance at $t = 0$). This was done for each trace, and ΔA values were averaged in the same way as for the k_{obs} values. Assuming that the absorption of the initial [Ru(edta)NO] complex at 370 nm is negligible compared to the one of the product, $[Ru(edta)NO_2]^{2-}$, and using the mass balance for both of the species and the expression of K_{eq}, we get equation 3.3 for ΔA.

$$\Delta A = \frac{\varepsilon C_T [OH^-]^2 K_{eq}}{1 + K_{eq}[OH^-]^2} \qquad (3.3)$$

In eq. 3.3, ε is the extinction coefficient of $[Ru(edta)NO_2]^{2-}$ and C_T is the total complex concentration. ΔA was fitted to this equation and the error in K_{eq} was estimated by finding the range of K_{eq} where the data could still be fitted.

3.3 Results and discussion

Table 3.1 displays the rate constants for the nucleophilic addition reactions of OH^- to the pentacyanonitrosylmetallates (Fe, Ru, Os),[8] as well as the values obtained in the present work for the rest of the $\{MX_5NO\}$ complexes. Also included are the corresponding values of ν_{NO}, $E_{NO^+/NO}$ and K_{eq}.

As a representative example, Figure 3.1 shows the successive spectra for the reaction of *trans*-$[Ru(4\text{-}Mepy)(NH_3)_4(NO)]^{3+}$ with OH^- The conversion of the nitrosyl complex to the *trans*-$[Ru(4\text{-}Mepy)(NH_3)_4(NO_2)]^+$ product, according to eq 3.1, is revealed by the onset of the intense band at 378 nm, which may be assigned

to a metal-to-ligand-charge-transfer (MLCT) from Ru(II) to the nitro-ligand. The isosbestic point shows that a clean conversion occurs. The reaction is reversed, to give the reactants, upon acidification. These general features are repeated for all the similar conversions of the complexes of Table 3.1, in fact *all of them* show the formation of a strong absorption band between 330 nm and 470 nm upon reaction with OH^-.

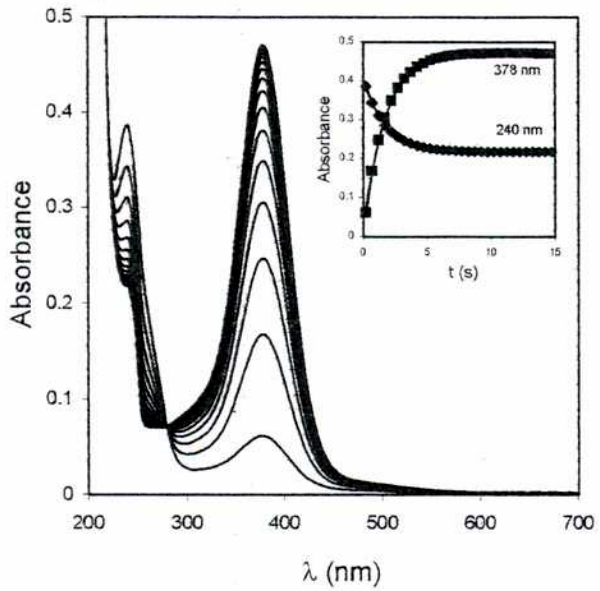

Figure 3.1. Kinetic study for the reaction of *trans*-$[Ru(4\text{-}Mepy)(NH_3)_4(NO)]^{3+}$ with OH^-. I = 1 M (NaCl); T = 35.0 °C; $[OH^-]$ = 0.015 M; [complex] = 4 x 10^{-6} M; cycle time 0.5 s. Inset: Plots of Absorbance *vs* time at 378 and 240 nm. k_{obs} = 0.386 s^{-1}.

The increase and decrease of the absorbance traces for the above reaction, at 378 nm and 240 nm, respectively, are displayed at the inset of Figure 3.1. They agree with a pseudo-first order behavior, up to at least three half-lives. Figure 3.2 shows the plot of k_{obs} against the concentration of OH^- for the [Ru(Hedta)NO] complex, which can be represented by:

$$k_{obs} = a[OH^-] + \frac{b}{[OH^-]} \tag{3.4}$$

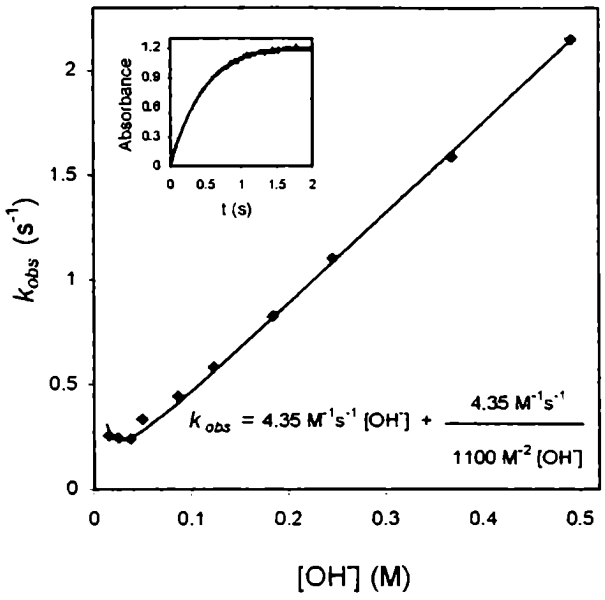

Figure 3.2. [OH$^-$]-concentration dependence for the observed rate constant (k_{obs}) during the reaction between [Ru(Hedta)NO] and OH$^-$. I = 1 M (NaCl); [Ru(Hedta)NO] = 5.0 mg/50ml; [OH$^-$] = 0.5 – 0.005 M; T = 25.0 ± 0.1 °C; k_{OH^-}= 4.35 M^{-1} s^{-1}, K_{eq} = 1.1 x 10^3 M^{-1} s^{-1}. Inset: kinetic trace at 370 nm.

An expression of the same form has been derived for k_{obs},[8b,d] assuming the following general mechanistic scheme:

$$[MX_5NO]^n + OH^- \rightleftarrows \{[MX_5NO]^n.OH^-\} \qquad K_{ip} \qquad (3.5)$$

$$\{[MX_5NO]^n.OH^-\} \rightleftarrows [MX_5NO_2H]^{(n-1)} \qquad K_6, k_6, k_{-6} \qquad (3.6)$$

$$[MX_5NO_2H]^{(n-1)} + OH^- \rightleftarrows [MX_5NO_2H]^{(n-2)} + H_2O \qquad K_7 \qquad (3.7)$$

The mechanism includes a fast ion-pair formation pre-equilibrium, eq 3.5, prior to the relevant nucleophilic addition step, eq 3.6. The latter leads to the $[MX_5NO_2H]^{(n-1)}$ intermediate, which may go back to the reactants or react as in eq 3.7 to form the final product.[8]

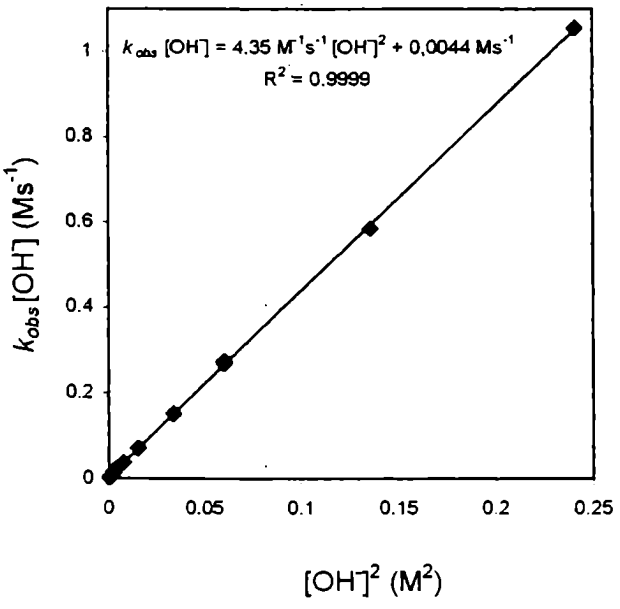

Figure 3.3. Plot of k_{obs}[OH⁻] *vs* [OH⁻]^2 for the reaction between [Ru(Hedta)NO] and OH⁻. I = 1.0 M (NaCl); [Ru(Hedta)NO] = 5.0 mg/50ml; [OH⁻] = 0.5 – 0.005 M; T = 25.0 ± 0.1 °C; k_{OH} = 4.35 ± 0.02 M^{-1} s^{-1}, K_{eq} = 1.0 ± 0.4 x 10^3 M^{-1} s^{-1}.

The values of K_{ip} (M^{-1}) were estimated by using electrostatic models[17] (see Experimental section, eq. 3.2). The values of a and b in eq 3.4 can be traced to a = k_{OH^-} and b = k_{OH^-}/K_{eq}, with k_{OH^-} = $K_{ip}k_6$ and K_{eq} = $K_{ip}K_6K_7$.[8d] Thus, plots like Figure 3.2 or Figure 3.3 afforded values of k_{OH^-} (M^{-1} s^{-1}) as well as of K_{eq} (M^{-2}), although the latter may be measured more accurately by independent equilibrium measurements. For many of the reactions (when [OH⁻] and K_{eq} are sufficiently high), the influence of the k_{OH^-}/K_{eq}[OH⁻] term is negligible, and k_{OH^-} may be obtained from the slope of the plot of k_{obs} against [OH⁻]. Then, the value of k_6 (s^{-1}),

corresponding to the elementary step for nucleophilic addition, can be calculated using estimated values of K_{ip} (see Table 3.1).[8d]

Figure 3.4 displays the Eyring plot for the [Ru(Hedta)NO] complex, from which the activation parameters were obtained. A similar procedure afforded the activation parameters of other selected complexes, which are listed in Table 3.1.

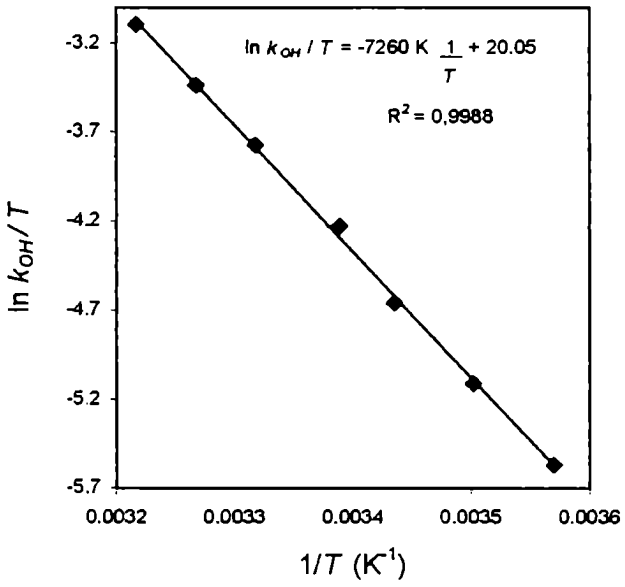

Figure 3.4. Eyring plot for the reaction between [Ru(Hedta) NO] and OH^-. I = 1.0 M (NaCl); [Ru(Hedta)NO] = 5.0 mg/50ml; [OH^-] = 0.48 – 0.12 M; T = 10 - 40 °C. $\Delta H^{\#}$ = 60 ± 1 kJ/mol, $\Delta S^{\#}$ = -31 ± 3 J/K mol.

(2) *cis*-$[Ru(bpy)_2(CH_3CN)NO]^{3+}$	$(5.60 \pm 0,07) \times 10^6$	2.31×10^6			0.35	1960	
(3) *cis*-$[Ru(bpy)(NO)(tpy)]^{3+}$	$(3.17 \pm 0.02) \times 10^5$	1.31×10^5	89 ± 1	159 ± 5	0.25	1946	2.1×10^{23} [10e]
(4) *cis*-$[Ru(bpy)_2(NO_2)NO]^{2+}$	$(5.06 \pm 0.02) \times 10^4$	2.75×10^4	83 ± 7	120 ± 20	0.18	1942	
(5) *cis*-$[Ru(bpy)_2ClNO]^{2+}$	$(8.5 \pm 0.1) \times 10^3$	4.6×10^3	100 ± 3	164 ± 8	0.05	1933	1.6×10^{15} [10e]
(6) *trans*-$[NCRu(py)_4CNRu(py)_4NO]^{3+}$	$(9.2 \pm 0.2) \times 10^3$	3.4×10^3	91 ± 4	135 ± 10	0.22	1917	3.2×10^{15}
(7) *trans*-$[RuClNO(py)_4]^{2+}$	$(4.6 \pm 0,3) \times 10^1$	3.1×10^1	62 ± 1	-6 ± 5	0.09	1910	
(8) *trans*-$[Ru(NCS)NO(py)_4]^{2+}$	$(2.03 \pm 0,01) \times 10^2$	1.36×10^2			0.12	1902	
(9) *trans*-$[Ru(OH)NO(py)_4]^{2+}$	$(2.4 \pm 0,1) \times 10^{-1}$	1.6×10^{-1}			-0.22	1866	
(10) *trans*-$[Ru(NH_3)_4NO(pz)]^{3+}$	$(1.77 \pm 0,04) \times 10^2$	$9.,55 \times 10^2$	76 ± 2	54 ± 6	-0.11	1942	6.0×10^{8} [13]
(11) *trans*-$[Ru(NH_3)_4(nic)NO]^{3+}$	$(3.3 \pm 0,1) \times 10^1$	1.8×10^1	78 ± 1	44 ± 4	-0.18	1940	5.9×10^{7} [13]
(12) *trans*-$[Ru(Clpy)(NH_3)_4NO]^{3+}$	$(2.60 \pm 0,05) \times 10^1$	1.40×10^1			-0.19	1927	6.0×10^{6} [14]
(13) *trans*-$[Ru(NH_3)_4NO(py)]^{3+}$	$(1.45 \pm 0,02) \times 10^1$	7.82×10^0			-0.22	1931	2.2×10^{5} [13]
(14) *trans*-$[Ru(4\text{-}Mepy)(NH_3)_4NO]^{3+}$	$(9.54 \pm 0,06) \times 10^0$	5.14×10^0	75 ± 1	26 ± 4	-0.25	1934	7.7×10^{5} [14]
(15) *trans*-$[Ru(hist)(NH_3)_4NO]^{3+}$	$(7.6 \pm 0,4) \times 10^{-1}$	4.12×10^{-1}			-0.39	1921	4.6×10^{13} [13]
(16) [Ru(Hedta)NO]	$(4.35 \pm 0.02) \times 10^0$	1.06×10^1	60 ± 1	-31 ± 3	-0.29	1890	$(4 \pm 2) \times 10^2$ [c]
(17) $[Fe(CN)_5NO]^{2-}$	$5.5.10^{-1}$ [8d]	3.9×10^0	53 [8d]	-49 [8d]	-0.29 [15]	1945 [8d]	1.5×10^{5} [8d]
(18) $[Ru(CN)_5NO]^{2-}$	$9.5.10^{-1}$ [8d]	6.4×10^0	57 [8d]	-54 [8d]	-0.35 [15]	1926 [8d]	4.4×10^{6} [8d]
(19) $[Os(CN)_5NO]^{2-}$	$1,37.10^{-4}$ [8d]	8.63×10^{-4}	80 [8d]	-73 [8d]	-0.68 [15]	1897 [8d]	$4.2 \times .10^{1}$ [8d]

[a] Derived from the rate-law. [b] Obtained through $k_6 = k_{OH}/K_{ip}$, with K_{ip} from eq. 3.2. [c] This work. [d] Values obtained from the literature.

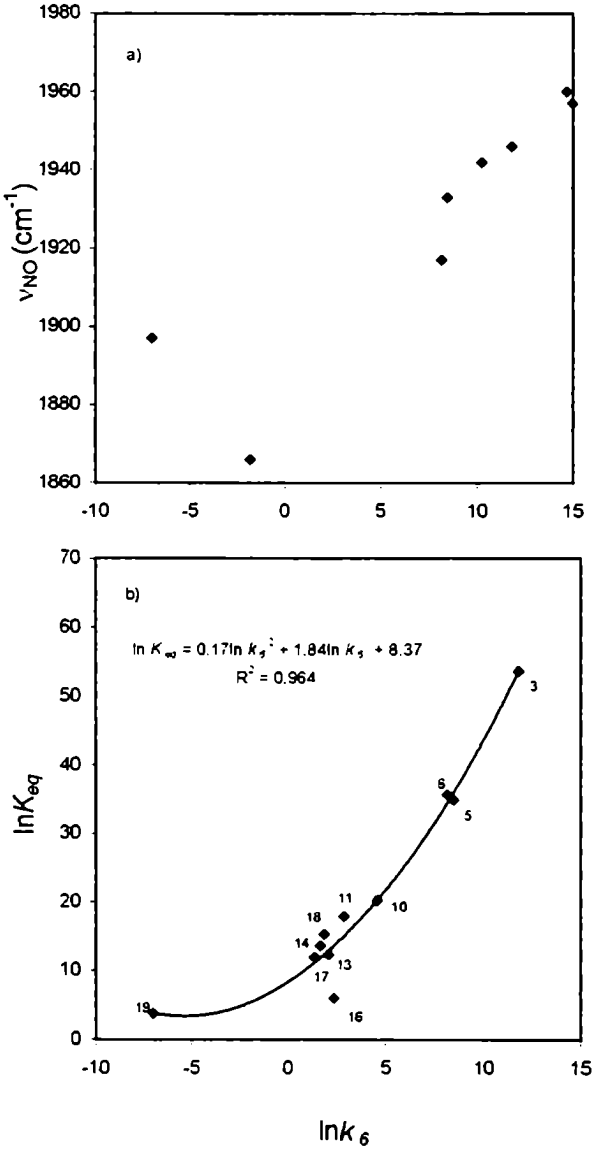

Figure 3.5. a) Plot of ν_{NO} and b) ln K_{eq}, against the nucleophilic rate constant, ln k_6,. See Table 3.1 for the assignment of numbers.

Figure 3.5a shows a correlation between ln k_6 against ν_{NO}, with a high dispersion in the intermediate region. Indeed, ν_{NO} is an uncertain parameter for predicting the electrophilic reactivity of a given nitrosyl complex. Figure 3.5b

shows also a correlation (not linear but quadratic) between ln k_6 and ln K_{eq}, giving some justification to the current use of K_{eq} as an indicator of nucleophilic reactivity.*

Figure 3.6 shows a plot of ln k_6 against $E_{NO^+/NO}$. A good correlation is obtained ($r^2 = 0.985$) for most of the complexes studied, with the exception of those corresponding to the *trans*-$[Ru(py)_4(X)NO]^{n+}$ series, which lay in a parallel line, showing lower rates than expected.** The slope of the main line is 19.5 V^{-1}. Remarkably, the correlation spans around 10 orders of magnitude in the values of k_6, covering a range of around 1 V in the redox potentials.

Figure 3.6 a *linear-free-energy-relation* (LFER), as frequently found in the correlations of kinetic *vs* thermodynamic parameters for a set of reactions governed by the same mechanism.[22] The value of the slope is very close to the one predicted for LFER's in weakly coupled outer-sphere one-electron transfer reactions (19.4 V^{-1}, or 0.5/RT) following Marcus' treatment for cross reactions.[23,24] Marcus extended the theory to atom-transfer reactions, with the prediction that a slope of 0.5 in the plot of $\Delta G^{\#}$ *vs* ΔG^{o} could also be found in the case of substitution reactions proceeding through an associative mechanism.[25] The value of the slope is associated to the bond order of the bond being formed[25] or to a measure of the fractional displacement of the transition state along the reaction coordinate from

---

* Complex 15 has been reported with a strikingly high value of K_{eq}. This is probably due to perturbing acid-base equilibria associated with the histidine ligand. On the other hand, both redox potential and rate constant values are consistent with the linear correlation shown in Figure 3.6

** Steric hindrance is probably a main reason for the tetrapyridine-complexes 6 - 9 falling out of the correlation between ln k_6 *vs* E, with a lower rate than predicted. In these complexes, the pyridines are free to rotate, and they are expected to favor a staggered configuration. In this position, the H points to the NO group, leaving less space to be attacked by OH^-.[21] For other complexes the coligands are smaller, or they are fixed in a planar configuration (polypyridines).

reactants to products.[22b] The appearance of such an LFER for an addition reaction as described by eqs 3.4 – 3.7 is, to our knowledge, a first situation found in mechanistic inorganic chemistry. The result is consistent with an increase in coordination number for the *N*-atom in nitrosyl, with a formal change in hybridization from linear M-N-O to angular M-NO_2H.

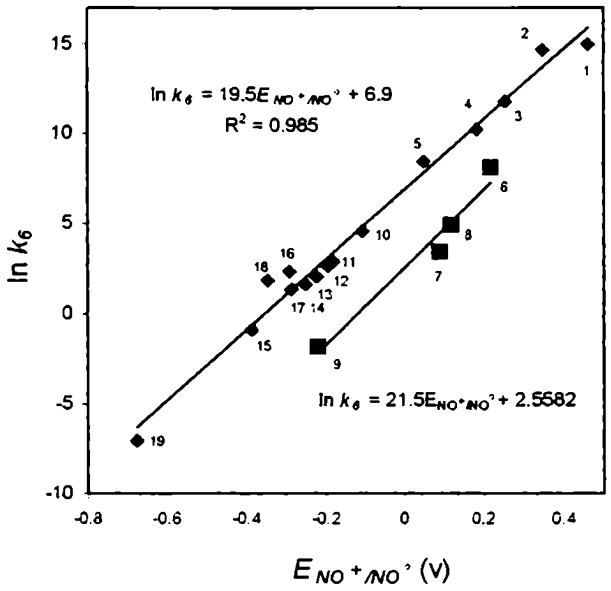

Figure 3.6. LFER plot of ln k_6 against $E_{NO^+/NO}$ for the reactions of a series of $\{MX_5NO\}^n$ complexes with OH^- See Table 3.1 for the assignment of numbers.

Figure 3.7 shows an *isokinetic relationship*, i.e. the trends in the activation parameters for the reactions of complexes in Table 3.1. The increase in rate constants and redox potentials goes in parallel with an *increase* in *both* the activation enthalpies and entropies. On this basis, the reactions appear as entropically driven. While the trends in the entropies can be reasonably explained considering the different solvational changes related to the reactions of species

carrying equal or opposite charges,[26*] the consideration of enthalpy changes is not so straightforward. We propose that the rate of addition in eq 3.6 should be controlled mainly by the energetically costly steps involving the reorganization of the linear MNO moiety to angular M-NO_2H, as anticipated previously.

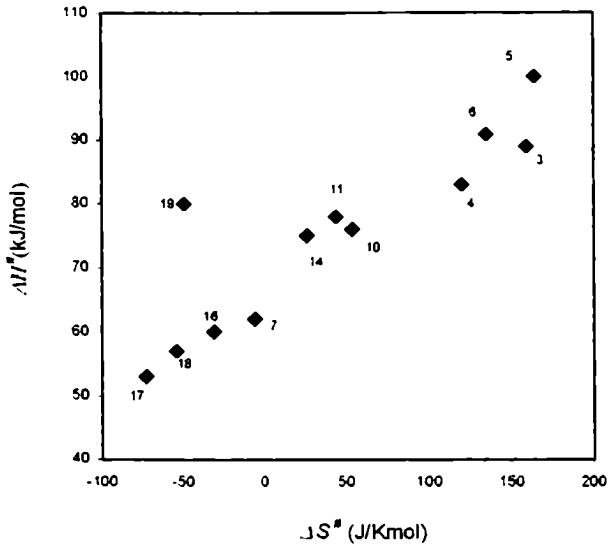

Figure 3.7. Plot of the activation enthalpies against the activation entropies for the reactions of $\{MX_5NO\}$ complexes with OH^- (see Table 3.1).

* In Figure 3.7, the osmium cyano-complex (19) deviates from the correlation because the low rate is associated mainly with an enthalpy effect. Activation entropy changes are similar for the three pentacyanonitrosylmetallates.[3d]

3.4 Conclusions

A detailed experimental picture has been shown for an important reaction in coordination chemistry, namely the nucleophilic addition of OH^- to a broad set of nitrosyl complexes. By measuring the relevant rate constants and activation parameters, along with the spectroscopic and electrochemical information sensing the variable electronic densities at the {MNO} moieties, we could place this reaction type under a rigorous scrutiny. We found that no significant correlation exists between the stretching frequency of the NO in the IR (ν_{NO}) with the reactivity, as has been proposed earlier.[9] We observed an appreciable correlation between the reactivity and the equilibrium constant for the addition of OH^- (K_{eq}). Finally, there is a very good correlation between the reactivity and the redox potential of the couple NO^-/NO° (E_{NO^-/NO°), (LFER). The LFER covers an impressive range of rates and redox potentials, showing to be a useful predictive tool. The interpretation of activation parameters suggests that both electronic and solvation effects influence the nucleophilic reaction rates. The results may be compared with those found for the reactions comprising additions of bases to bound carbonyl,[27] and also with the general situation in organic chemistry, where the variable electrophilicities at carbon must be afforded in terms of empirical parameters dealing with substituent effects.[28]

We propose that the rate of addition in eq 3.6 should be controlled mainly by the energetically costly steps involving the reorganization of the linear MNO moiety to angular M-NO_2H, as well as the geometry changes ascribed to the OH^- reactant upon coordination. Moreover, we expect a stronger stabilization of the MNO moieties for complexes receiving a smaller back-bonding interaction arising from the coligands. Back bonding to the antibonding LUMO, increasing the electronic density of this orbital, decreases the bond order. Bond reorganization becomes favored and the activation enthalpy decreases. For the complexes at the

top of Table 3.1, showing a higher triple bond character, bond reorganization is disfavored and the reaction is more endothermic. DFT calculations support these ideas.[29]

The analysis could seemingly be extended to other nucleophiles, and this is important for the predictions having a more general validity. Although different rates are operative for a given complex by changing the nucleophile, we should expect similar trends for any nucleophile considering the $\{MX_5NO\}$ series, if the relevant rate constants do reflect the adduct-formation step. In this context, in Chapter 4, we present a systematic study of the reaction of cysteine with several complexes of Table 3.1.

Acknowledgments. I thank Mara E. Ruggiero for the preparation of the complexes 10 – 15 and collaboration in the kinetic measurements.

3.5. References

1. Richter-Addo, G. B.; Legzdins, P. *Metal Nitrosyls*; Oxford University Press: New York, 1992.

2. Swinehart, J. H. *Coord. Chem. Rev.* **1967**, *2*, 385.

3. Mc Cleverty, J. A. *Chem. Rev.* **1979**, *79*, 53-76.

4. (a)Bottomley, F., in *Reactions of Coordinated Ligands, Vol.2*, Braterman, P. S., Ed. Plenum, New York, 1985, p. 115. (b) Ford, P. C.; Lorkovic, I. M. *Chem. Rev.* **2002**, *102*, 993.

5. Enemark, J. H.; Feltham, R. D. *Coord. Chem. Rev.* **1974**, *13*.

6. Averill, B. A. *Chem. Rev.* **1996**, *96*, 2951.

7. Butler, A. R.; Glidewell, C. *Chem. Soc. Rev.* **1987**, *16*, 361. (b) Clarke, M. J. Gaul, J. B. *Struct. Bonding (Berlin)* **1993**, *81*, 147. (c) Stamler, J. S.; Singel, D. J.; Loscalzo, J. *Science* **1992**, *258*, 1898. (d) Moradno, P. J.; Borghi, E. B.; Schteingart, L. M.; Blesa, M. A. *J. Chem. Soc. Dalton Trans.* **1981**, 2, 435.

8. Swinehart, J. H.; Rock, P. A. *Inorg. Chem.* **1966**, *5*, 573. (b) Masek, J.; Wendt, H. *Inorg. Chim. Acta* **1969**, *3*, 455. (c) Olabe, J. A.; Gentil, L. A.; Rigotti, G. E.; Navaza, A. *Inorg. Chem.* **1984**, *23*, 4297. (d) Baraldo, L. M.; Bessega, M. S.; Rigotti, G. E.; Olabe, J. A. *Inorg. Chem.* **1994**, *33*, 5890.

9. Bottomley, F. *Acc. Chem. Res.* **1978**, *11*, 158.

10. Callahan, R. W.; Meyer, T. J. *Inorg. Chem.* **1977**, *16*, 574. (b) Nagao, H.; Nishimura, H.; Funato, H.; Ichikawa, Y.; Howell, F. S.; Mukaida, M.; Kakihana, H. *Inorg. Chem.* **1989**, *28*, 3955. (c) Pipes, D. W.; Meyer, T. J. *Inorg. Chem.* **1984**, *23*, 2466. (d) Godwin, J. N.; Meyer, T. J. *Inorg. Chem.* **1971**, *10*, 2150. (c) Nagao, H.; Nimishura, H.; Funato, H.; Ichikawa, Y.; Howell, F. S.; Mukaida, M.; Kakihana, H. Inorg. Chem. **1989**, 28, 3955.

11. Bottomley, F.; Mukaida, M. *J. Chem. Soc. Dalton Trans.* **1982**, 1933.

12. Zanichelli, P. G.; Miotto, A. M.; Estrela, H. F. G.; Soares, F. R.; Grassi-Kassisse, D. M.; Spadari-Bratfish, R. G.; Castellano, E. E.; Roncaroli, F.; Parise, A. R.; Olabe, J. A.; Regina, A; Franco, D. W. *J. Inorg. Biochem.* **2004**, 98, 1921.

13. Gomes, M. G.; Davanzo, C. U.; Silva, S. C.; Lopes, L. G. F.; Santos, P. S.; Franco, D. W. *J. Chem. Soc. Dalton Trans.* **1998**, 601.

14. (a) Borges, S.; Davanzo, C. U.; Castellano, E. E.; Schpector, J. Z.; Silva, S. C.; Franco, D. W. *Inorg. Chem.* **1998**, *37*, 2670. (b) Gomes, M. G.; Davanzo, C. U.; Silva, S. C.; Lopes, L. G. F.; Santos, P. S.; Franco, D. W.; *J. Chem. Soc. Dalton Trans.* **1998**, 601.

15. (a) Fiedler, J. *Collect. Czech. Chem. Comm.* **1993**, *58*, 461. (b) Baumann, F.; Kaim, W.; Baraldo, L. M.; Slep, L. D.; Olabe, J. A.; Fiedler, J. *Inorg. Chim. Acta* **1999**, *285*, 129.

16. (a) Binstead, R. A.; Zuberbuhler, A. D. Spectrum Software Associates: Chapel Hill, N.C., 1993-1999. (b) Zuberbuhler, A. D. *Anal. Chem.* **1990,** *62*, 2220.

17. (a) Haim, A. *Comments Inorg. Chem.* **1985**, *4*, 113. (b) Miralles, A. J.; Szecsy, A. P.; Haim, A. *Inorg. Chem.* **1982**, *21*, 697. (c) Curtis, J. C.; Meyer, T. J. *Inorg. Chem.* **1982**, *21*, 1562.

18. Cambridge Structural Database System, version 5.23; Cambridge Crystallographyc Data Center: Cambridge, 2001.

19. Burton D. J.; Shinya S., Howells R. D.; J. Am. Chem. Soc. **1973**, 101, 3688.

20. Bessel, A.; Leising, R. A.; Szcepura, L. F.; Perez, W. J.; Vo, H.; My, H; Takeuchy, K. J. Inorg. Synth. **1988**, 32, 186.

21. Coe, B. J.; Meyer, T. J.; White, P. S. *Inorg. Chem.* **1995**, *34*, 593)

22. (a) Edwards, J. O. *Inorganic Reaction Mechanisms*, W. A. Benjamin, Inc., 1965, NY. (b) Swaddle, T. W. *Coord. Chem. Rev.* **1974**, *14*, 217. (c)

Swaddle, T. W. *Advances in Inorg. and Bioinorg. Mechanisms, Vol. 2*, A. G. Sykes, Ed.; Academic Press: London,1983, 95.

23. (a) Marcus, R. A. *J. Phys. Chem.* **1963**, *67*, 853, 2889. (b) Sutin, N. *Ann. Rev. Phys. Chem.* **1966**, *17*, 119.

24. (a) Oliveira, L. A. A.; Giesbrecht, E.; Toma, H. E. *J. Chem. Soc. Dalton Trans.***1979**, 236. (b) Parise, A. R.; Baraldo, L. M.; Olabe, J. A. *Inorg. Chem.* **1996**, *35*, 5080.

25. (a) Marcus, R. A.; *J. Phys. Chem.* 1968, *72*, 891. (b) Cohen, A. O.; Marcus, R. A. *J. Phys. Chem.* **1968**, *72*, 891.

26. (a) Wilkins, R. W. *Kinetics and Mechanism of Reactions of Transition Metal Complexes, 2nd Edition,* VCH, Weinheim, 1991.

27. Ford, P. C.; Rokicki, A. *Adv. Organometallic Chem.* **1988**, *28*, 139.

28. March, J. *Advanced Organic Chemistry*, 4th. Edition, Wiley, 1992.

29. Roncaroli, F.; Ruggiero, M. E.; Franco, D. W.; Estiú, G. L.; Olabe, J. A. *Inorg. Chem.* **2002**, 41, 5760.

4. The reactions of nitrosyl-complexes with cysteine

4.1. Introduction

The reactivity of nitrogen monoxide (NO) bound to transition metal centers is of particular concern in the context of the chemistry of NO relevant to biochemistry.[1] On discussing the ability of NO to bind or to dissociate from a given metal, it is crucial to define the redox state of the nitrosyl-bound species. Thus, the redox interconversions in the MNO moieties can lead to species with different electron contents, which may be described, in limiting approximations, as $M(NO^+)$, MNO or $M(NO^-)$. The electronic structures can be discussed with the aid of spectroscopic tools (mainly IR and/or EPR) or theoretical calculations, corresponding, in each case, with different reactivity patterns, including the formation-dissociation rates, as well as other types of redox reactivity.[2] The nitroprusside ion (NP, $[Fe(CN)_5NO]^{2-}$) is unique among iron-nitrosyl complexes with biological activity.[3] In addition to its hypotensive action, other physiological roles have been described, and these have recently reviewed.[4] The long known reversible additions of nucleophiles have been studied with NP and other metallonitrosyls by using OH^-, amines, thiolates and other reactants.[5] In these reactions the electrophilic nitrosyl ligand can be best described as a nitrosonium (NO^+) species, with the N-atom being the site for the addition of the nucleophiles.[3,5]

The mechanistic study of the reaction of NP with OH^- has been extended in Chapter 3 to a great variety of nitrosyl complexes of formula type $\{X_5MNO\}^n$, with X comprising ligands of different donor-acceptor abilities, such as amines, polypyridines, cyanides, etc.[5,6] Most of these studies have been performed with ruthenium, but a similar picture emerges with other low-spin d^6 metals such as Fe(II), Os(II), Ir(III). The reactions with OH^- are the most simple mechanistically, because they can be considered as acid-base reactions evolving in two steps: first,

OH^- adds forming the MNO_2H intermediate, which may go back to $M(NO^-)$ or subsequently lose the proton rapidly under attack of another OH^- to give the final nitro-complex. In Chapter 3, the redox potentials of the MNO^+/MNO couples were shown to be the crucial parameters controlling the electrophilic reactivity of the different $\{X_5MNO\}^n$ complexes.

The reactions with other potentially reductant nucleophiles such as amines or thiolates are more complicated than with OH^-, because irreversible processes (namely, intramolecular redox reactions) operate subsequently to adduct formation. The reactions with *N*-binding nucleophiles (ammonia and amines, hydrazine, hydroxylamine, azide) have been reviewed recently,[7] and lead in most instances to gas evolution (N_2 or N_2O) as a result of the adduct-decompositions, with complex mechanistic issues that become specifically dependent on the structure of the nucleophile. On the other hand, the reactions of different thiolates have been addressed exclusively with NP.[8] Adduct-intermediates intensively absorbing around 520 nm have been observed for the fast reactions of NP with diverse thiolates, with ensuing redox decomposition processes involving the reduction of NO^- and the oxidation of the thiolates.[8,9] These reactions are of great biological relevance, because NP is currently injected in the body fluids for blood-pressure control, and the question arises on the mechanistic role of thiolates in the mobilization of NO, in order for it to be accessible in solution for the vasodilation process.[3,4] In this work, we refer to the latter issue in a complementary way to existing work, because our main goal is to introduce a broader picture for the reactivity studies of thiols with metal nitrosyls, in addition to the recent work published for the NP ion, which have revealed a complex mechanistic picture, involving radical and non-radical paths associated with the role of thiolates, as well as a significant influence of pH and oxygen availability on the reaction process.[8] We have selected cysteine $\{(H^-)H_2NCH(CO_2^-)CH_2S^-)\}$ as the S-binding nucleophile, because of its biological relevance, and we use a variety of nitrosyl-

complexes already well characterized in the literature. We focus on the stoichiometry and mechanism of the steps arising after mixing the nitrosyl complexes with an excess of cysteine, under anaerobic and pH-controlled conditions.

4.2 Experimental section

Materials. All chemicals were analytical grade and were used without further purification. *L*-cysteine hydrocloride monohydrate was purchased from Anedra. Sodium nitroprusside dihydrate (NP) was from Aldrich. The following ruthenium complexes were prepared as previously described: $[Ru(bpz)NO(tpy)](PF_6)_3$;[10a] *cis*-$[Ru(AcN)(bpy)_2NO](PF_6)_2$;[10b] *cis*-$[Ru(bpy)_2(NO_2)$-$NO](PF_6)_2$;[10c] *cis*-$[Ru(bpy)_2ClNO](PF_6)_2$;[10c] $[Ru(bpy)NO(tpy)](PF_6)_3$;[10d] *trans*-$[Ru(NH_3)_4NOpz](BF_4)_3$;[10e] [Ru(Hedta)NO];[10f] *trans*-$[NCRu(py)_4CNRu(py)_4NO]$-$(PF_6)_3$;[10g] (tpy: terpyridine; bpz: 2,2′-bipyrazine; bpy: 2,2′-bipyridine; pz: pyrazine; py: pyridine) The purities were checked by IR and ^{1}H-NMR spectroscopies. Solutions were deoxygenated by saturation with N_2 or Ar. They were protected from light and were handled using gas-tight syringes. 1 M NaCl was used for adjusting the ionic strength, and acetic, phosphate and borate buffers were employed to control the pH.

Instrumentation and General Procedures. pH measurements were done with a Metrohm 744 pH meter at room temperature. NMR spectra were recorded on a Brucker 500 MHz spectrometer. A Thermo Nicolet Avatar 320 FT-IR spectrometer and a Spectratech IR-liquid-cell (with two 32 × 3 mm CaF_2 disks and a 0.1 mm spacer) were used for the IR measurements. Usually a 10–15 mM solution in *cis*-$[Ru(bpy)_2ClNO]Cl_2$ was prepared in D_2O or H_2O, after saturation with Ar. The necessary amount of cysteine was added together with some sodium acetate or sodium carbonate to reach the desired pH. A 273A Princeton Applied Research Potentiostat was used for square wave voltammetry (SWV) and

electrolysis. For SWV, a solution containing 1M NaCl and 0.1 M sodium acetate at pH 4 was used as electrolyte. Vitreous carbon, Ag/AgCl (3 M KCl), and a platinum wire were used as working, reference and counter electrodes, respectively. EPR measurements were done on the X-band of a Brucker ER 200D spectrometer. The spectra were recorded at 9.57 GHz, 140 K. For these experiments, 1 mM *cis*-$[Ru(bpy)_2ClNO](PF)_6$ was prepared (I = 1 M, pH 4.0, 0.1 M acetate) and 0.8 mg or 20 mg of cysteine were added to 10 ml of the complex solution, depending on the experiment. UV-vis spectra were recorded in the range 200–1100 nm with a Hewlett Packard 8453 diode array spectrophotometer. For the titrations of the complexes with cysteine, 20 ml of a 5×10^{-5} M complex solution (0.1 M acetic buffer, pH 4.0, I = 1 M) were placed in a cuvette attached to a flask. After bubbling N_2, 0.1 mL aliquots of a 2×10^{-3} M solution of cysteine were added. The UV-vis spectral changes were recorded during the process as described before. The titrations were done in duplicates. The temperature was kept constant at 25.0 □ 0.1 °C by means of a Lauda RC 20 thermostat.

Kinetic Experiments. A solution containing the complex (7×10^{-5}–5×10^{-4} M depending on the complex and the concentration of cysteine, with 1M NaCl) and some HCl (pH ca. 2 to discard any reaction with OH^-) were mixed using stopped flow (SF) techniques with another solution containing cysteine (6×10^{-4}–1.4×10^{-2} M), the buffer system (0.1–0.5 M) and NaCl to reach a total I = 1 M. At least a 10-fold excess of cysteine over the concentration of complex was always kept to ensure pseudo-first order conditions. To get an overall picture of the reaction, the solutions were mixed using an RX 1000 Applied Photophysics rapid kinetic accessory, and the spectral changes were recorded on the diode array spectrophotometer. To make the systematic studies as a function of the concentration of cysteine or of the pH, a Hi Tech PQ/SF-53 stopped flow and a Hi Tech SU-40 spectrophotometric unit were used. The data was acquired by a Hewlett Packard 54600A oscilloscope. This last instrument was interfaced to a

computer. The wavelength was always selected close to the absorption maximum of the Intermediate 1 (410–470 nm for the ruthenium complexes, and 526 nm for NP, see Table 4.1). Kinetic traces were always fitted to a single exponential at least for 3 half lives, usually 5, with the aid of a home-made-program. Under each condition, about 10 measurements were done. Values, which differed less than 20 %, usually less than 10 % were averaged. In this way, k_{obs} values were obtained. Plots of k_{obs} *vs* cysteine-concentration afforded the formation second order rate constant, with an intercept value equal to the dissociation constant (see eq 4.1). The formation of Intermediate 1 could only be studied using the Hi Tech SF technique. Similar values on the decomposition of the Intermediate 1 (to produce Intermediate 2) were obtained using both groups of instruments. For the experiments as a function of pH, a 9×10^{-5} M solution of $[Ru(bpy)_2ClNO]^{2+}$ and a 8.2×10^{-3} M solution of cysteine were used. The second order rate constant was calculated from the observed rate constants and the cysteine concentration (neglecting the intercept). At pH 4 this procedure introduced an error of ca. 20%, which was smaller at higher pH's.

Some complementary experiments using either substoichiometric or a small excess of cysteine were done using the diode array spectrophotometer and the rapid kinetic accessory described above. The concentration ranges of complex and cysteine were $0.7\text{-}1.5 \times 10^{-4}$ M and $0.17\text{-}1.5 \times 10^{-4}$ M, respectively. The experiments were done at pH 4.0 (0.1 M acetate buffer), $I = 1$ M, NaCl.

4.3. Results and discussion

We analyze first our selected reaction conditions, on the basis of the previous work with NP.[8] The most significant studies on the adduct-formation reactions of NP with thiols were done in the pH-range 8-10, i.e., under conditions

in which the thiols are (nearly) fully deprotonated ($pK_{a(SRH)}$ = ca. 8)[8], with the upper limit of 10 being appropriate for avoiding the competitive attack of OH^-.[3] A fast equilibrium is settled in the red-adduct formation process, eq 4.1, and both the forward and reverse rate constants have been determined for different thiols (I = 0.4 M, 25 °C). For *L*-cysteine, $k_1 = 2.2 \times 10^4\ M^{-1}s^{-1}$ and $k_{-1} = 3.4 \times 10^2\ s^{-1}$, at pH 10.0.[8b] Independently of the broad range of studied thiols, the absorption maxima lay at ca. 520 nm, with ϵ = ca. ($5\text{-}10 \times 10^3\ M^{-1}\ cm^{-1}$).[8,9]

$$[Fe(CN)_5NO]^{2-} + RS^- \rightleftarrows [Fe(CN)_5N(O)SR]^{3-} \qquad k_{1(SR^-)},\ k_{-1(SR^-)} \quad (4.1)$$

The unreactivity of RSH species toward NP was demonstrated in the pH range 4-10.[8b] In the kinetic studies, substoichiometric cysteine was used with respect to NP. Under these conditions, the subsequent redox decay of $[Fe(CN)_5N(O)SR]^{3-}$ leads to $[Fe(CN)_5NO]^{3-}$ and the disulfide oxidized species, cystine, as revealed by UV-vis and EPR results.[8c] The same products have been claimed under working conditions of excess-cysteine.[8a] N_2O has also been found however in related work with NP and thiolates,[11] and the two-electron reduced nitrosyl-bound intermediate, nitroxyl (NO^-, HNO), could be proposed as its precursor.

Reaction 4.1 has been studied with T-jump techniques, because the fast reactions of NP with thiolates are in the detection limit of the SF procedure.[8b] In the present work, we were able to reproduce the values for both rate constants in reaction 4.1 even under these extreme SF conditions. Given that the addition reactions of thiolates are significantly faster than with OH^-,[5] we could anticipate that the reactions with the ruthenium nitrosyl-complexes could be hardly studied by SF procedures, at least at pH 10. A preliminary check corroborated this negative prediction, but we took advantage of the fact that only the deprotonated thiols, SR^-, are the active species in the nucleophilic process, the reactivity of SRH being

negligible.[8] In this way, we were able to control the effective concentration of SR^- by lowering the pH. The work was performed under excess of cysteine over the ruthenium complex. This situation is seemingly the one present in the body fluids containing a high concentration of reduced sulfur species *in vivo*.[6]

The results will be ordered according to the different time scales for the events occurring after mixing. First, we address the adduct-formation reactions for cysteine adding to the different nitrosyl-complexes, as detailed in Table 4.1. Second, we consider the decay of these adducts, as observed in the UV-vis spectral runs, giving additional intermediates in the route to final products.

Adduct formation reactions. Figure 4.1 shows the successive spectra after the addition of aliquots of a solution of cysteine to a solution of $[Ru(bpy)NO(tpy)]^{3+}$.

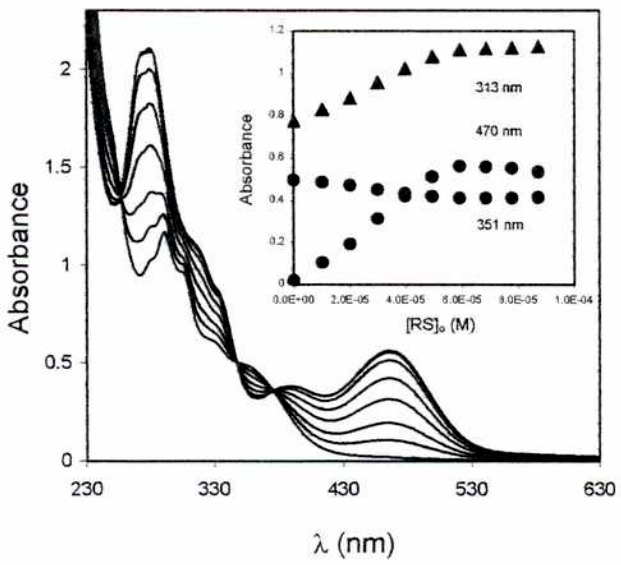

Figure 4.1. Successive spectra recorded during the addition of 0.1 ml aliquots of a solution 2.02 x 10^{-3} M in cysteine to a solution 5.71 x 10^{-5} M in the $[Ru(bipy)NO(tpy)]^{3+}$ complex. pH 4.0 (0.1 M acetate buffet), I = 1 M (NaCl), T = 25 °C.

During this process a new band centered at 467 nm, a shoulder at 390 nm and other new bands below 340 nm can be appreciated. The presence of isosbestic points at 347 and 376 nm are evidence for a clean reaction. The spectra remain constant after the addition of 0.95 equivalents of cysteine. This is a clear evidence of a 1:1 stoichiometry. We refer to the product of the primary interaction between cysteine and $[Ru(bpy)NO(tpy)]^{3-}$ as Intermediate 1, I_1. Upon addition of larger amounts of cysteine, new spectral changes were observed due to further reactivity of I_1 (see below). We propose that I_1 is an adduct between cysteine and the nitrosyl complex, similar to the one described in eq 4.1. Although no solid state characterizations are available for these adducts, strong support for the coordination of a nitrosothiolate ligand, $N(O)SR^-$ (with S binding to the N atom of nitrosyl) into the X_5M moieties, is provided by the IR evidence, mainly by the shifts in the NO-stretching vibration, which goes from 1936 cm^{-1} in NP to 1380 cm^{-1} in the red adduct (studied with EtS^- and NP).[12] On the other hand, the similarly intense visible bands in NP and the presently reported complexes can be traced to metal-to-ligand charge transfer (MLCT) transitions in the $\{X_5MN(O)SR\}$ adducts, which are expectedly shifted to the blue for the ruthenium-based adducts compared to those for the NP-thiolate adducts.

A similar experiment was performed with the *cis*-$[Ru(bpy)_2ClNO]^{2+}$ complex. In this case a new band at 450 nm and a shoulder at 410 nm were observed. A three-fold-excess of cysteine over complex concentration had to be added in order to reach a maximum conversion into I_1. This is consistent with the establishment of an equilibrium reaction, similar to the one described in eq 4.1 for the reaction with NP. Figure 4.2 shows the spectral changes observed during the reaction of the *cis*-$[Ru(bpy)_2ClNO]^{2+}$ complex with an excess of cysteine.

During the first reaction step, I_1 was formed (Figure 4.2a), showing the characteristic bands observed during the titration (*vide supra*). By measuring at different wavelengths, the same values of k_{obs} were obtained.

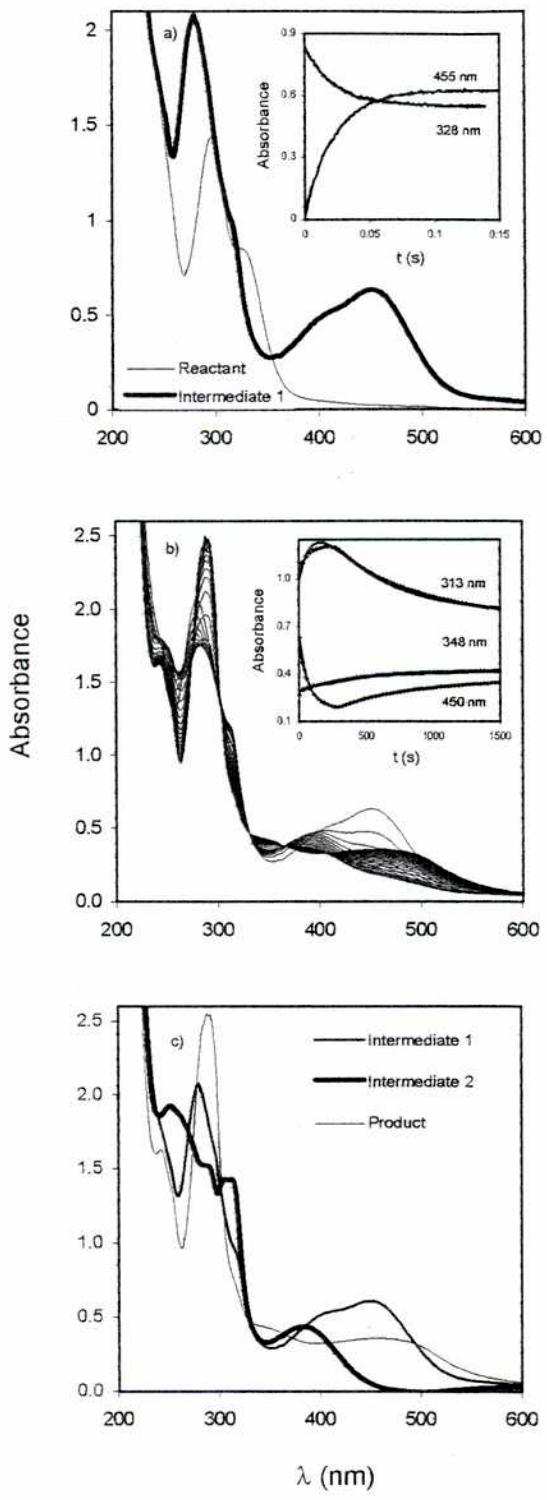

Figure 4.2. UV-vis-spectral changes for the reaction of 8.1 x 10^{-5} M $[Ru(bipy)_2ClNO]^{2+}$ complex with 3.8 x 10^{-3} M cysteine, pH 4.0 (0.1 M acetic

buffer), I = 1 M (NaCl), T = 25.0 °C. a) Spectra of the $[Ru(bipy)_2ClNO]^{2+}$ complex solution without the addition of cysteine (Reactant) and after the addition of cysteine (Intermediate 1). Inset: kinetic traces at 455 and 328 nm corresponding to the formation of Intermediate 1, $k_{1(obs)}$ = 43 s^{-1}. b) Successive spectra for the decomposition of Intermediate 1 to produce Intermediate 2 and Product. $k_{2(obs)}$ = 1.0 x 10^{-2} s^{-1} and $k_{3(obs)}$ = 3 x 10^{-3} s^{-1}. Inset: kinetic traces. c) Spectra of Intermediates 1 and 2 and Product, obtained through SPECFIT analysis of b).

Figure 4.3 shows the cysteine-concentration dependence of k_{1obs} for the adduct formation reaction with *cis*-$[Ru(bpy)_2ClNO]^{2+}$ (first step). A linear distribution appears, with a slope that can be traced to k_1 and an appreciable intercept assignable to k_{-1}.

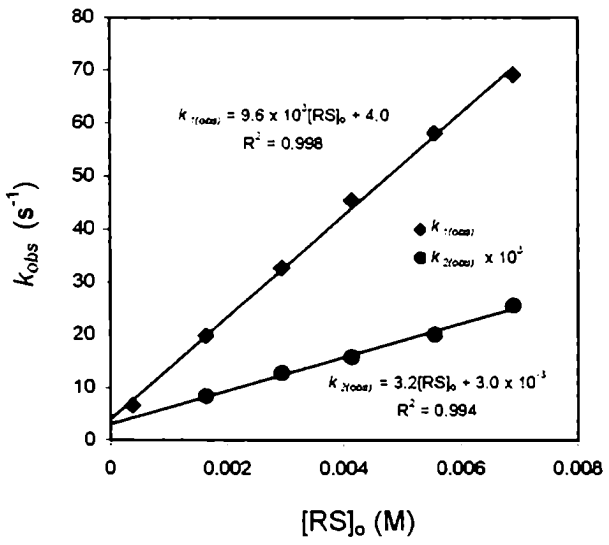

Figure 4.3. Cysteine-concentration dependence of the observed rate constant of the first reaction step ($k_{1(obs)}$) and the second reaction step ($k_{2(obs)}$) for the *cis*-$[Ru(bipy)_2ClNO]^{2+}$ complex. T = 25.0 °C, pH 4.0 (0.1 M acetate buffet), I = 1 M (NaCl). $k_{2(obs)}$ values were multiplied by 10^3 to fit the scale.

In order to assign these rate constants, we must consider the acid base equilibrium of cysteine, eq 4.2,[8b] and the reactions of RS^- and RSH with the nitrosyl complex.(reactions 4.3 and 4.4). In this way we obtain eqs 4.5 and 4.6, where k_1 is the second order rate constant for the first step (i = 1), and k_{-1} is the intercept corresponding to the plots of k_{obs} *vs* $[RS]_o$ (analytical concentration of cysteine).

$$RSH \rightleftarrows RS^- + H^+ \qquad K_a \quad (4.2)$$

$$[(X)_5RuNO]^n + RS^- \rightleftarrows [(X)_5RuN(O)SR]^{n-1} \qquad k_{1(SR^-)},\ k_{-1(SR^-)} \quad (4.3)$$

$$[(X)_5RuNO]^n + RSH \rightleftarrows [(X)_5RuN(O)SR]^{n-1} + H^+ \qquad k_{1(SRH)},\ k_{-1(SRH)} \quad (4.4)$$

$$k_i = \frac{k_{i(RS^-)}K_a + k_{i(RSH)}[H^+]}{K_a + [H^+]} \qquad (4.5)$$

$$k_{-i} = k_{-i(SR^-)} + k_{-i(SRH)}[H^+] \qquad (4.6)$$

From literature data, pK_a is 8.3 for cysteine.[8,13] When $[H^+] >> K_a$, according to eq 4.5, a plot of the second order rate constant k_1 *vs* $1/[H^+]$ should be linear, with a slope equal to $k_{1(RS^-)}K_a$ and an intercept equal to $k_{1(RSH)}$. Figure 4.4 shows this plot for the first reaction step. A linear distribution is observed with no meaningful intercept. This means that $k_{1(RSH)}$ is negligible in our reaction conditions.

The spectral changes during the reactions of cysteine with the rest of the complexes of Table 4.1 were similar to those observed with the *cis*-$[Ru(bpy)_2ClNO]^{2-}$ complex. The bands for the adduct-intermediates I_1 were observed in the range 410–470 nm (see Table 4.1). In all cases, the formation of I_1 was studied as a function of the concentration of cysteine. The reactions showed

again a linear distribution, with appreciable intercepts in most cases, thus affording values for k_{-1}. The values of the rate constants are shown in Table 4.2.

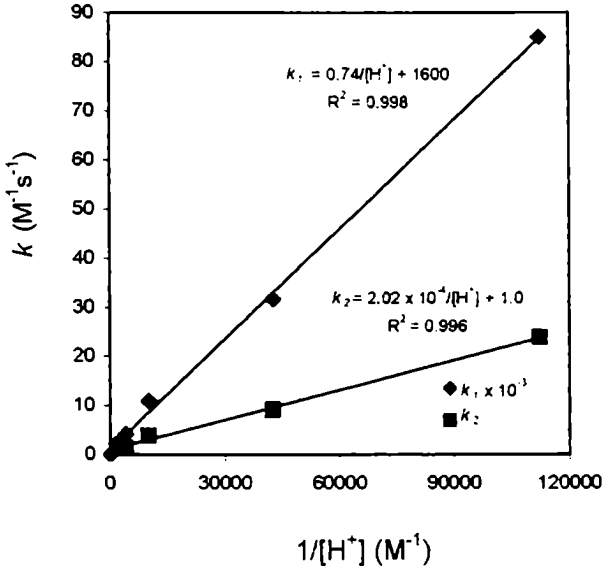

Figure 4.4. Plot of the second order rate constant for the first (k_1) and second (k_2) reaction steps *vs* 1/[H$^+$], for the *cis*-[Ru(bipy)$_2$ClNO]$^{2+}$ complex. T = 25.0 °C, pH 3.2 – 5.0 (0.1 M acetate buffet), I = 1 M (NaCl), [complex] = 9 × 10^{-5} M, [RS]$_o$ = 8.2 × 10^{-3} M. k_1 values were multiplied by 10^{-3} to fit the scale.

The values obtained for k_1 cannot be compared, because they have been measured at different pH's. With the assumption that only the deprotonated form of cysteine is reactive, and considering pK_a = 8.3,[8,13] we calculate $k_{1(SR^-)}$ for the different complexes by using eq 4.5 (see Table 4.2). Figure 4.5 shows a plot of ln $k_{1(SR^-)}$ *vs* $E_{NO^+/NOO}$ (redox potential of the coordinated nitrosyl). A linear correlation is observed for the lower potential range, i.e., for the least reactive complexes. The most reactive ones show values of $k_{1(SR^-)}$ close to the diffusion limit of 10^9 M^{-1}s^{-1} Values corresponding to the addition of OH$^-$ to the same complexes are also shown in Table 4.2 and in Figure 4.5 for comparative purposes.

Table 4.1. UV-vis spectral data for Intermediates 1 and 2.

Complex	Intermdiate 1	Intermediate 2
1.$[Fe(CN)_5NO]^{2-}$	526 (10^3-10^4)[a]	
2.[Ru(Hedta)NO]	405[b]	340[b]
3.*trans*-$[Ru(NH_3)_4NO(pz)]^{3+}$	421[c]	336[c]
4.*cis*-$[Ru(bpy)_2ClNO]^{2+}$	450 (8.0×10^3)	384 (5.3×10^3)
	410 (sh) (6.8×10^3)	
5.*cis*-$[Ru(bpy)_2(NO_2)NO]^{2+}$	451 (7.6×10^3)	372 (6.6×10^3)
	376	
6.*trans*-$[NCRu(py)_4CNRu(py)_4NO]^{3+}$	461	425 (sh)
7.$[Ru(bpy)(NO)(tpy)]^{3+}$	467 (9.0×10^3)	394 (6.2×10^3)
	390 (6.0×10^3)	
8.*cis*-$[Ru(bipy)_2(CH_3CN)NO]^{2+}$	448 (3×10^3)	390
9.$[Ru(terpy)(bipz)NO]^{3+}$	467 (5.6×10^3)	

Values in parenthesis correspond to molar absorptions. Values obtained at pH 4.0 (0.1 M acetate buffer, I = 1 M (NaCl), T = 25.0 °C, using at least 10 fold excess of cysteine over complex concentration, otherwise stated. [a] From ref. 8. [b] pH 9.9 (0.1 M borate buffer), I = 1 M (NaCl). [c] pH 7.0 (0.1 M phosphate buffet), I = 1 M (NaCl).

The rate constants for the additions of thiolates, SR^-, are expectedly greater than for OH^-, given the greater relative nucleophilic ability of sulfur. However, it can be seen that the values of the slopes are similar, close to 20 V^{-1}, for the lines corresponding to the reactions with OH^- and the meaningful values for the reactions with SR^-. The significance of this LFER has been analyzed in Chapter 3 for the adduct formation reactions in which the linear M-NO moieties are transformed into the angular M-NO_2H ones in the respective addition processes. The increase in the rates for the complexes with more positive reduction potentials was shown to be related to an increase in the positive charge at the electrophilic MNO moiety. Interestingly, the activation parameters indicated that the rate-increase was also associated with an activation enthalpy *increase*, overcompensated by the large activation entropies displayed by the positively charged complexes when reacting with OH^-. Given the similar slopes in Figure 4.5, we can reasonably assume an analogous behavior for the SR^- nucleophiles as well.

Table 4.2. Kinetic data for the reactions of cysteine with nitrosyl-complexes.

Complex	E_{NO^+/NO^0} (v) [a]	k_1 ($M^{-1}s^{-1}$)	k_{-1} (s^{-1})	k_2 ($M^{-1}s^{-1}$)	k_{-2} (s^{-1})	$k_{1(SR^-)}$ ($M^{-1}s^{-1}$)[b]	$k_{2(SR^-)}$ ($M^{-1}s^{-1}$)[b]	k_{OH} ($M^{-1}s^{-1}$)[a]
1.$[Fe(CN)_5NO]^{2-}$	-0.29	$(2.2 \pm 0.4) \times 10^4$ [c]	$(5.6 \pm 0.2) \times 10^2$ [c]	1 – 2 [e]		2.2×10^4	1 – 2 [e]	5.5×10^{-1}
2.[Ru(Hedta)NO]	-0.30	$(4.9 \pm 0.6) \times 10^4$ [c]	$(2.6 \pm 0.2) \times 10^2$ [c]	*ca.* 50 [c]	Not measured	4.9×10^4	*ca.* 50	4.35×10^0
3.*trans*-$[Ru(NH_3)_4NO(pz)]^{3+}$	-0.11	$(1.6 \pm 0.3) \times 10^5$ [d]	$(1.1 \pm 0.4) \times 10^2$ [d]	$(6.0 \pm 4) \times 10^1$ [d]	$(2.8 \pm 0.6) \times 10^{-2}$ [d]	3.2×10^6	1.2×10^3	1.77×10^2
4.*cis*-$[Ru(bpy)_2ClNO]^{2+}$	0.05	$(9.6 \pm 0.2) \times 10^3$	$(4.0 \pm 0.9) \times 10^0$	$(3.2 \pm 0.1) \times 10^0$	$(3.0 \pm 0.7) \times 10^{-3}$	1.5×10^8	4.0×10^4	8.5×10^3
5.*cis*-$[Ru(bpy)_2(NO_2)NO]^{2+}$	0.18	$(1.36 \pm 0.03) \times 10^4$	$(2 \pm 1) \times 10^0$	$(1.16 \pm 0.02) \times 10^1$	$(2.9 \pm 0.9) \times 10^{-3}$	2.7×10^8	2.3×10^5	5.06×10^4
6.$[NCRu(py)_4CNRu(py)_4NO]^{3+}$	0.22	$(7.00 \pm 0.09) \times 10^3$	$(1.5 \pm 0.3) \times 10^0$	$(3.5 \pm 0.1) \times 10^1$	$(1.9 \pm 0.5) \times 10^{-2}$	1.4×10^8	7.0×10^5	9.2×10^3
7.$[Ru(bpy)NO(tpy)]^{3+}$	0.25	$(2.67 \pm 0.08) \times 10^4$	< 3	$(3.5 \pm 0.2) \times 10^1$	$< 9 \times 10^{-3}$	5.3×10^8	7.0×10^5	3.17×10^5
8.*cis*-$[Ru(bipy)_2(CH_3CN)NO]^{2+}$	0.35	$(2.89 \pm 0.07) \times 10^4$	$(4 \pm 2) \times 10^0$	$(1.8 \pm 0.4) \times 10^1$	$(9 \pm 1) \times 10^{-2}$	5.8×10^8	3.6×10^5	5.60×10^6
9.$[Ru(bpz)NO(tpy)]^{3+}$	0.46	$(3.56 \pm 0.08) \times 10^4$	< 5	$(1.79 \pm 0.04) \times 10^2$	$(2 \pm 1) \times 10^{-2}$	7.1×10^8	3.6×10^6	7.6×10^6

Values obtained at pH = 4.0 (0.1 M acetate buffer), I = 1 M (NaCl), T = 25.0 °C, otherwise stated.
[a] From Chapter 3.
b Calculated from equation 4.5, using $pK_a = 8.3$
c pH = 9.9 (0.1 M borate buffer), I = 1M (NaCl).
d pH = 7.0 (0.1 M phosphate buffer), I = 1M (NaCl).
e From ref. 8a.c.

The decay of the adduct Intermediate I_1, with Formation of Intermediate I_2. For $[Ru(bpy)_2ClNO]^{2+}$, I_1 reacts in a second reaction step to produce a second intermediate, I_2, which shows a well defined band at 384 nm (see Figure 4.2b and Table 4.1). Figure 4.3 shows the plot of k_{obs} against the concentration of cysteine for this second reaction step, showing again a first-order behavior in both reactants, as for the first step.

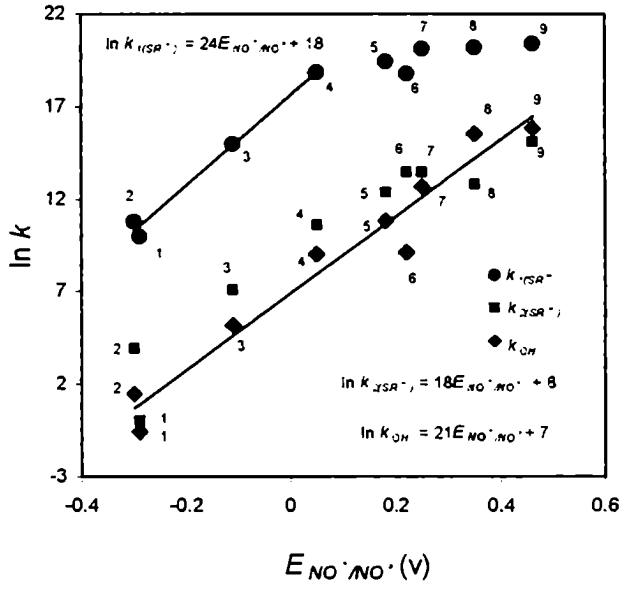

Figure 4.5. Linear free energy relationships for $k_{1(SR^-)}$, $k_{2(SR^-)}$ *and* k_{OH^-}, against the redox potential for the nitrosyl-couples. For number assignments, see Table 4.1 or 4.2.

We propose that I_2 is a second adduct with two coordinated, deprotonated cysteines, eq 4.7.

$$[(X)_5RuN(O)SR]^{n-1} + RS^- \rightleftarrows [(X)_5RuN(O)(SR)_2]^{n-2} \qquad k_{2(SR^-)},\ k_{-2(SR^-)} \quad (47)$$

This type of intermediate has been proposed in the analysis of the reaction of NP with excess of thiolates.[8a] No direct spectroscopic evidence was shown, but a

linear dependence of the pseudo-first order rate constant for the decay of $[Fe(CN)_5N(O)SR]^{3-}$ on the concentration of cysteine was reported,[8a,c] as described here. Also, similar structures comprising two bound thiolates to the N-atom of NO have been proposed during the transnitrosation reactions of thiols,[14a,b] and recent NMR evidence, together with DFT calculations, have been provided for these elusive intermediates.[14c] In Figure 4.4, the linear plot of the second order rate constant, k_2, against the inverse of $[H^+]$ shows again that reaction 4.8, involving the protonated cysteine, RSH, is negligible, as found for the formation of I_1 (eq 4.4).

$$[(X)_5RuN(O)SR]^{n-1} + RSH \rightleftarrows [(X)_5RuN(O)(SR)_2]^{n-2} + H^+ \quad k_{2(SRH)},\ k_{-2(SRH)} \quad (4.8)$$

By plotting the values of ln $k_{2(SR^-)}$ for the second-step in eq 4.7 (again, k_2 was corrected for the pH effect using eq 4.5, $i = 2$) against the redox potential for the same series of complexes as previously shown, Figure 4.5 shows again a linear behavior. The alignment of the points together with the ones for the OH^--additions is fortuitous. However, it is entirely reasonable that the rates for the addition of a SR^--nucleophile in reaction 4.7 must be lower than in reaction 4.3, because the first bound-thiolate has already diminished the nucleophilic ability of the MNO group compared to the one for NP. Overall, the plots in Figure 4.5 provide consistent evidence on the successive SR^--additions on the nitrosyl-complexes, as described by eqs 4.3 and 4.7.

The decay of I_2. Finally, I_2 decomposes slowly (third reaction step, k_3) to a product with bands at 470 and 350 nm. Figure 4.2c shows the spectra corresponding to both intermediates, I_1 and I_2, together with the one for the final product, as obtained through a SPECFIT analysis.[15] Further reactions of the product were not investigated in detail. Its spectrum closely resembles that of the

cis-$[Ru(bpy)_2Cl(H_2O)]^+$.[16] Moreover, a new wave at 0.49 V *vs* Ag/AgCl was observed during this reaction by performing the SWV experiments. A wave in the same position appeared after reduction of *cis*-$[Ru(bpy)_2ClNO]^{2+}$ at −1.0 V *vs* Ag/AgCl (it is well known that the last procedure generates the $[Ru(bpy)_2Cl(H_2O)]^+$ complex in a clean way, consistent with the two-electron reduction process occurring at the stated potential).[16]

During this third reaction step N_2O was also produced, as detected by IR spectroscopy through its characteristic band at 2230 cm^{-1}.[11b] We propose reaction 4.9 for describing the decomposition of I_2 in the *cis*-$[Ru(bpy)_2ClNO]^{2+}$ complex, and we assume that similar processes are also operative for the remaining Ru-complexes.

$$cis\text{-}[Ru(bpy)_2ClN(O)(SR)_2]^{o} + H^{-} \rightleftarrows cis\text{-}[Ru(bpy)_2Cl(HNO)]^{-} + RS\text{-}SR \quad (4.9)$$

Equation 4.9 assumes a two-electron reduction of NO^+ giving the nitroxyl ligand, HNO, favored by the coordination of the two thiolate reductants. HNO is a labile ligand, and a fast coupling process will lead to N_2O, as described elsewhere.[17] The lability of HNO in the ruthenium complexes is strongly suggested by the irreversible character of the two-electron reduction waves in electrochemical experiments.[10b] We observed a white precipitate of cystine in the aged solutions, in the experiments with the most concentrated solutions, as found previously by other authors.[8] A comprehensive study of the reaction of NP with thiolates, in a wide range of relative concentrations for the latter species,[8a] accounts for the production of only the one-electron reduction production, $[Fe(CN)_5NO]^{3-}$. Some reports have also found N_2O, however.[11,*] In our experiments (including some assays with

---

* N_2O has been reported as a delayed product during the reaction of glutathione with NP, through IR detection (reference 11b). We have also demonstrated (see Chapter 6) that upon the one-

substoichiometric cysteine), we also observed $[Fe(CN)_5NO]^{3-}$ when using NP, but we could not observed any one-electron reduction products for the ruthenium complexes 4,5,7,8 (Table 4.1). For complex 4, no IR absorptions were found in the range 1600-1800 cm^{-1}, as expected for reduced-nitrosyl.[7] A very weak EPR signal at ca. 3400 gauss was measured, which cannot be assigned to the NO-bound complex.

The reason for the different behavior of NP compared to the more oxidizing ruthenium-complexes may be traced to the different stability and reactivity of the adducts. Although NP is the least oxidizing species, it can be easily reduced by one electron;[3] thus, I_1 leads to $[Fe(CN)_5NO]^{3-}$. In the case of I_2 (which should be a less stable adduct compared to the Ru-analogs because of the negative charge of NP), it also produces $[Fe(CN)_5NO]^{3-}$,[8a] probably because the two-electron reduction is not thermodynamically allowed. On the other hand, the more oxidizing ruthenium nitrosyl-complexes favor a fast two-electron reduction in the more stable I_2 adducts.* The influence of the structure of the nucleophile in the one-electron or multielectronic reductions of bound NO^- in NP has been recently discussed by

---

electron reduction of NP to the $[Fe(CN)_5NO]^{3-}$ or to the $[Fe(CN)_4NO]^{2-}$ ions (pH range 6-10), N_2O appears in the *hours* time scale. The slowly dissociating NO (k = ca. 10^{-5} s^{-1} at 25 °C) enters the labile *trans*-position generated by cyanide-loss, thus forming a dinitrosyl species. This is an intermediate that decomposes to NP and N_2O in a 2:1 ratio. This type of N_2O-generation is not certainly occurring in the presently reported fast reactions of nitrosyl-ruthenium complexes with cysteine.

* An intermediate character can be envisaged for the less reactive Ru-complexes 2 and 3. In the reaction of $[Ru(NH_3)_4pzNO]^{3+}$ with cysteine, a new absorption at ca. 1850 cm^{-1} developed, which could probably be ascribed to a one-electron reduction process.

using hydrazine and substituted hydrazines as nucleophiles. HNO-bound intermediates have been proposed in some of these systems as precursors of N_2O.[18]

4.4. Summary and conclusions

The nucleophilic reactions under excess of cysteine were studied for a number of ruthenium nitrosyl-complexes. The reactions were very fast, compared with previously reported additions of OH^- and *N*-binding nucleophiles. The primary interaction of cysteine with the complexes generated 1:1 adduct-intermediates, I_1, with intense absorption bands in the range 410–470 nm, assigned to MLCT transitions, structurally related to the similar adduct with NP. The formation kinetics showed a first order behavior for both of the reactants and a first order one for adduct-dissociations.

The visible bands of I_1 decay in the presence of an excess of cysteine, to form a second intermediate I_2 showing intense absorption bands between 340-400 nm. The formation of I_2 is slower than I_1, but the kinetic order in the formation and dissociation reactions of both intermediates were the same. We propose that I_2 is another adduct, with a 2:1 stoichiometry (thiolate *vs* nitrosyl-complex). Additional evidence of these successive adduct-formation reactions is provided by the linear free energy plots of the addition-rate constants against the reduction potentials of the NO^+/NO couples. As in the reactions with OH^- with a set of nitrosyl-complexes, the addition of thiolates are faster for the complexes affording more positive reduction potentials.

I_2 decays further, with formation of the corresponding aqua-complexes, $\{X_5Ru(H_2O)\}$, N_2O and cystine. Negative evidence was obtained (IR, EPR) for most of the complexes as to the presence of bound NO-complexes, in contrast with NP. The observed products account for a two-electron reduction of the initial NO^+-bound species, favored by the strong oxidizing abilities of the Ru-NO^+ complexes

and by the structures of the I_2 adducts containing the two reductant thiolates. Scheme 4.1 summarizes our proposed mechanism.

$$[(X)_5RuNO]^n \underset{-RS^{\cdot}}{\overset{RS^{\cdot}}{\rightleftharpoons}} [(X)_5RuN(O)SR]^{n-1} \underset{-RS^{\cdot}}{\overset{RS^{\cdot}}{\rightleftharpoons}} [(X)_5RuN(O)(SR)_2]^{n-2} \longrightarrow [(X)_5Ru(H_2O)]^{n-1} + N_2O + RSSR$$

Scheme 4.1. Proposed mechanism for the reactions of cysteine with ruthenium nitrosyl complexes.

A final comment is in order on the connection of these mechanistic issues with the role of thiolates on the release of free NO to the medium when NP is injected, a crucial point for triggering the vasodilation process. We shall show in Chapter 6 that bound NO is very inert toward dissociation, independently of the pH, i.e. when we consider it as predominantly $[Fe(CN)_5NO]^{3-}$ (at pH's greater than 8) or as $[Fe(CN)_4NO]^{2-}$ (at lower pH's). Therefore, the role of thiolates should be ascribed to the ability of reducing NO^+ to NO, still as a bound species, but not to any other specific effect favoring the mobilization of NO to the enzymatic targets. Intracellular conditions appropriate to first favoring the prior release of cyanides should be met for NO-labilization from NP,[4] thus accounting for the fast response (minute time scale) upon injection of NP in the body fluids.

4.5. References

1. (a) McCleverty, J. A. *Chem. Rev.* **2004**, *104*, 403-418. (b) Stamler, J. S.; Feelisch, M., in *Methods in Nitric Oxide Research*; Feelisch, M.; Stamler, J. S., Eds.; Wiley, Chichester: UK, 1996, Chapter 2. (c) *Nitric Oxide:*

Biology and Pathobiology; Ignarro, L. J., Ed.; Academic Press: San Diego, 2000. (d) Moncada S.; Palmer, R. M. J.; Higgs, E. A. *Pharmacological Reviews*, **1991**, *43*, 109-142.

2. (a) Westcott, B. L.; Enemark, J. H. In *Inorganic Electronic Structure and Spectroscopy*; Solomon, E. I., Lever, A. B. P., Eds.; Wiley-Interscience: New York, 1999; Vol. 2. Chapter 7, pp. 403-450. (b) Enemark, J. H.; Feltham, R. D. *Coord. Chem. Rev.* **1974**, *13*, 339-406.

3. (a) Swinehart, J. H. *Coord. Chem. Rev.* **1967**, *2*, 385-402. b) Clarke, M. J.; Gaul, J. B. *Struct. Bonding (Berlin)*, **1993**, *81*, 147-181. (c) Butler, A. R.; Glidewell, C. *Chem. Soc. Rev.* **1987**, *16*, 361-380.

4. Butler, A. R.; Megson, I. L. *Chem. Rev.* **2002**, *102*, 1155-1165.

5. (a) Bottomley, F., in *Reactions of Coordinated Ligands*; Braterman, P. S., Ed.; Plenum Press: New York, 1989; Vol. 2, pp 115-222.

6. (a) Ford, P. C.; Lorkovic, I. M. *Chem. Rev.* **2002**, *102*, 993-1018. (b) Ford, P. C.; Laverman, L. E.; Lorkovic, I. M. *Adv. Inorg. Chem.* **2003**, *54*, 203-257.

7. Olabe, J. A. *Adv. Inorg. Chem.* **2004**, *55*, 61-126.

8. (a) Szacilowski, K.; Wanat, A.; Barbieri, A.; Wasielewska, E.; Witko, M.; Stochel, G.; Stasicka, Z. *New J. Chem.* **2002**, *26*, 1495-1502. (b) Johnson, M.; Wilkins, R. G. *Inorg. Chem.* **1984**, *23*, 231-235. (c) Morando, P. J.; Borghi, E. B.; Schteingart, L. M.; Blesa, M. A. *J. C. S. Dalton Trans.* **1981**, 435-440. (d) Butler, A. R.; Calsy-Harrison A. M.; Glidewell, C. *Polyhedron*, **1988**, *7*, 1197-1202.

9. Szacilowski, K.; Stochel, G.; Stasicka, Z.; Kisch, H. *New J. Chem.* **1997**, *21*, 893-902.

10. (a) see Chapter 3. (b) Callahan, R. W.; Meyer, T. J. *Inorg. Chem.* **1977**, *16*, 574-581. (c) Godwin, J. B.; Meyer, T. J. *Inorg. Chem.* **1971**, *10*, 471-474. (d) Murphy, R. W.; Takeuchi, K.; Barley, M. H.; Meyer, T. J. *Inorg. Chem.* **1985**, *25*, 1043. (e) Gomes, M. G.; Davanzo, C. V.; Silva, S. C.; Lopes, L. G. F.; Santos, P. S.; Franco, D. W. *J. C. S. Dalton Trans.* **1998**, 601-607. (f) Zanichelli, P. G.; Miotto, A. M.; Estrela, H. G.; Rocha Soares, F.; Grassi-Kassisse, D. M.; Spadari-Bratfisch, R. C.; Castellano, E. E.; Roncaroli, F.; Parise, A. R.; Olabe, J. A.; de Brito, A. R. M. S.; Franco, D. W. *J. Inorg. Biochem.* **2004**, *98*, 1921-1932. (g) see Chapter 2.

11. (a) Smith, J. N.; Dasgupta, T. P. *Inorg. Reaction Mech.*, **2002**, *3*, 181-195. (b) Sampath, V.; Rousseau, D. L.; Caughey, W., in *Methods in Nitric Oxide Research*; Feelisch, M.; Stamler, J. S., Eds.; Wiley, Chichester: UK, 1996, Chapter 29.

12. Schwane, J. D.; Ashby, M. T. *J. Am. Chem. Soc.* **2002**, *124*, 6822-6823.

13. CRC Handbook of Chemistry & Physics, 75th ed., CRC Press, 1994.

14. (a) Dicks, A.; Li, E.; Munro, A.; Swift, H.; Williams, D. *Can. J. Chem.* **1998**, *76*, 789-794. (b) Houk, K. N.; Hietbrink, B. N.; Bartberger, M. D.; Mc Carren, P. R.; Choi, B. Y.; Voyksner, R. D.; Stamler, J. S.; Toone, E. J. *J. Am. Chem. Soc.* **2003,** *125*, 6972-6976. (c) Perissinotti, L. L.; Estrín, D. A.; Doctorovich, F., unpublished results.

15. Binstead, R. A.; Zuberbülher, A. D. Spectrum Software Associates: Chapel Hill, N. C., 1993-1999.

16. Togniolo, V.; Santana da Silva, R.; Tedesco, A. C. *Inorg. Chim. Acta* **2001**, *316*, 7-12.

17. Bonner, F. T.; Stedman, G., in *Methods in Nitric Oxide Research*; Feelisch, M.; Stamler, J. S., Eds.; Wiley, Chichester: UK, 1996, Chapter 1.

18. Gutiérrez, M. M.; Amorebieta, V. T.; Estiú, G. L.; Olabe, J.- A. *J. Am. Chem. Soc.* **2002**, *124*, 10307-10319.

5. Spectroscopic characterization of reduced ruthenium nitrosyl complexes

5.1. Introduction

Formation, reactivity, spectroscopy and structures of nitrosyliron complexes have been investigated for more than a century.[1-3] The question of the appropriate electronic description of such species in terms of oxidation and spin states has been highlighted recently by the examples of simple $[(H_2O)_5Fe(NO)]^{2+}$,[4] of complexes $[(L)Fe(NO)]^{n-}$ with multidentate N,S-donor ligands L,[5] and of nitrosyliron porphyrins inside or outside of hemoproteins.[6,7] Various iron oxidation states, from -II[8] to +IV[9] can be discussed in conjunction with nitrosyl (NO^-), nitric oxide ($NO^\bullet$) or nitroside (NO^-) ligands.[10] Paramagnetic neutral $NO^\bullet$ is of particular interest, its presence being evidenced frequently through vibrational or EPR spectroscopy.[11,12]

The current surge of such studies is attributed to the recognition of the essential role of iron-NO interactions in physiological context,[13] including the formation,[14] binding, and release[15] of this ubiquituous messenger (neurotransmitter) molecule.[16] Copper-[17] or iron-coordinated NO also plays an important role in the biological nitrogen cycle.[18] In yet another line of interest, the metal-influenced chemistry of NO is of relevance for catalytic exhaust gas conversion.[19]

Recently, corresponding compounds of the higher homologue ruthenium have also found attention in the search for NO-scavenging[20] or NO-releasing (delivering) agents.[14,15,21] Scavenging by specifically designed ruthenium(III) complexes was reported recently to involve a fast NO coordination, leading to formally $Ru^{II}(NO^-)$ complexes.

On the other hand, photochemical or electron transfer activation can be envisaged for the labilization of bound NO from its usual, kinetically stable Ru^{II}-(NO^-) = $\{RuNO\}^6$ configuration.[21] Following more recent assumptions[22] on the

transition from Ru^{II}-(NO^+) to Ru^{II}-($NO^\bullet$) some EPR data on chemically generated Ru^{II}-($NO^\bullet$) species and pertinent quantum-chemical calculations were published in the last years.[21b,23-30]

A similar situation holds for the infrared spectroscopy. Previous reports show that the NO stretching frequency in reduced ruthenium nitrosyl complexes, ν_{NO}, is around 1650 cm^{-1} [23] which is a value close to the data reported for iron complexes.[42,43] Some crystalline structures were resolved and they show an hexacoordinated structure with a coordinated *bent* NO.[30b,42]

Herein we describe EPR results from the *in situ*-reduction of several more such complexes $[L_nRu(NO)]^k$, we summarize and critically discuss the data of 18 different such species and compare the unexpectedly uniform result with the situation in corresponding iron complexes. We also present some infrared spectroscopic data, which complements the previous information.

5.2. Experimental section

Materials: All chemicals were analytical grade and used without further purification. Anhydrous acetonitrile for IR measurements was from Aldrich.

The complexes *trans*-$[Ru(py)_4(Cl)_2]$,[35] *trans*-$[RuCl(NO)(py)_4](PF_6)_2$,[32] *trans*-$[Ru(NO)(OH)(py)_4](PF_6)_2$,[32] *trans*-$[Ru(NH_3)(NO)(py)_4](BF_4)_3$,[33a] *cis*-$[Ru(bpy)_2Cl(NO)](PF_6)_2$,[23] *cis*-$[Ru(bpy)_2(CH_3CN)(NO)](PF_6)_2$ [33b] and $[Ru(bpy)(NO)(tpy)](PF_6)_3$ [34] were prepared as previously described. The synthesis of the $[Ru(bpz)(NO)(tpy)](PF_6)_3$ and *trans*-$[Ru(NO)(py)_4(SCN)](PF_6)_2$ complexes was described in Chapter 3. The purity was checked by IR and ^{1}H-NMR spectroscopies.

Instrumentation. IR spectra were measured on a Thermo Nicolet Avatar 320 FT-IR instrument. The purity of the complexes was checked using KBr pellets.

To determine the IR spectra of the reduced species, 10 mg of complex and 8 mg of *trans*-[$Ru(py)_4(Cl)_2$] were dissolved in dried and deoxygenated acetonitrile. The solution thus obtained was transferred by a gas tight syringe to a Spectratech liquid-cell containing two 32 × 3 mm CaF_2 disks and a 0.1 mm spacer. ^{1}H-NMR spectra were obtained on a Bruker 500 MHz spectrometer.

UV-vis spectra were recorded in the range 200 – 1100 nm with a Hewlett Packard 8453 diode array spectrophotometer. For the UV-vis spectroelectrochemical experiments, a Princeton Applied Research potentiostat 273A and a 1-cm-quartz-cuvette attached to a glass container were used. The electrolyte was a solution 1 M in NaCl and 0.1 M in acetate buffer pH 4.0. A Platinum gauze and a Ag/AgCl (KCl 3 M) electrode were used as working and reference electrodes respectively. The counter electrode was a Platinum wire separated by a frit glass. Electrolysis were preformed under continuous bubbling of N_2, at 25 °C and at -0.1 V *vs* Ag/AgCl.

EPR spectroscopy: The ruthenium-nitrosyl complexes were reduced for *in situ* EPR studies in a two-electrode capillary described earlier.[31] The electrolyte was CH_3CN/0.1 M Bu_4NPF_6. Whereas the brief (ca. 10 min) electrolysis was performed at 295 K, the EPR spectra were recorded at 110 K in glassy frozen solutions due to the EPR silence of the complexes at room temperature. A Bruker ESP 300 spectrometer was used, and the *g* factors were determined with a Bruker ER035M gaussmeter and a HP 5350B microwave counter. The spectra were simulated (program Bruker WinSimfonia) without incorporating the unresolved hyperfine splitting of g_1 and g_3 components.

5.3. Results and discussion

EPR spectrosopy. Although the Ru^{II}-($NO^{\cdot}$) precursor complexes referred to in the Experimental Section are reduced reversibly at room temperature, there were no EPR signals detectable for the one-electron reduced forms under those conditions. EPR silence at room temperature has been reported before for the related species from Table 5.1.[22-25] In glassy frozen solution a typical pattern[17,23-30] of rhombic g splitting with ^{14}N nitrosyl hyperfine coupling of the central component emerges a representative spectrum from the *in situ*-electrolysis of a precursor, $[Ru(bpz)(NO)(tpy)]^{3+}$, in CH_3CN/0.1 M Bu_4NPF_6 is shown together with a computer simulation in Figure 5.1.

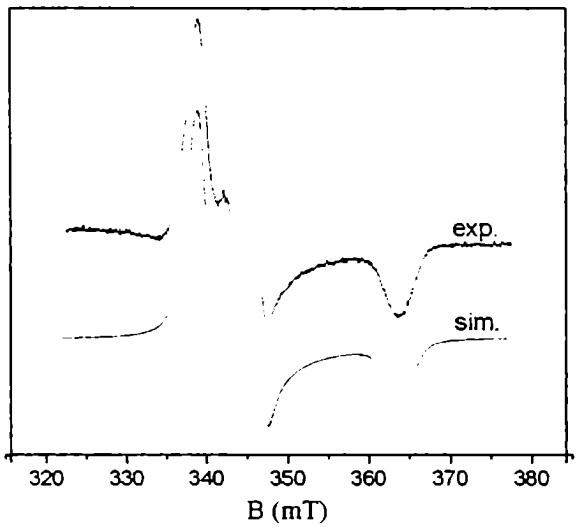

Figure 5.1. EPR spectrum of $[Ru(bpz)(NO)(tpy)]^{2+}$ at 110 K in CH_3CN/0.1 M Bu_4NPF_6 (top) with computer simulation (bottom).

The results for the reversibly reduced systems are summarized together with literature data in Table 5.1. Most previously reported species were obtained through chemical reduction with e.g. Zn/Hg[29] or Eu^{2+}.[21b,24,25b]

Table 5.1. EPR Data of Ruthenium-Nitrosyl Complexes [a,b]

Complex	g_1	g_2	g_3	g_{av}	Δg	A_1	A_2		ref.
$[Ru(NH_3)(NO)(py)_4]^{2+}$	2.0215	1.9875	1.878	1.963	0.1435	n.o.			[b]
$[Ru(NO)(py)_4(SCN)]^+$	2.0225	1.9895	1.877	1.963	0.1455	n.o.	2.9		
$[Ru(Cl)(NO)(py)_4]^+$	2.025	1.990	1.886	1.967	0.139	n.o.	3.1		
$[Ru(Cl)(NO)(py)_4]^+$	2.033	1.989	1.874	1.965	0.159	1.51	3.18		28[c]
$[Ru(NO)(OH)(py)_4]^-$	2.0235	1.991	1.886	1.967	0.1375	n.o.		n.o.	
$[Ru(bpy)_2(CH_3CN)(NO)]^{2+}$	2.028	1.9925	1.882	1.968	0.146	n.o.	3.3	n.o.	
$[Ru(bpy)_2Cl(NO)]^+$	2.029	1.992	1.881	1.968	0.148	n.o.	3.2	n.o.	
$[Ru(bpy)(NO)(tpy)]^{2+}$	2.0175	1.998	1.883	1.967	0.1345	n.o.	3.4	n.o.	
$[Ru(bpz)(NO)(tpy)]^{2+}$	2.0215	1.999	1.886	1.969	0.1355	n.o.	3.4	n.o.	
$[NC(py)_4RuCNRu(py)_4NO]^{2+}$	2.024	1.990	1.865	1.960	0.159	1.55	3.39	0.97	28[c]
$[Ru(cyclam)Cl(NO)]^+$	2.035	1.995	1.883	1.971	0.152	1.7	3.21	1.5	24, 25b[d]
$[Ru(bpydip)Cl(NO)]^+$	2.027	1.991	1.889	1.969	0.138	1.69	3.23	1.48	29[e]
$[Ru(Cl)(dppe)_2(NO)]^+$	2.011	1.976	1.867	1.951	0.144	1.71	1.85[m]	1.43	25[f]
$[Ru(Cl)(depe)_2(NO)]^+$	2.010	1.984	1.888	1.961	0.122	1.8	3.5	1.9	25b[d]
$[Ru(NC)_5(NO)]^{3-}$	2.004	2.002	1.870	1.959	0.134	n.o.	3.8	n.o.	27[g]
$[Ru(C_5Me_5)(NO)(Ph_3P)_2]^+$	2.0115	1.983	1.900	1.965	0.111	1.63	2.10[n]	2.29	30a[h]
	1.995	1.995	1.896	1.962	0.099	n.o.	2.85	n.o.	30a[i]
$[Ru(C_5Me_5)(NO)(PhMe_2P)_2]^+$	2.000	1.998	1.915	1.970	0.085	1.06	3.38	1.07	30a[h]
	1.996	1.996	1.964[j]	1.985[j]	0.032[j]	n.o.	3.25	n.o.	30a[i]
$[Ru(C_5Me_5)(Me_3P)_2(NO)]^+$	2.007	2.002	1.918	1.976	0.089	1.15	3.37	1.20	30a[h]
	2.001	1.994	1.912	1.969	0.089	0.6	3.3	1.3	30a[i]
$[Ru(HCl)(NO)(OC)(^iPr_3P)_2]$	2.006	1.993	1.910	1.970	0.096	n.o.	3.45	n.o.	30b[k]
$[Ru(DCl)(NO)(OC)(^iPr_3P)_2]$	2.001	1.994	1.910	1.968	0.091	n.o.	3.45	n.o.	30b[k]

[a] ^{14}N hyperfine coupling A in mT. [b] In CH_3CN/0.1 M Bu_4NPF_6, measured at 110 K. [c] In CH_3CN/0.1 M Bu_4NPF_6, measured at 10 K. [d] In ethylene glycol + 30% H_2O, measured at 77 K; cyclam = 1,4,8,11-tetraazacyclotetradecane; depe = 1,2-bis(diethylphosphino)ethane. [e] In CH_3CN, measured

at 110 K; bpydip N,N'-bis(7-methyl-2-pyridylmethylene)-1,3-diiminopropane. [f] In CH_2Cl_2, measured at 77 K, dppe = 1,2-bis(diphenylphsophino)ethane. [g] In CH_3CN/0.1 M Bu_4NPF_6, measured at 3.5 K. [h] In CH_2Cl_2, measured at 113 K. [i] In acetone, measured at 100 K. [j] Probably erroneous value. [k] In toluene, measured at 77 K. Additional ^1H hyperfine coupling observed at about 3.5 mT.

Given the wide variety of ligands L for the species $[RuL_n(NO)]^k$ in Table 5.1 (L = pyridine, polypyridines, imines, amines, nitriles, phosphines, carbonyl, cyclopentadienide, halides, hydride, hydroxide, thiocyanate, cyanide), the small degree of EPR parameter variation is surprising: g_1 = 2.015 ±0.02, g_2 = 1.990 ±0.015, g_3 = 1.892 ±0.03, g_{av} = 1.968 ±0.02, $\Delta g = g_1 - g_3$ = 0.122 ±0.037, $A_2(^{14}N)$ = 3.3 ±0.5 mT. The variance is still smaller if organometallic derivatives[30] are excluded.

Paramagnetic nitrosyliron complexes, even those involving only low-spin systems,[4,5,7,36] exhibit a distinctly greater variation. In part this may reflect contributions from the more accessible valence-tautomeric $M^I(NO^-)$ state for M = Fe which has a $(d_z^2)^1$ configuration and leads to $g_{1,2} \approx 2.07$, $g_3 \approx 2.0$ and $g_{av} \approx 2.03$ for clearly established $Fe^I(NO^+)$ cases.[25,36b]

As an average, the g anisotropy $\Delta g = g_1 - g_3$ is about twice as large for the ruthenium complexes than for related nitrosyliron(II) species.[27] This is an immediate consequence of the higher spin-orbit coupling constant $\xi(Ru) \approx 2\ \xi(Fe)$.[37]

Despite the rather uniform EPR results for the species in Table 5.1 there are some slight variations: The most symmetrical species $[Ru(NC)_5(NO)]^{3-}$ displays a g component splitting approaching the axial limit with "$g_\perp$" > $g_\parallel$. The average g is smallest for this species whereas it is slighly larger (by 0.012) for $[Ru(cyclam)Cl(NO)]^+$, however, all Ru^{II}-($NO^\bullet$) complexes have g_{av} well below 2, indicating the closeness of both π^* orbitals of NO[27] and thus of both $^2\Pi_x$ and $^2\Pi_y$

states.[38,39] The presence of states lying close to the radical ground state is al responsible for the rapid relaxation as evident from the EPR silence at temperature. The relatively large A_2 hyperfine value of 3.8 mT for $^{14}N(NO)$ may in part reflect the reluctance of negatively charged cyanide ligands in $[Ru(CN)_5(NO)]^{3-}$ to accommodate the unpaired electron. On the other hand, the A_2 values are smallest, at about 3.0 mT, for the series of complexes $[Ru(py)_4X(NO)]$ with rather weak donor ligands (Tab. 5.1).

The total g anisotropy $\Delta g = g_1 - g_3$ is highest for the dinuclear $[(NC)(py)_4Ru(CN)(py)_4Ru(NO)]^{2+}$, possibly reflecting an effect of the second, not NO-coordinating metal center with its high spin-orbit coupling constant. On the other side, $[Ru(CN)_5(NO)]^{3-}$ and the phosphine-containing compound $[(depe)_2ClRu(NO)]^{+}$ (depe = 1,2-bis(diethylphosphino)ethane), both with strong σ donor/π acceptor ligation, display relatively small Δg values, indicating smaller metal contributions as supported also by rather high nitrosyl ligand coupling constants $A_2(^{14}N)$.

Exchange of CH_3CN by DMF in the case of $[RuCl(NO)(py)_4]^{+}$ yielded identical EPR prarameters. Although the cyanoiron radical compounds $[Fe(CN)_5(L)]^{2-}$, L = NO^{+} or N-methylpyrazinium (mpz^{+}), can lose one cyanide ligand on reduction[40,41] we found no evidence for conversion to five-coordination in the paramagnetic ruthenium species studied here.

IR spectroscopy. Table 5.2 shows the infrared spectroscopic data for some reduced ruthenium nitrosyl complexes together with some literature data. The complexes under study show a ν_{NO} near 1650 cm^{-1} and the intensity of this band did not change significantly within 1 hour. These findings are consistent with previous reports (see Chapter 2), which claim that these reduction products are very stable.[23] Several complexes showing ν_{NO} at these frequencies have been reported, including nitrosyliron complexes.[42,43] The structure of some of these compounds

has been resolved, they are octahedral and the M-N-O is bent with an angle close to 150°.[42,30b]

Table 5.2. IR spectroscopic data for the reduction products of some ruthenium complexes.

Complex	ν_{NO} (cm^{-1})
cis-$[Ru(bpz)(tpy)NO]^{2+}$	1670 [a]
cis-$[Ru(CH_3CN)(bpy)_2NO]^{2+}$	1666 [a,b]
cis-$[Ru(bpy)(tpy)NO]^{2+}$	1656 [a]
cis-$[Ru(bpy)_2(NO_2)NO]^{+}$	1649 [a]
cis-$[Ru(bpy)_2(Cl)NO]^{+}$	1640 [a,b]
trans-$[Ru(NH_3)(py)_4(NO)]^{2+}$	1639 [a]
trans-$[NC(py)_4RuCNRu(py)_4NO]^{2+}$	1626 [c]
trans-$[Ru(Cl)(py)_4(NO)]^{+}$	1610 [c]
$[Fe(CN)_5NO]^{3-}$	1648 [d]
$[Os(CN)_5NO]^{3-}$	1560 [e]

[a] This work, in acetonitrile, in the precence of *trans*-$[Ru(Cl)_2(py)_4]$ as reducing agent. [b] From ref. 23. [c] See chapter 2. [d] From ref. 43. [e] From ref. 44.

Some authors have found a very small shift for ν_{NO} upon reduction of the nitrosyl complexes. The reduction product of the $[Ru(cyclam)(Cl)NO]^{2+}$ complex shows ν_{NO} at 1850 cm^{-1} [24] and a similar situation was found for the $[Ru(bpydip)Cl(NO)]^{+}$ complex.[29] For these compounds some evidence for the *trans*-ligand-labilization was observed.[24] Nevertheless, their reduction products show the typical EPR spectra of the ruthenium complexes (see Table 5.1). Moreover, in the case of nitroprusside, $[Fe(CN)_5NO]^{2-}$, the reduction product shows a ν_{NO} at 1648 cm^{-1} [43], which shifts to 1800 cm^{-1} upon *trans*-CN-labilization.[43] The EPR spectrum of a sample of $[Fe(CN)_4NO]^{2-}$ also shows signals

assignable to $[Fe(CN)_5NO]^{3-}$. This has been explained in terms of the · ture dependence of the equilibrium between both species. The [Fe(CN) on is comparatively more stable at lower temperatures, which are the conditions se cted for the EPR experiments. [45]

Putting together these comments, it is probable that the appa wrong values for ν_{NO} reported in references 24,29, while being associated to correct EPR spectra for the hexacoordinate species, are in fact a consequence of ligand labilization, i.e. the pentacordinate species is the one really present in the medium.

UV-vis spectroscopy. The UV-vis spectra during the controlled potential reduction of cis-$[Ru(bpy)_2(Cl)(NO]^{2+}$ and $[Ru(bpy)(NO)(tpy)]^{3+}$ were measured in water. The results obtained for the first complex are very simlar to the ones previously reported in acetonitrile.[23] The wavelength maxima and the molar absorbances are listed in Table 5.3. The spectral changes during the reduction of the complexes *trans*-$[NCRu(py)_4CNRu(py)4NO]^{3+}$ and *trans*-$[Ru(Cl)NO(py)_4]^{2+}$ have already been analysed in Chapter 2. Figure 5.2 shows the spectra arising upon reduction of $[Ru(bpy)NO(tpy)]^{3+}$

5.4. Conclusions

Several reduced ruthenium nitrosyl complexes have been characterized through EPR, IR and UV-vis spectroscopies.

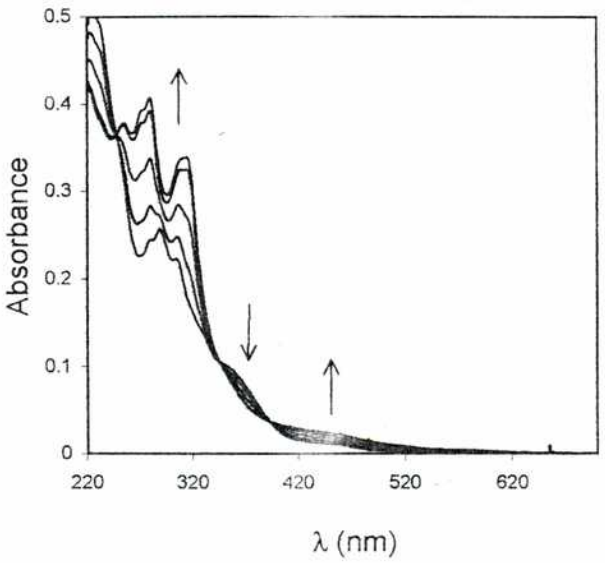

Figure 5.2. UV-vis spectral changes recorded during electrochemical reduction of $[Ru(bpy)(NO)(tpy)]^{3+}$ at –0.1 v *vs* Ag/AgCl. T = 25 °C, pH = 4.0 (0.1 M acetate buffer), I = 1 M (NaCl), [complex] = 1.2 x 10^{-5} M.

In the EPR spectra, the small variation in g tensor splitting and hyperfine coupling for all 18 compounds in Table 5.1 suggest very similar electronic structures, described essentially by the Ru^{II}-($NO^{\bullet}$) formulation. The surprising invariance of EPR parameters points to a higher degree of covalency in the $\{RuNO\}^7$ situation than in corresponding $\{FeNO\}^7$ arrangements, the latter having more accessible options between the limiting structures $Fe^{II}(NO^{\bullet})$ and $Fe^{I}(NO^{+})$ and between low-spin and high-spin states.

The IR and the UV-vis spectra also show similarities among the studied compounds and the literature data. The first technique appears to be quite sensitive to the *trans*-ligand-labilization effect. More work should be done in order to assess if IR measurements are able to differentiate between penta- and hexacoordinate-nitrosyl species.

Table 5.3. UV-vis spectroscopic data for some ruthenium complexes

Complex	λ_{max} (nm)[a]	ε ($M^{-1}cm^{-1}$)[a]
$[Ru(bpy)(NO)(tpy)]^{3+}$	281 (sh)	1.8×10^4
	291	2.0×10^4
	305 (sh)	1.7×10^4
	325 (sh)	1.1×10^4
	351 (sh)	8.7×10^3
	465 (sh)	3.5×10^2
$[Ru(bpy)(NO)(tpy)]^{2+}$	254	3.3×10^4
	279	3.5×10^4
	312	2.9×10^4
	440(sh)	2.0×10^3
cis-$[Ru(bpy)_2(Cl)NO]^{2+}$	297	1.7×10^4
	325 (sh)	1.0×10^4
cis-$[Ru(bpy)_2(Cl)NO]^{+}$	252	2.3×10^4
	293	1.9×10^4
	310 (sh)	1.8×10^4
	370 (sh)	3.5×10^3

[a] Electrochemical reduction in water, pH = 4.0 (0.1 M acetate buffer), I = 1 M (NaCl), T = 25 °C.

Aknowledgements. I thank Stéphanie Frantz and Prof. Wolfgang Kaim for the EPR measurements, data analysis and result discussions.

5.5. References

1. Playfair, L. *Proc. Roy. Soc. (London)* **1849**, *5*, 846. (b) Playfair, L. *Liebigs Ann. Chem.* **1850**, *74*, 317.
2. Swinehart, J. H. *Coord. Chem. Rev.* **1967**, *2*, 385.
3. Olabe, J. A. *Adv. Inorg. Chem.*, 2004, 55, 61-126.
4. Wanat, A.; Schneppensieper, T.; Stochel, G.; van Eldik, R.; Bill, E.; Wieghardt, K. *Inorg. Chem.* **2002**, *41*, 4.
5. Li, M.; Bonnet, D.; Bill, E.; Neese, F.; Weyhermüller, T.; Blum, N.; Sellmann, D.; Wieghardt, K. *Inorg. Chem.* **2002**, *41*, 3444.
6. Averill, B. A. *Chem. Rev.* **1996**, *96*, 2951; (b) Trofimova, N. S.; Safronov, A. Y.; Ikeda, O. *Inorg. Chem.* **2003**, *42*, 1945, and references cited.
7. Wayland, B. B.; Olson, L. W. *J. Am. Chem. Soc.* **1974**, *96*, 6037; (b) Chen, Y.; Sweetland, M. A.; Shepherd, R. E. *Inorg. Chim. Acta* **1997**, *260*, 163.
8. (a)Couture, C.; Morton, J. R.; Preston, K. F.; Strach, S. J. *J. Magn. Reson.* **1980**, *41*, 88. (b)Dieck, H.; Bruder, H.; Kühl, E.; Junghans, D.; Hellfeldt, K. *New. J. Chem.* **1989**, *13*, 259.
9. Hauser, C.; Glaser, T.; Bill, E.; Weyhermüller, T.; Wieghardt, K. *J. Am. Chem. Soc.* **2000**, *122*, 4352.
10. Olabe, J. A.; Slep, L., in *Comprehensive Coordination Chemistry II* (McCleverty, J. A.; Meyer, T. J., Eds.); Pergamon, 2004, p. 603-623.
11. Enemark, J. H.; Feltham, R. D. *Coord. Chem. Rev.* **1974**, *13*, 339.
12. Richter-Addo, G. B.; Legzdins, P. *Metal Nitrosyls*; Oxford University Press., New York, 1992.
13. Feelisch, M.; Stamler, J. S. (eds.) *Methods in Nitric Oxide Research*; Wiley, Chichester, 1996.

14. Ford, P. C.; Lorkovic, I. M. *Chem. Rev.* **2002**, *102*, 993.

15. Wang, P. G.; Xian, M.; Tang, X.; Wu, X.; Wen, Z; Cai, T.; Janc ak, A. *Chem. Rev.* **2002**, *102*, 1091. (b) Hrabie, J. A.; Keefer, L. K. *Chem. Rev.* **2002**, *102*, 1135.

16. Murad, F. *Angew. Chem. Int. Ed.* **1999**, *28*, 1856.

17. Ruggiero, C. E.; Carrier, S. M.; Antholine, W. E.; Whittaker, J. W.; Cramer, C. J.; Tolman, W. B. *J. Am. Chem. Soc.* **1993**, *115*, 11285.

18. Ferguson, S. J. *Current Opinion in Chem. Biol.* **1998**, *2*, 182.

19. Iwamoto, M.; Hamada, H. *Catal. Today* **1991**, *10*, 57; (b) Groothaert, M. H.; van Bokhoven, J. A.; Battiston, A. A.; Weckhuysen, B. M.; Schoonheydt, R. A. *J. Am. Chem. Soc.* **2003**, *125*, 7629.

20. Cameron, B. R.; Darkes, M. C.; Yee, H.; Olsen, M.; Fricker, S. P.; Skerlj, R. T.; Bridger, G. J.; Davies, N. A.; Wilson, M. T.; Rose, D. J.; Zubieta, J. *Inorg. Chem.* **2003**, *42*, 1868. (b) Serli, B.; Zangrando, E.; Gianferrara, T.; Yellowlees, L.; Alessio, E. *Coord. Chem. Rev.* **2003**, *245*, 73.

21. Wolak, M.; van Eldik, R. *Coord. Chem. Rev.* **2002**, *230*, 263. (b) Tfouni, E.; Krieger, M.; McGarvey, B.R.; Franco, D.W. *Coord. Chem. Rev.* **2003**, *236*, 57.

22. Borges, S. S. S.; Davanzo, C. U.; Castellano, E. E.; Z-Schpector, J.; Silva, S. C.; Franco, D. W. *Inorg. Chem.* **1998**, *37*, 2670. (b) Bezerra, C. W. B.; Silva, C. S.; Gambardella, M. T. P.; Santos, R. H. A.; Plicas, L. M. A.; Tfouni, E.; Franco, D. W. *Inorg. Chem.* **1999**, *38*, 5660.

23. Callahan, R. W.; Meyer, T. J. *Inorg. Chem.* **1977**, *16*, 574. The EPR spectrum of $[(bpy)_2ClRu(NO)]^+$ shown in this publication was not analyzed.

24. Lang, D. R.; Davis, J. A., Lopes, L. G. F.; Ferro A. A.; Vasconcellos, L. C. G.; Franco, D. W.; Tfouni, R.; Wieraszko, A.; Clarke, M. J. *Inorg. Chem.* **2000**, *39*, 2294.

25. Zampieri, R. C. L.; Von Poelhsitz, G.; Batista, A. A.; Nascimento, O. R.; Ellena, J.; Castellano, E. E. *J. Inorg. Biochem.* **2002**, *92*, 82. (b) McGarvey, B. R.; Ferro, A. A.; Tfouni, E.; Brito Bezerra, C. W.; Bagatin, I.; Franco, D. W. *Inorg. Chem.* **2000**, *39*, 3577.

26. Gomez, J.A.; Guenzburger, D. *Chem. Phys.* **2000**, *253*, 73.

27. Wanner, M.; Scheiring, T.; Kaim, W.; Slep, L. D.; Baraldo, L. M.; Olabe, J. A.; Zalis, S.; Baerends, E. J. *Inorg. Chem.* **2001**, *40*, 5704.

28. See chapter 2.

29. de Souza, V. R.; de Costa Ferreira, A. M.; Toma, H. E. *Dalton Trans.* **2003**, 458

30. Diversi, P.; Fontani, M.; Fuligni, M.; Laschi, F.; Marchetti, F.; Matteoni, S.; Pinzino, C.; Zanello, P. *J. Organomet. Chem.* **2003**, *675*, 21. (b) Marchenko, A. V.; Vedernikov, A. N.; Dye, D. F.; Pink, M.; Zaleski, J. M.; Caulton, K.G. *Inorg. Chem.* **2004**, *43*, 351.

31. Kaim, W.; Ernst, S.; Kasack, V. *J. Am. Chem. Soc.* **1990**, *112*, 173.

32. Bottomley, F.; Mukaida, M. *J. Chem. Soc., Dalton Trans.* **1982**, 1933.

33. Nishimura, H.; Matsuzawa, H.; Togano, T.; Mukaida, M.; Kakihana, H. *J. Chem. Soc., Dalton Trans.* **1990**, 137. (b) Nagao, H; Ito, K.; Tsuboya, N.; Ooyama, Dai.; Nagao, N.; Howell, S. F.; Mukaida, M. *Inorg. Chim. Acta* **1999**, *290*, 113 .

34. Pipes, D. W.; Meyer, T. J. *Inorg. Chem.* **1984**, *23*, 2466

35. Evans, I. P.; Spencer, A.; Wilkinson, G. *J. Chem. Soc. Dalton Trans.* **1973**, 2, 204.

36. van Voorst, J. D. W.; Hemmerich, P. J. *Chem. Phys.* **1966**, *45*, 3914. (b) Reginato, N.; M.cCrory, C. T. C.; Pervitsky, D.; Li, L. *J. Am. Chem. Soc.* **1999**, *121*, 10217.

37. Weil, J. A.; Bolton, J. R.; Wertz, J. E. *Electron Paramagnetic Resonance*; Wiley: New York, 1994.

38. Pietrzyk, P.; Piskorz, W.; Sojka, Z.; Broclawik, E. *J. Phys. Chem. B* **2003**, *107*, 6105.

39. Neyman, K. M.; Ganyushin, D. I.; Nasluzov, V. A.; Rösch, N.; Pöppl, A.; Hartmann, M. *Phys. Chem. Chem. Phys.* **2003**, *5*, 2429.

40. EPR of $[(NC)_4Fe(NO)]^{2-}$: Glidewell, C.; Johnson, I. L. *Inorg. Chim. Acta* **1987**, *132*, 145.

41. Waldhör, E.; Kaim, W.; Olabe, J. A.; Slep, L. D.; Fiedler, J. *Inorg. Chem.* **1997**, *36*, 2969.

42. Sellmann, D.; Blum, N.; Heinemann, F. W.; Hess, B. A. *Chem. Eur. J.* **2001**, 7, 9.

43. Schwane, J. D.; Ashby, M. T. *J. Am. Chem. Soc.* **2002**, 124, 6822.

44. Baumann, F.; Kaim, W.; Baraldo, L. M.; Slep, L. D.; Olabe, J. A.; Fiedler, J.; *Inorg. Chim. Acta* **1999**, 285, 129.

45. Kruszyna, H.; Kruszyna, R.; Rochelle, L. G.; Smith, R. P.; Wilcox, D. E. *Biochem. Pharmacol.* **1993**, 46, 95.

6. The release of NO from reduced Nitroprusside. Metal-Dinitrosyl Formation and NO-Disproportionation Reaction

6.1. Introduction

Different compounds identified as "NO donors" are currently employed in medical or pathological situations by introducing them into the biological fluids, in order to play key roles in bioregulatory functions, including immune stimulation, platelet inhibition, neurotransmission, and smooth muscle relaxation.[1,2] These compounds may contain explicitly the NO group, as in metallonitrosyls, *N*-nitrosamines, nitrosothiols, etc., or may be other *N*-containing substances able to generate NO *in situ* through the reaction with endogenous reactants, as is the case with organic nitrates and nitrites or with hydroxylamine. Then, NO will diffuse or will be transported in some way to an enzyme target, e.g., soluble guanylate cyclase (sGC), producing a cascade of events leading to vasodilation.[2]

Among the metallonitrosyls, sodium pentacyanonitrosylferrate ($Na_2[Fe(CN)_5NO].2H_2O$, nitroprusside, NP) is widely used in physiological and medical experimentation as a "gold-standard" NO donor drug.[3] NP has a number of clinical uses, the most common of which is hypotensive anaesthesia during surgery. This $\{FeNO\}^6$ species in the Enemark-Feltham formalism[4] is best described as an Fe(II) centre (d^6, low spin) containing a NO^+ (nitrosonium) ligand.[5] As such, it is extremely inert toward thermal dissociation, although a photoredox process readily delivers NO upon irradiation with visible-UV light, with additional formation of $[Fe^{II}(CN)_5H_2O]^{2-}$.[6] On the other hand, NP shows electrophilic reactivity toward different nucleophiles (OH^-, amines, thiolates, etc),[7] and can be reduced either chemically or electrochemically forming the one-electron reduction product,

$[Fe^{II}(CN)_5NO]^{3-}$, or ill defined two-electron reduction products, presumably related to the nitroxyl anion, NO^-.[8] The addition of thiolates to bound NO^- in NP leads to the fast formation of bound nitrosothiolates, which could be the appropriate intermediates for the mobilization and rapid release of NO to the medium *via* subsequent processes that finally lead to sGC activation.[1a,9] Fundamental questions still remain as to the detailed mechanistic steps involving metal-bound nitrosothiolate formation and decomposition. The latter process involves mainly a redox event with formal reduction of NO^- to NO and oxidation of thiolate.[10] However, it is still unclear if this process occurs through the bound or free nitrosothiolate species, or both.

The $[Fe^{II}(CN)_5NO]^{3-}$ ion could be considered an alternative direct precursor of NO, released to the medium after the reduction of NP by biologically relevant reductants. A recent kinetic and mechanistic study revealed that NO dissociates from $[Fe^{II}(CN)_5NO]^{3-}$ with a rate constant of 1.6×10^{-5} s^{-1} at 25 °C, pH 10,[11] and this value seems too low to account for the fast physiological response upon NP injection (minute time scale).[3] The $[Fe^{II}(CN)_5NO]^{3-}$ ion releases cyanide rapidly forming $[Fe(CN)_4NO]^{2-}$, and appreciable concentrations of both anions may exist in equilibrium at pH's around 7.[12] The $[Fe(CN)_4NO]^{2-}$ ion has been proposed as the labile precursor of NO-release[13] when NP is reduced by different thiols, in a process comprising the *subsequent* dissociation of cyanides and rearrangements leading to $[Fe^{II}(CN)_6]^{4-}$, with the claimed intermediacy of $[Fe(CN)_4]^{2-}$.[14] Also, the $[Fe(CN)_4NO]^{2-}$ ion leads to paramagnetic dinitrosyl-iron complexes (DNICs, the so-called "g = 2.03" complexes with formula $\{Fe(L)_2(NO)_2\})^{3a,15}$ which may behave as NO-carriers in the presence of an excess of thiolates.[14] EPR signals assignable to these DNICs have been found in tissue of ascites tumors of mice upon injection of NP.[13f]

In the studies of coordination of NO to the $[Fe^{II}(CN)_5H_2O]^{3-}$ ion, we found that the product was unstable under excess of NO, at pH 7.[11] A preliminary

investigation revealed that $[Fe(CN)_4NO]^{2-}$ was the active species promoting decomposition, and that NP was formed as one of the products, among others. This result suggested that an NO-disproportionation process could be involved, in the context of an unknown reactivity picture of bound NO, probably relevant to the complex process of NP decomposition in biological media. Herein we present the results of a stoichiometric and kinetic study in the pH-range 4-10, through the measurement of the decay of $[Fe^{II}(CN)_5NO]^{3-}$ and/or $[Fe(CN)_4NO]^{2-}$ by using UV-vis, IR, EPR, electrochemical and mass-spectrometric techniques. Through this *in vitro* approach, we aim to contribute to finding a reasonable assignment of the possible chemical events leading to the rapid vasodilatory action of NP. This study involves a careful avoidance of light exposure,[3a] as well as the maintenance of anaerobic conditions. The latter point becomes important, because oxygen can rapidly transform $[Fe^{II}(CN)_5NO]^{3-}$ back to NP in aerobic media.[10] Our studies are placed in the context of a still underdeveloped chemistry of bound NO in transition metal centers,[16] and we address specifically the nitrosyl transfer problem from a metal-NO donor (*viz.*, NP) to another M′-NO acceptor,[17] including the possible intermediacy of dinitrosyl compounds.

6.2. Experimental section

All chemicals were of analytical grade and were used without further purification. 85 % sodium dithionite ($Na_2S_2O_4$) was from Acros. Acetate, Bis-Tris or phosphate and borate buffers were used, with NaCl for adjusting the ionic strength. The measurements of pH in the range 4-10 were done at room temperature with a 744 Metrohm pH meter. The preparation of the solutions was done in Schlenk tubes. The necessary amount of reducing agent, usually sodium dithionite ($Na_2S_2O_4$) or sodium tetrahydroborate ($NaBH_4$), was added as a solid to

N_2- or Ar-saturated solutions of NP, containing the appropriate buffer and ionic strength. At least a two-fold excess of NP over the reducing agent was always employed. The solutions were always protected from light, and were transferred using gas tight syringes and a vacuum/Ar or N_2 line. NO was purchased from Air Liquide and purified from higher nitrogen oxides by passing through an ascarite II column. The concentration of NO in the saturated solutions prepared under NO-bubbling was 1.8 mM.

Studies on the reaction products. 2–3.5 mg of NP were dissolved in 10 ml of a 0.01M buffer solution (I = 0.1 M, NaCl). $Na_2S_2O_4$ was added and an aliquot was immediately transferred to a spectrophotometric cell to record the UV-vis spectrum. The initial concentration of reduced NP species, either $[Fe(CN)_5NO]^{3-}$ or $[Fe(CN)_4NO]^{2-}$, was calculated considering the molar absorbances reported in the literature[12] (these values were also checked experimentally in this study). The concentrations usually ranged between 0.2–0.5 mM. The samples were allowed to react for two days in the Schlenk tubes. Then, aliquots were extracted and different ions present in the final solutions were analyzed using spectrophotometric techniques. A Hewlett Packard 8453A diode array spectrophotometer was employed for the UV-vis measurements. The latter procedures were not performed under anaerobic conditions. The *o*-phenantroline and SCN^- reagents were used for determining the concentrations of $[Fe(H_2O)_6]^{2+}$ and $Fe(H_2O)_6]^{3+}$, respectively.[18] Nitrite was quantified using the *Griess* reaction.[1a] Free CN^- or HCN were determined with an Aquaquant 14429 kit from Merck. NP was determined through the reaction with thiosuccinic acid,[19] as described elsewhere.[20] The final value was corrected by using the initial concentration of NP. By knowing the amount that was reduced from the initial spectrum, we obtained the concentration of NP that was effectively obtained through reoxidation of $[Fe(CN)_5NO]^{3-}$ The concentration of $[Fe(CN)_6]^{4-}$ was determined through the reaction with $[Fe(H_2O)_6]^{3+}$, producing Prussian-Blue.[21] The sample was mixed with an equal volume of a 0.1 M HNO_3

solution containing 1 mM $Fe(NO_3)_3$. Calibration was achieved by preparing standard solutions of $[Fe(CN)_6]^{4-}$ in the range (0 – 0.2) mM. Samples and standard solutions were allowed to react for two hours and the absorbance at 705 nm was measured. No precipitation of Prussian-Blue was observed under these conditions and the calibration curve showed a good linear distribution.

Mass spectrometric determinations. A 0.5 M buffered solution containing 100 mg of NP in 10 ml was transferred to a mechanically stirred reactor (volume *ca* 24 cm^3), attached to a vacuum system. After evacuation, 30 mg of $Na_2S_2O_4$ was added from a side flask. The reactor was linked through a capillary to a SenSym SX15A pressure sensor, and to an Extrel Emba II mass spectrometer. The temperature was controlled at 25 °C. The evolution of the total pressure as a function of time was recorded during the experiment. At the end, the composition of the gaseous products was analyzed with the mass spectrometer.[22]

UV-vis spectroscopy. Samples (*ca*. 0.2 mM in the reduced species, 0.01 M in buffer and I = 0.1 M) were transferred to a cell with a 1 cm optical path, under N_2. The absorbance changes in the range 300 – 800 nm were recorded on a double beam Varian Cary 5G spectrophotometer, equipped with a temperature control set up. The results were analyzed with the SPECFIT program,[23] using a two exponential model (A → B → C) for the reaction at pH 4 – 8 and a single exponential model (A → B) at pH 9 – 10. The molar absorbances of the intermediates were estimated by calculating the initial complex concentration through the molar absorbances reported in the literature.[12] All the reactions were done at 25.5 ± 0.2 °C.

EPR spectroscopy. Samples (0.3 mM in the reduced species, 0.01 M in buffer and I = 0.1 M) were prepared as described before and kept at 25.5 °C during the experiment. From time to time aliquots were extracted and transferred under N_2 to EPR quartz tubes. Each sample was frozen immediately in liquid N_2. After collecting all the samples, they were measured in the X-band of a Bruker ESP 300E

spectrometer. The spectra were recorded at 9.44 GHz, 0.635 mW power, 100 kHz modulation frequency and 9.3434 G modulation amplitude. To study the reaction between NO and the $[Fe(CN)_4NO]^{2-}$ complex, solutions were prepared as already described and NO was bubbled through them. They were then transferred to the EPR tube and frozen. The *g* values were estimated by using the magnetic field and the microwave frequency, without performing a calibration.

IR spectroscopy. 100 mg of NP were dissolved in 10ml of a solution 0.5 M in buffer (without addition of NaCl), in H_2O or D_2O, depending on the spectral range under study. 30 mg of $Na_2S_2O_4$ were added after saturation with Ar, and then immediately transferred to the IR-liquid-cell. The rest of the solution was stored in a syringe, which was kept in a big Schlenk tube under Ar to prevent any reaction with air. From time to time, aliquots of the solution were loaded in the cell and the IR spectrum was recorded with a Thermo Nicolet Avatar 320 FT-IR spectrometer, and a Spectratech liquid-cell containing two 32 × 3 mm CaF_2 disks and a 0.1 mm spacer. The spectral ranges were 1750 – 2800 cm^{-1}, and 2150 – 1300 cm^{-1} in the H_2O- and D_2O-solutions, respectively. The reaction of NO with the $[Fe(CN)_4NO]^{2-}$ complex was studied preparing a solution as described above and bubbling NO through it.

NO detection. An amiNO electrode from Innovative Instruments, Inc. was used. The electrode was attached to a home-made potentiostat interfaced to a computer. For these measurements 10 mg of NP were dissolved in 10 ml of Ar saturated 0.1 M buffer solutions. After allowing for equilibration of the electrode output, 3 mg of $Na_2S_2O_4$ were added and the current was recorded as a function of time. To study the influence of metal ions, $FeSO_4$, $CuSO_4$, $CoSO_4$, $MnSO_4$ and $NiCl_2$, (9 – 10) mM at pH 7.0, were used. 20 mM KSCN, *o*-phenantroline or disodium ethylenediaminetetraacetate were used to study the influence of other ligands.

Stopped-Flow measurements. NO-saturated solutions were prepared as described elsewhere.[20] The ionic strength was 0.1 M (NaCl) and the buffer concentration was 0.01 M (pH 5 – 7). NP was reduced with $Na_2S_2O_4$ in the buffer solutions and the final reduced complex was 10-fold substoichiometric with respect to NO. The NO and complex solutions were mixed with a SX 18MV Applied Photophysics stopped flow instrument at 25.0 ± 0.1 °C. Kinetic traces were recorded at 620, 420 and 330 nm and fitted to a single exponential over more than 3 half-lives. The observed rate constants did not differ significantly at the different wavelengths.

DFT calculations. Geometry optimizations and frequency calculations were performed with Gaussian 98[35a] at the DFT level of theory, using the B3LYP functional.[35b] The employed basis sets were Double-Z with polarization. This combination functional and basis has already proven success in the study of iron nitrosyls.[35c]

6.3. Results and discussion

By using dithionite or tetrahydroborate as reducing agents, and working in excess of NP, the one-electron, nitrosyl-centered reduction of NP could be assured, leading to $[Fe(CN)_5NO]^{3-}$, with the exclusion of potential multi-electron reduction processes on bound NO (dithionite generates sulfite as a product, and this is inactive toward NP reduction).[13c] It was established earlier that $[Fe(CN)_5NO]^{3-}$ generates the $[Fe(CN)_4NO]^{2-}$ ion through the release of *trans*-cyanide,[12] according to eq 6.1:

$$[Fe(CN)_5NO]^{3-} \rightleftarrows [Fe(CN)_4NO]^{2-} + CN^- \qquad k_1, k_{-1} \quad (6.1)$$

Given the values of 2.7×10^2 s^{-1} and of 4×10^6 $M^{-1}s^{-1}$ at 25.0 °C for k_1 and k_{-1} in eq 6.1, respectively, and considering the protonation equilibrium of cyanide

(pK_a = 9.3 for HCN),[12] it follows that substantial amounts of $[Fe(CN)_4NO]^{2-}$ may be present when decreasing the pH, particularly around pH 7 or lower. The products formed after NP reduction on the *hours* time scale are strongly pH-dependent. It is convenient to analyze the results for defined pH-ranges.

pH´s 9-10. The $[Fe(CN)_5NO]^{3-}$ ion is the highly predominant initial species after the fast reduction of NP and the establishment of equilibrium (6.1). Slow dissociation of NO is observed, according to eq 6.2:

$$[Fe(CN)_5NO]^{3-} + H_2O \rightleftarrows [Fe(CN)_5H_2O]^{3-} + NO \qquad (6.2)$$

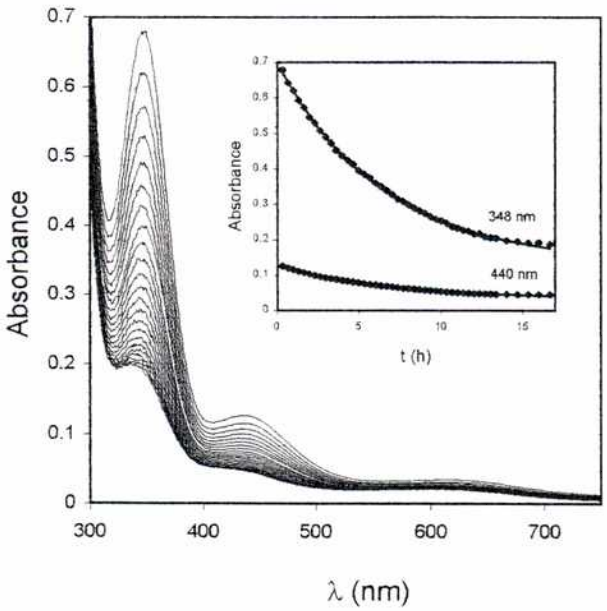

Figure 6.1. UV-vis spectral changes observed during the decomposition of a *ca.* 0.2 mM solution of nitroprusside reduced with $Na_2S_2O_4$ at pH 9.0 (I = 0.1 M, T = 25.5 °C, 0.01 M borate buffer), cycle time 2400 s. Inset: kinetic traces at 348 nm and 440 nm fitted to a single exponential by SPECFIT, $k_{obs} = 4.0 \times 10^{-5}$ s^{-1}.

Figure 6.1 shows the successive UV-vis spectra, revealing a decrease in the intensity of the absorption bands of $[Fe(CN)_5NO]^{3-}$, at 348 and 440 nm. Note that traces of $[Fe(CN)_4NO]^{2-}$ can also be observed through the weak absorption at 620 nm.[12] The single exponential decay is valid over three half-lives, affording a value of $k_2 = 4 \times 10^{-5}$ s^{-1}, at pH 9. Figure 6.2 shows the same kinetic behavior for the IR measurements, by following the intensity decrease in the stretching vibrations of the cyano- and NO-groups, at 2088 and 1650 cm^{-1}, respectively.[24] Product formation is associated with the absorption increase of a new band at 2037 cm^{-1}, typical of the $[Fe(CN)_6]^{4-}$ ion.[21,24] This ion was also determined in the solutions (ca. 20-30% with respect to initially reduced species), although a strictly quantitative evaluation is disturbed by the formation of precipitates. The formation of hexacyanoferrate(II) occurs through a rapid follow-up to reaction 6.2, namely the thermal decomposition of $[Fe(CN)_5H_2O]^{3-}$, which evolves according to the following stoichiometry, eq 6.3:

$$[Fe(CN)_5H_2O]^{3-} \rightarrow 5/6\ [Fe(CN)_6]^{4-} + 1/6\ Fe^{2+} + H_2O \qquad (6.3)$$

Reaction 6.3 has been previously analyzed mechanistically on the basis of a set of competitive-consecutive reactions. The rate-determining first order decay of $[Fe(CN)_5H_2O]^{3-}$ leads to $[Fe(CN)_4(H_2O)_2]^{2-}$, with $k = 1.25 \times 10^{-4}$ s^{-1} (25 °C, I = 1 M). The successive release of the remaining cyanides is fast, as is also the reverse coordination of CN^- to the reacting $[Fe(CN)_5H_2O]^{3-}$ ion.[25]

Minor quantities of $[Fe(CN)_4NO]^{2-}$ were also detected in the IR experiments (Fig. 6.2, bands at 2110 and 1800 cm^{-1}).[24] A weak shoulder at 1910 cm^{-1} can be assigned to the formation of $[Fe(CN)_4(OH)(NO)]^{2-}$.[12]

Remarkably, an additional important, although minor, product of the decomposition process is the NP ion. Although NP is in excess in these

experiments, Figure 6.2 allows to detect some gradual increase in the characteristic absorptions at 2142 and 1936 cm^{-1}.[24] The quantitative determination showed around a 10% yield of NP with respect to initial $[Fe(CN)_5NO]^{3-}$, at pH 10. N_2O was also observed in the IR spectra, after *ca* 10 hs of reaction, through its characteristic band at 2230 cm^{-1}.[1a] This result anticipates that a disproportionation reaction is occurring, and is discussed below along with the experimental results at lower pH´s.

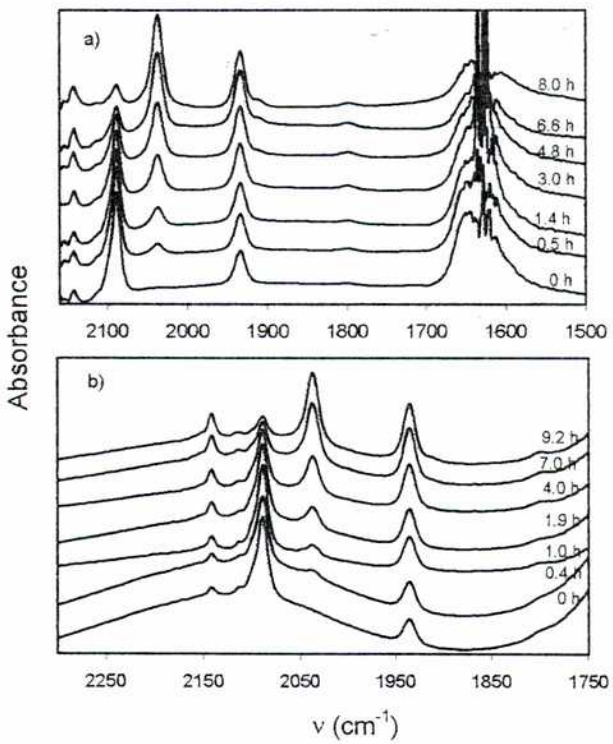

Figure 6.2. IR spectral changes recorded during the decomposition of a *ca*. 17 mM solution of nitroprusside reduced with $Na_2S_2O_4$ at pH 10 (T = 25 °C, 0.5 M borate buffer). a) D_2O k_{obs} *ca* 4×10^{-5} s^{-1}. b) H_2O, k_{obs} *ca*. 3×10^{-5} s^{-1}. A detailed description of the spectral changes is given in text.

The value of k_2 is in close agreement with the recent determination of k_{-NO}, 1.6×10^{-5} s^{-1},[11] performed under slightly different conditions of excess cyanide,

thus providing for the near exclusion of tetracyanonitrosyl species, as well as the faster scavenging of the $[Fe(CN)_5H_2O]^{3-}$ ion following reaction 6.2.

In the present work, NO was detected electrochemically during the first 15 min, and was absent after 24 hs (2-3 half-lives, cf. eq 6.2). Nitrite was also detected over the whole pH range 4-10, yield < 5%; this is presumably associated with some oxygen leakage during the very long reaction times

Table 6.1. UV-vis kinetic data obtained for the spontaneous decomposition of the mixture of $[Fe(CN)_5NO]^{3-}$ and $[Fe(CN)_4NO]^{2-}$ as a function of pH.

pH	$k_{1st} \times 10^5$ (s^{-1})	$k_{2nd} \times 10^5$ (s^{-1})
10	2.5	–
9	3.5	–
8	5.3	1.5
7	2.7	1.1
6	5.5	1.6
5	20	1.4
4	200	not measured

T = 25.5 ± 0.2 °C; 0.01 M buffer; I = 0.1M (NaCl). See text for the rate constants determination.

pH's 6-8. Both iron complexes in reaction 6.1 are present in the initial mixture immediately after reduction of NP, with significant quantities of $[Fe(CN)_4NO]^{2-}$ Figure 6.3a shows the successive UV-vis spectra. The inset includes the absorbance traces at two selected wavelengths, fitted to a two-exponential model. A monotonous decay at 615 nm along with an initial increase and subsequent decrease of an Intermediate (I_1) with maximum at 336 nm can be

observed. The output leads to values of $k = 3\text{-}6 \times 10^{-5}$ s^{-1} for the first reaction step, and of $k = 1\text{-}2 \times 10^{-5}$ s^{-1} for the second one, involving the formation and decay of the intermediate I_1, respectively. In Figure 6.3b, the three spectra correspond to a Specfit output for the reactant, the Intermediate I_1 and the product. The absorbance maxima for I_1 are at 333 ± 10; 425 ± 15; 600 ± 15 nm, with molar absorbances of ca. 600 ± 100, 200 ± 60 and 120 ± 50 M^{-1} cm^{-1}, respectively. Similar spectral and kinetic data were obtained by using either dithionite or tetrahydroborate as reducing agents. Table 6.1 shows the kinetic results as a function of pH.

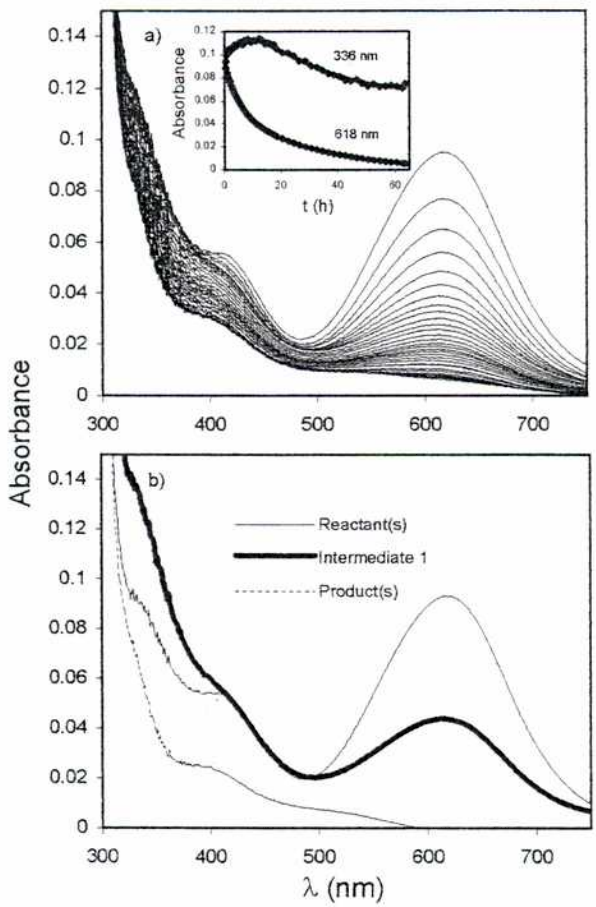

Figure 6.3. a) UV-vis spectral changes observed during the decomposition of a *ca.* 0.25 mM solution of NP, reduced with $Na_2S_2O_4$, at pH 6.0 (I = 0.1 M, T = 25.5 °C, 0.01 M Bis-Tris buffer), cycle time 7200 s. Inset: kinetic traces at 336 nm and 618

nm fitted to a double exponential model by SPECFIT, $k_{1st} = 5.37 \times 10^{-5}$ s^{-1} $k_{2nd} = 2.6 \times 10^{-5}$ s^{-1}. b) Spectra of the reactants, intermediates and products obtained from the SPECFIT analysis.

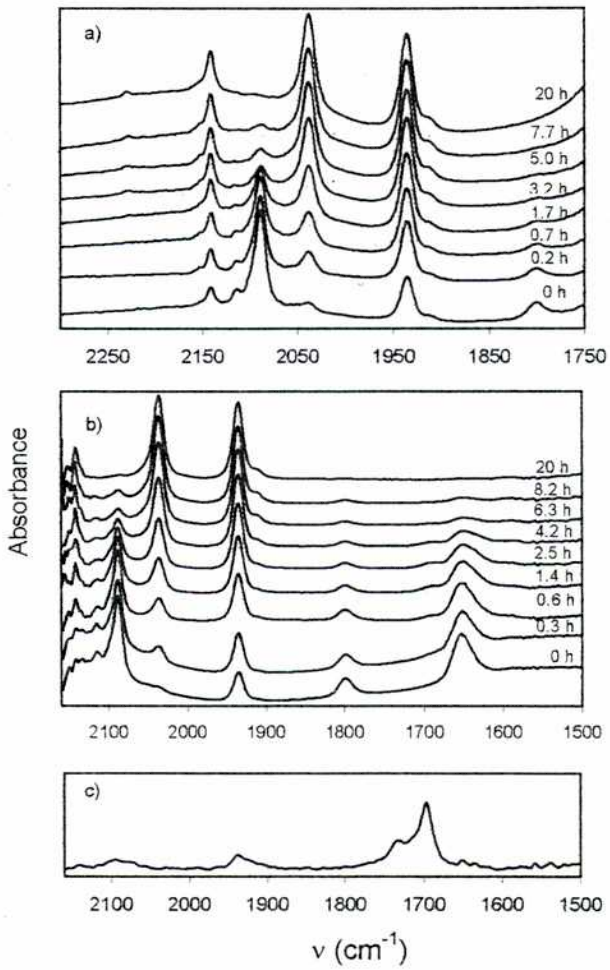

Figure 6.4. IR spectral changes observed during the decomposition of a *ca.* 17 mM solution in NP, reduced with $Na_2S_2O_4$, at pH 7 ($T = 25$ °C, 0.5 M phosphate buffer). a) H_2O, k_{obs} *ca* 8×10^{-5} s^{-1}. b) D_2O, k_{obs} *ca.* 5×10^{-5} s^{-1}. c) Spectrum obtained after bubbling NO trough a reduced nitroprusside solution, until first color change (17 mM in D_2O). A detailed description of the spectral changes is given in text.

The formation of products can still be explained by reactions 6.2-6.3 for the decay of $[Fe(CN)_5NO]^{3-}$, and a similar reaction may be proposed for the decay of $[Fe(CN)_4NO]^{2-}$, eq 6.4. At the end of the reaction, free $[Fe(CN)_6]^{4-}$ was found in low yields, in contrast with *free cyanides* (60-200% with respect to initial reduced complex), together with some ferrous and ferric ions and a white precipitate associated presumably with $[Fe(CN)_6]Fe_2$.[21]

In the EPR measurements (not shown) the intensity of the reactant's signal decreases with a rate constant of ca. 5×10^{-5} s^{-1}, affording an *EPR-silent* product. Values of the same order (k = ca. 5-8 $\times$ 10^{-5} s^{-1}) may be estimated from the IR data in Figure 6.4a-b, showing an intensity decrease in the bands for both the $[Fe(CN)_5NO]^{3-}$ and $[Fe(CN)_4NO]^{2-}$ ions, along with an absorption increase at 2037 cm^{-1} ($[Fe(CN)_6]^{4-}$ and/or other Fe-cyano-aqua-complexes). The absorption *increase* at 2141 and 1934 cm^{-1} corresponding to NP is again clearly observed, and a peak at 2230 cm^{-1} (N_2O) is already apparent at 3-6 hs after the onset of reaction 6.1. Another outstanding feature is given by the appearance of a very weak absorption at 1695 cm^{-1} (whose maximum value is also attained in 3-4 hs), which is absent at the beginning and end of the process, suggesting its intermediate character. Finally, Figure 6.4c shows a peak at 1695 cm^{-1} and a weaker absorption at ca. 1740 cm^{-1} obtained by performing a complementary experiment with $[Fe(CN)_4NO]^{2-}$ reacting with NO (see below). This peak disappears under a further excess of NO.

On the basis of the above reported evidence, we propose that the Intermediate I_1 is a *trans*-dinitrosyl species, which forms after dissociation of NO from the $[Fe(CN)_4NO]^{2-}$ ion, eq 6.4, and subsequent coordination to the same complex, eq 6.5:

$$[Fe(CN)_4NO]^{2-} + 2H_2O \rightleftarrows [Fe(CN)_4(H_2O)_2]^{2-} + NO \qquad (6.4)$$

$$[Fe(CN)_4NO]^{2-} + NO \rightleftarrows \textit{trans}\text{-}[Fe(CN)_4(NO)_2]^{2-} \qquad (6.5)$$

The EPR-silent properties of I_1 can be ascribed to a low-spin Fe(II) centre containing two antiferromagnetically coupled NO ligands, and will be discussed later in the context of some DFT calculations. Support for the intermediate identification is provided by recent reports on the coordination of NO to ferrous nitrosyl porphyrins (P), giving *trans*-Fe(P)$(NO)_2$ in low-temperature solutions (P = TPP, *meso*-tetraphenylporphinato and TmTP, *meso*-tetra-*m*-tolyl-porphinato).[26] These are also EPR-silent complexes, and have been characterized by UV-vis, NMR and IR spectroscopies, showing in the latter case an intense band at 1695 cm^{-1}, together with a much weaker one at 1777 cm^{-1}. As a result of theoretical calculations, a *trans-syn* (C_{2v}) conformation has been proposed for Fe(TPP)$(NO)_2$.[27]

In the present work, we propose that I_1 decomposes through a disproportionation process, as described by eq 6.6. The ability to detect I_1 is consistent with the values of k shown in Table 6.1, and also agrees with the UV-vis and IR evidences on the time scale of intermediate detection. In agreement with the trends in the IR spectra, the increase in the concentration of NP has been verified quantitatively. Around 40 % of the initially reduced complex is oxidized again in these experiments. Besides, N_2O was observed at pH 7 through mass-spectrometry, with a 20 % yield and an exponential formation rate leading to $k = 1.4 \times 10^{-5}$ s^{-1}. The systematic appearance of rate-constant values around 10^{-5} s^{-1}, obtained through different type of measurements, either with the reactants decay or with the products development, strongly suggest that the time scales for NO dissociations, either from $[Fe(CN)_5NO]^{3-}$ or from $[Fe(CN)_4NO]^{2-}$ (eqs 6.2, 6.4), are of the same order as for the formation and decay of I_1, eqs 6.5, 6.6. In fact, considering the concentration of NO under steady-state conditions for reactions 6.4 – 6.6, the observed rate constant for the first reaction step is two times k_4. The mechanistic picture is consistent with rate-limiting NO dissociations that control the nitrosyl transfer to other acceptors, as previously observed with intermolecular NO transfer

from Mn- to Fe-tropocoronand complexes.[28] The distribution of products (a 2:1 molar ratio for NP:N_2O) provides evidence on the stoichiometry described by eqs 6.6, 6.7:

$$\textit{trans}\text{-}[Fe(CN)_4(NO)_2]^{2-} + CN^- + H^+ \rightleftarrows [Fe(CN)_5NO]^{2-} + HNO \qquad (6.6)$$

$$2\ HNO \rightarrow N_2O + H_2O \qquad (6.7)$$

However, we are not able to provide a detailed analysis of the elementary steps involved in eq 6.6. We may reasonably propose an intramolecular electron-transfer in I_1, leading to bound NO^+ and NO^-(HNO), followed by the release of the latter species and fast coupling to give N_2O, eq 6.7.[29]

Disproportionation processes have been observed following coordination of NO to several metal centres (Mn, Re, Fe, Ru, Os, Ni, Cu), forming initially mononitrosyl complexes with the subsequent, proposed intermediacy of different types of dinitrosyl species. Further attack by more NO to give N_2O and nitrite (O- or N-bound) shows a different picture for each of the considered metals, with some ambiguity remaining on the detailed mechanistic issues.[16] We also verified that I_1 can further react with excess NO. Nevertheless, under our experimental conditions, the quotient $[NO]/[Fe(CN)_4NO^{2-}]$ is always << 1, supporting the proposed reactions 6.4 – 6.7. A related dinitrosyl complex (proposed as a *cis*-dinitrosyl octahedral ion) has been detected chemically in the reaction of $[Fe(H_2O)_5NO]^{2+}$ with NO. It is an apparent intermediate in the reduction of NO by aqueous Fe(II), forming N_2O and aqueous Fe(III). In contrast to I_1, however, this *cis*-dinitrosyl complex appears as an ill-defined paramagnetic species.[30]

An interesting situation recently occurred with the above-mentioned $Fe(P)(NO)_2$ complexes. In controversy with previous studies regarding disproportionation,[31] it remains stable for hours even at ambient temperature, in contrast with the Ru-analogue, which readily leads to bound nitrite and N_2O.[32]

Remarkably, the disproportionation process is readily observed with Fe(TPP)(NO) only if trace amounts of NO_2 are present.[33]

As detailed above, I_1 presents a close structural analogy with the $Fe(P)(NO)_2$ complex, supported by the EPR-silent properties and IR features. As to the reactivity differences, the onset of an intramolecular redox process in reaction 6.6 seems consistent with the low value for the $Fe(NO^-)/Fe(NO)$ redox couple (-0.37 V *vs* SCE)[8] which makes NP a very stable product when one of the NO-ligands in I_1 induces an electron transfer to the opposite NO. On the other hand, a potential of 0.74 V has been reported for the formal Fe(III)/Fe(II) couple in Fe(TPP)NO,[34] suggesting a high comparative stability of the Fe(II)NO fragment in the dinitrosyl species.

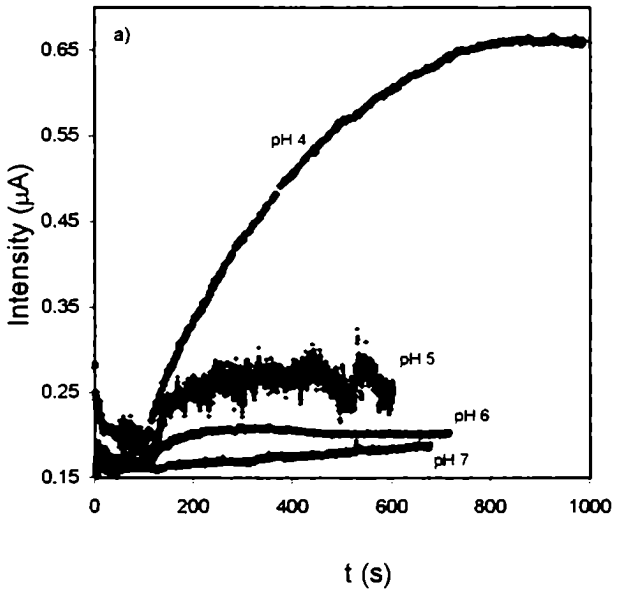

Figure 6.5. Chronoamperograms for the release of NO after addition of 3 mg of $Na_2S_2O_4$ to 10 ml of 3.4 mM nitroprusside solution as a function of pH.

The chronoamperograms in Figure 6.5 show that NO is generated rapidly during the first minutes, with the rates increasing with decreasing pHs. The

concentration of NO remains constant or decreases with time, supporting the onset of reaction 6.5.

pH's 4-5. A significant increase in the decomposition rate for the $[Fe(CN)_4NO]^{2-}$ ion is observed (Table 6.1). NP is also formed in 50 % yield, along with high yields of cyanide (300%), aqueous Fe(III) and Prussian-Blue precipitates. N_2O was also observed in the IR spectra.

Figure 6.6a shows the successive EPR spectra obtained at pH 5 upon reduction with tetrahydroborate. It can be seen that the initial spectrum of the reactant* evolves through an apparently silent intermediate (second spectrum from bottom) to reach a final different spectrum similar to those reported in the literature for the four-coordinate $\{Fe(L)_2(NO)_2\}$ compounds (S = ½, L = thiolates, imidazole, CO, etc.), referred to as "g = 2.03" DNIC complexes.[3a,15] The final spectrum is similar as the one obtained after bubbling NO to the reduced NP solution (Figure 6.6b). We propose that the EPR silent intermediate in Figure 6.6 is the previously described I_1. The latter may evolve through disproportionation, as detailed above, but can also react competitively as a precursor of the new four-coordinate dinitrosyl species described above, I_2, eq 6.8:

$$\textit{trans}\text{-}[Fe(CN)_4(NO)_2]^{2-} + e^- \longrightarrow [Fe(CN)_2(NO)_2]^- + 2\ CN^- \qquad (6.8)$$

---

* The initial EPR spectrum in Figure 6a shows the presence of both the tetracyano- and the pentacyano-nitrosyl species. The percentage of each species is strongly affected by temperature. Only the tetracyanonitrosyl ion gives an EPR signal at 22 °C.[13d] The final spectrum in Figure 6a and the one in Figure 6b agree with those reported for the four-coordinated dinitrosyls.[15]

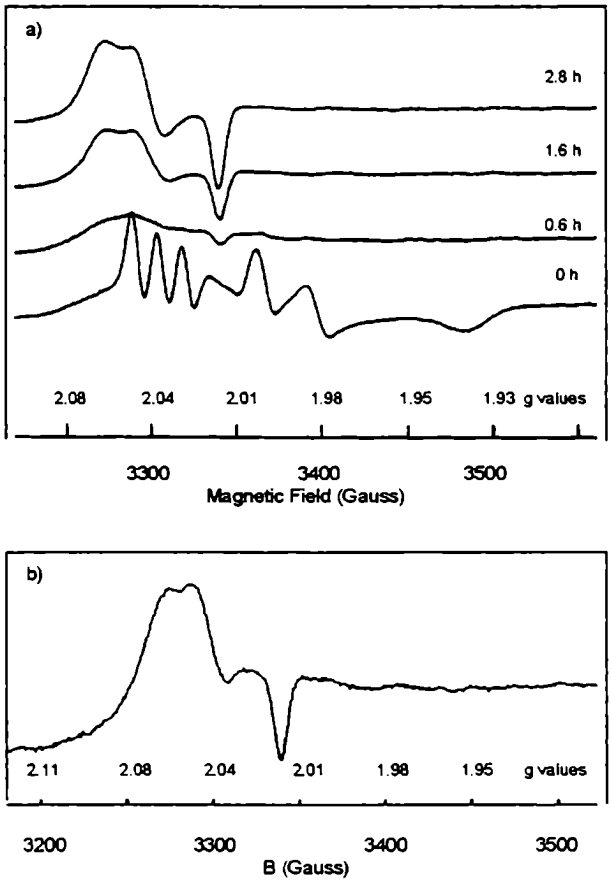

Figure 6.6. (a) EPR spectral changes recorded during the decomposition of a *ca.* 0.26 mM solution of nitroprusside reduced with $NaBH_4$ at pH 5.0 (I = 0.1 M, T = 25 °C, 0.01 M Acetate buffer). b) Spectrum obtained after bubbling NO through a reduced nitroprusside solution (0.26 mM, I = 0.1 M, 0.01 M acetate buffer).

It must be stressed however that when using dithionite as a reductant, only the initial and final EPR spectra were coincident, as the silent intermediate I_1 can not be clearly observed (Figure 6.7).

The initial reactant, $[Fe(CN)_4NO]^{2-}$, is an $\{FeNO\}^7$ species, and its configuration has been described as a d^7 Fe(+I), with a NO^+ ligand.[36] Addition of NO to form intermediate I_1 leads to a six-coordinate $\{Fe(NO)_2\}^8$ species (eq 6.5), for which a distribution of d^6 Fe(II), with two NO radicals as ligands may be

envisioned. The conversion of I_1 to I_2 involves the release of two cyanides and formation of a four-coordinate species, $\{Fe(NO)_2\}^9$, (S = ½). The description of the electronic structure is still a matter of discussion, either d^7 Fe(+I) with two NO ligands, [15f] or d^9 Fe(–I) with two NO^+ ligands.[15j] The proposal requires an one-electron reduction (eq 6.8), which could be accomplished by free NO or by aqueous ferrous ions.

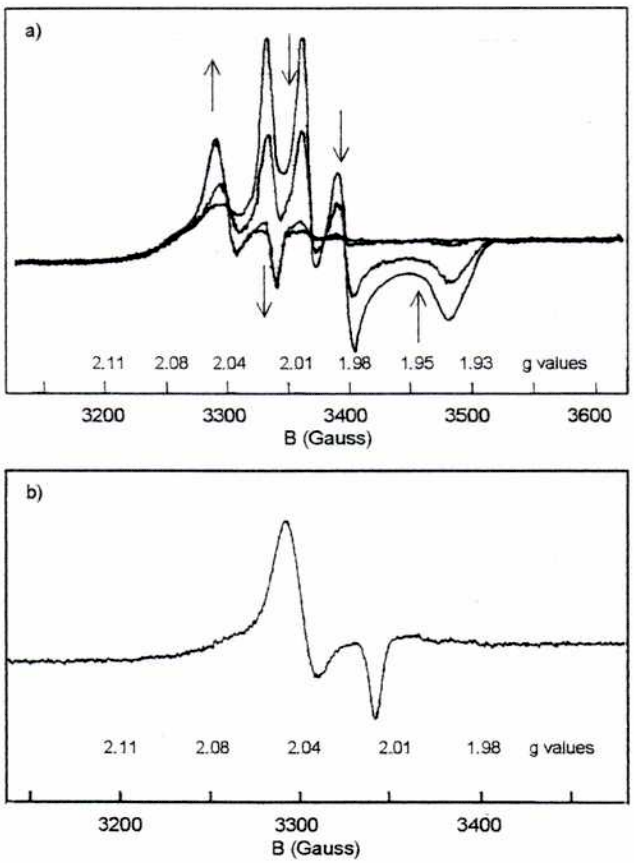

Figure 6.7. (a) EPR spectral changes during the decomposition of a *ca.* 0.26 mM solution in reduced nitroprusside with $Na_2S_2O_4$ at pH 5.0 (I = 0.1 M, T = 25 °C, 0.01 M Acetate buffer). Spectra recorded at 0, 0.3, 0.7 and 1.0 hours respectively. The arrows indicate the evolution of the intensities. (b) Spectrum obtained after bubbling NO trough a reduced nitroprusside solution (0.26 mM, I = 0.1 M, 0.01 M acetate buffer)

In Figure 6.8, both dinitrosyl intermediates can be detected in the UV-vis spectra when tetrahydroborate is used, following a Specfit analysis with a three exponential model. Only I_2 is observed when dithionite is used. I_2 presents absorption features at 330, 400 and 500 nm, with estimated molar extinction coefficients of ca. 650, 300 and 150 M^{-1} cm^{-1}, respectively.

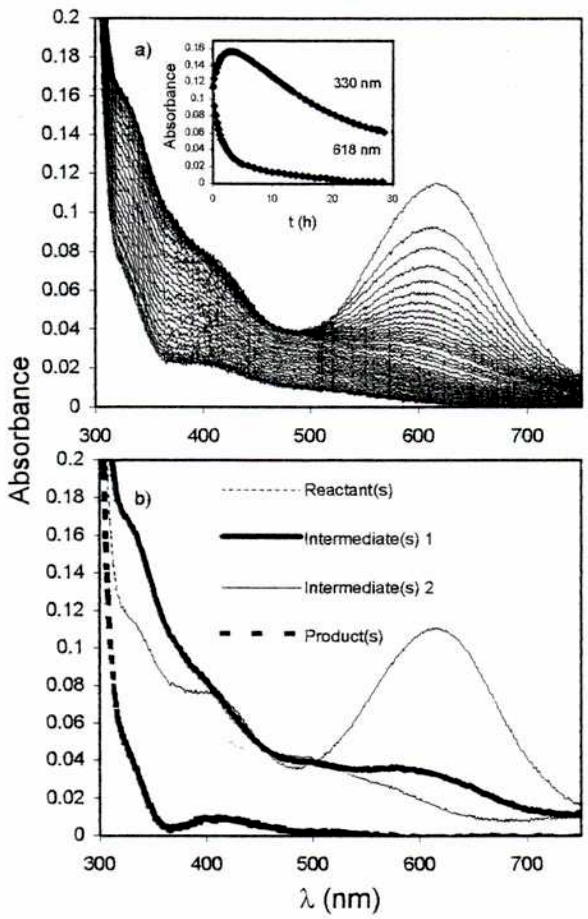

Figure 6.8. (a) UV-vis spectral changes recorded during the decomposition of a *ca.* 0.32 mM solution of nitroprusside reduced with $NaBH_4$ at pH 5.0 (I = 0.1 M, T = 25.5 °C, 0.01 M Acetate buffer), cycle time 900 s and 3600 s after 18000 s. Inset: Kinetic traces at 330 nm and 618 nm fitted to a three exponential model by SPECFIT, $k_{1st} = 2.4 \times 10^{-4}$ s^{-1} $k_{2nd} = 5.1 \times 10^{-5}$ s^{-1} and $k_{3rd} = 2.4 \times 10^{-5}$ s^{-1}. b) Spectra of the reactants, intermediates and products obtained from the SPECFIT analysis.

Figure 6.9 shows the IR spectra obtained in H_2O- and D_2O-solutions at pH 4. The absorptions found for I_2 (1810, 1737 cm^{-1}) can be observed in the spontaneous decomposition process (a-b), as well as in the products formed after bubbling NO (c).

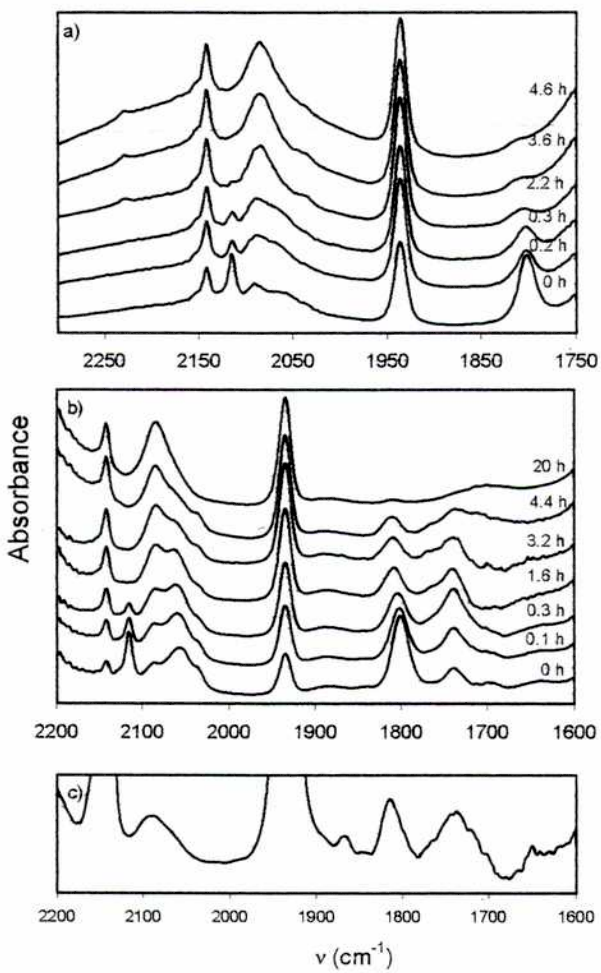

Figure 6.9. IR spectral changes observed during the decomposition of a *ca.* 17 mM solution of nitroprusside reduced with $Na_2S_2O_4$ at pH 4 (T = 25 °C, 0.5 M acetate buffer). a) H_2O k_{obs} *ca* 1×10^{-3} s^{-1}. b) D_2O, k_{obs} *ca.* 1×10^{-3} s^{-1}. c) Spectrum obtained after bubbling NO through a reduced nitroprusside solution (17 mM, 0.5 M acetate buffer) in D_2O. A detailed description of the spectral changes is given in text. .

The frequencies are remarkably close to those reported for $[Fe(CO)_2(NO)_2]^+$, [15c] 1810, 1767 cm^{-1}, and this is valuable evidence for proposing the *new* dinitrosyl complex, $[Fe(CN)_2(NO)_2]^-$, as the relevant intermediate, I_2, under our reaction conditions. The IR absorptions in DNICs have been shown to be significantly influenced by the binding properties of the coligands L.[15]

An interesting feature in the experiments at pH's 4,5 was that the addition of cyanide led to a behavior similar to the above reported one for higher pH's. Thus, the decomposition rate decreased, and the I_1 intermediate was observed again. Then, equilibrium reaction 6.9 can be proposed as a first step in the pH-dependent decomposition of $[Fe(CN)_4NO]^{2-}$:

$$[Fe(CN)_4NO]^{2-} + H^- \rightleftarrows [Fe(CN)_3NO]^- + HCN \qquad (6.9)$$

Some evidence on the existence of $[Fe(CN)_3(NO)]^-$ has been advanced.[8] We expect this species to decompose according to eq 6.10, releasing cyanide and NO to the medium, under pH conditions where HCN is stabilized.

$$[Fe(CN)_3NO]^- + 3\ H^- \rightarrow Fe^{2-} + 3\ HCN + NO \qquad (6.10)$$

A consistent increase in the rate and amount of NO production was observed at pH 4 within the first minutes. From the exponential display in Figure 6.5, we estimate a value for k of ca. $2 \times 10^{-3}\ s^{-1}$, in close agreement with the kinetic data in Table 6.1. It is predictable that at these low pH's, cyanide release will determine a conversion from low-spin to high-spin for Fe(II) complexes at a given stage of the decomposition process, thus favoring the fast release of cyanides and NO in the final stages of reaction 6.10. In this context, some formation of the labile species $[Fe(H_2O)_5NO]^{2+}$ could be predicted.[37] However, no EPR signal is detectable under our conditions. An IR-absorption at 1810 cm^{-1} suggests that it

could be present, but this band has been alternatively assigned above to I_2. The $[Fe(H_2O)_5NO]^{2+}$ ion decomposes yielding N_2O and Fe(III) over a long time scale.[38]

Complementary experiments with excess NO. The product obtained after the reaction of $[Fe(CN)_4NO]^{2-}$ with external NO at pH 7 was EPR-silent, showing only very weak signals of the starting complex. It was also characterized by IR measurements (Figure 6.4), confirming that I_1 is present. On the other hand, the experiments at pH's 5 and 4 (EPR and IR, respectively, cf. Figures 6.8, 6.9) showed the appearance of the $[Fe(CN)_2(NO)_2]^-$ intermediate, I_2.

On the above ground, definite evidence for the occurrence of eq 6.5 has been provided. A second-order rate law was found in an independent experiment for reaction 6.5, with $k_5 = 4.3 \times 10^4\ M^{-1}\ s^{-1}$. This value shows that NO may compete with cyanide for the vacant site in $[Fe(CN)_4NO]^{2-}$ (cf. k_5 with k_{-1}). Thus, even under the conditions of slow release of NO in eq 6.4 (rate-controlling step), reaction 6.5 becomes sufficiently fast in the absence of external NO, opening the route to disproportionation (eq 6.6).

Influence of added metal ions. Figure 6.10 shows the influence of different metal ions on the rate for release of NO. A rapid increase (Cu > Co > Fe) is observed for the short times after addition, followed by a slower increase for the last two ions and a distinctive decrease for copper. The influence of metal ions probably occurs because of association effects on bound cyanides, promoting the decomposition of $[Fe(CN)_4NO]^{2-}$, also related to the ability to form stable complexes with cyanide. This is equivalent to the pH-effect commented above. The presence of metal ions is highly feasible in biological media, thus allowing for a fast decomposition process even at pH conditions around 7, which are insufficiently low for promoting full cyanide-release. We also checked the influence of added ligands on the release of NO. We found that thiocyanate, *o*-

phenantroline and edta enhanced the decomposition rate of the complex (viz., cyanide release), but, surprisingly, no effect is observed on the release of NO.

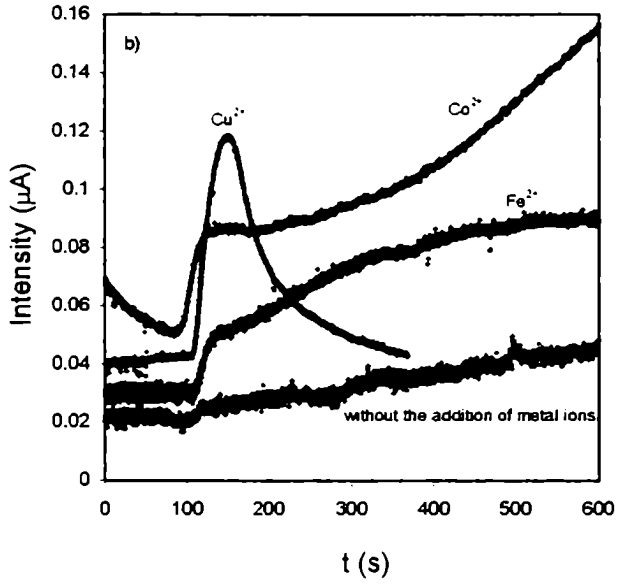

Figure 6.10. Chronoamperogram of the NO release after addition of 3 mg of $Na_2S_2O_4$ to 10 ml of 3.3 mM nitroprusside solution at pH 7 in the presence of 9 – 10mM of different metal ions.

DFT calculations for the *trans*-$[Fe(CN)_4(NO)_2]^{2-}$ ion. We performed calculations for the *trans*-$[Fe(CN)_4(NO)_2]^{2-}$ complex in the singlet and triplet spin states. The results for the corresponding complexes are shown in Table 6.2. Optimized structures are shown in Figures 6.11a and 6.11c respectively.

The singlet state shows a *syn* geometry with two asymmetric bent nitrosyls. In contrast, the triplet state, which has lower energy, has an *anty* geometry, and both nitrosyls are equivalent.

These two structures were obtained starting the calculations from both *anti* and *syn* geometries for the two states. For the singlet state, restricted and unrestricted calculations gave the same result.

Previous reports on dinitrosyl iron complexes show that although both nitrosyls are in a *trans-syn* geometry, they are, however, equivalent.[27] From the small energy difference of the two optimized geometries we cannot easily conclude which of the two states is the real ground state in vacuum. In fact this energy difference can be overcame by solvent effects.

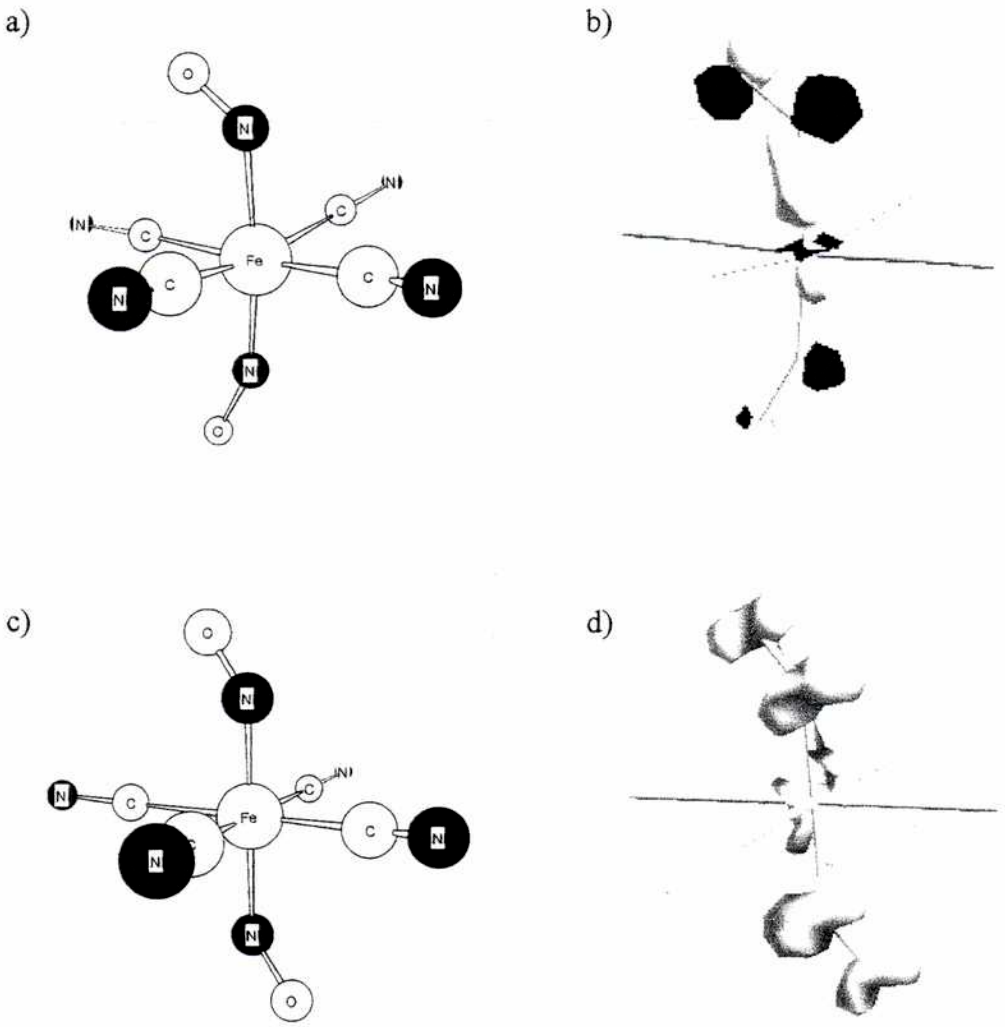

Figure 6.11. Computed structures for *trans*-$[Fe(CN)_4(NO)_2]^{2-}$ optimized using DFT and B3LYP functionals. a) Singlet state. c) Triplet state. b) Computed HOMO for the Singlet state. d) Spin density surface for the Triplet state.

Figure 6.11b shows the computed HOMO for the singlet state, which is mainly localized on the two nitrosyls. One of the nitrosyls contributes more to the HOMO, this is in agreement with its smaller angle Fe-N-O. It seems that the two electrons for the nitrosyls tend to be paired in an orbital mainly localized on one of the two nitrosyl, which takes more NO^- character and has therefore a smaller angle.

Table 6.2. Selected parameters calculated by DFT optimization for the *trans*-$[Fe(CN)_4(NO)_2]^{2-}$ complex.

	Singlet state	Triplet state.
d(Fe-N)[a] (Å)	1.958	1.849
	1.683	1.849
d(N-O)[a] (Å)	1.185	1.179
	1.177	1.179
< (Fe-N-O)[a] (deg)	126.8	143.6
	153.2	143.6
d(Fe-C)[b] (Å)	1.98	1.999
d(C-N)[b] (Å)	1.175	1.175
< (C-Fe-C) (deg)	176.0	180.0
	168.5	180.0
< (N-Fe-N) (deg)	172.9	180.0
Frecuencies[c] (cm^{-1})	1725 (1.00)	1782 (1.00)
	1826 (0.36)	2196 (0.10)
	2200 (0.11)	
Energy (kcal/mol)	3.8	0

[a] The first value corresponds to one nitrosyl, the second to the other. [b] Averaged values. [c] Relative intensities are between parentheses.

Figure 6.11d shows a total spin density surface for the triplet configuration. It can be observed that the spin density is localized on both nitrosyl in equal proportions, what accounts for its symmetry.

According to our experimental data we proposed a structure of *trans*-$[Fe(CN)_4(NO)_2]^{2-}$ for an EPR silent compound with a ν_{NO} at 1695 cm^{-1} and ν_{CN} *ca.* 2100 cm^{-1}. The computed IR frequencies show for the singlet three bands, an intense one at 1725 cm^{-1} and two less intense ones at 1826 and 2200 cm^{-1}. For the triplet configuration only two bands were observed: 1782 and 2196 cm^{-1}. We

consider that the *ca* 100 cm^{-1}-shift for all the computed frequencies could be traced to solvent effects.

The shoulder experimentally observed at 1740 cm^{-1} in the IR spectrum (Figure 6.9c) could give some justification for the less intense band at 1826 cm^{-1} of the singlet state.

In summary, the DFT calculations give evidence for the existence of the *trans*-$[Fe(CN)_4(NO)_2]^{2-}$ complex. The computed frequencies are in agreement with the experimental results. The EPR data together with the computed energies are evidence that the singlet state is a better description of the compound.

6.4. Conclusions

We present a description of the overall decomposition process in Scheme 6.1. The kinetic results show that the dissociation rates of NO from the penta- or tetracyanonitrosyl ions are too slow under physiological pH-conditions (k = ca. 10^{-5} s^{-1}, 25 °C) to account for the rapid vasodilatory action displayed by NP upon injection in the biological fluids.[3] Thus, even the well established fast release of the *trans*-cyano ligand from $[Fe(CN)_5NO]^{3-}$ is not enough to significantly labilize NO from the metal, as previously suggested.[13]

A substantial decrease in pH down to at least 4, or any other factor favoring the release of *all* of the cyanides from $[Fe(CN)_4NO]^{2-}$ and the consequent liberation of NO to the medium is needed. Bound cyanides are strong electron-donors by way of their free lone-pairs on nitrogen.[41] Thus, even in the absence of a decrease in pH, local situations may provide for protein attachment to cyanides,[3a,42] favoring a complete decomposition of the complex. This could also be aided by a ubiquitous presence of appropriate metal ions such as copper, as demonstrated in this work.

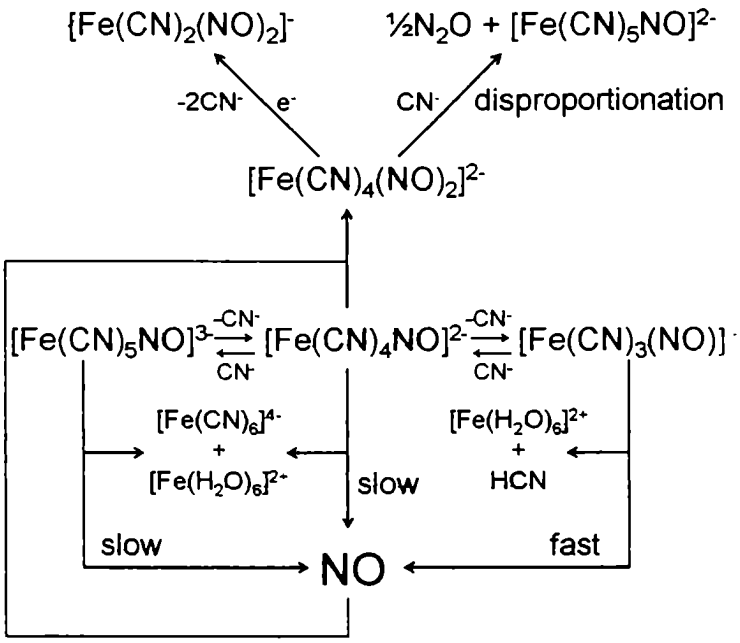

Scheme 6.1. Proposed overall mechanism for the decomposition of reduced nitroprusside.

Two types of dinitrosyl intermediates have been found and characterized under different conditions, at consecutive stages of the decomposition process. The EPR-silent *trans*-dinitrosyl complex $[Fe(CN)_4(NO)_2]^{2-}$, described as $\{Fe(NO)_2\}^8$, is formed through addition of NO to $[Fe(CN)_4NO]^{2-}$, and shows remarkable similarities with a recently described $Fe(TPP)(NO)_2$ complex, also formed by coordination of NO to Fe(TPP)NO.[26] Although the latter complex is stable, the *trans*-$[Fe(CN)_4(NO)_2]^{2-}$ complex appears as the precursor of disproportionation, regenerating NP and evolving N_2O. This reaction is probably not significant in biological media, because NO is in fact released rapidly, affording a very fast coordination to sGC ($k > 10^8$ M^{-1} s^{-1}).[39] DFT calculations give additional evidence for the intermediancy of the $[Fe(CN)_4(NO)_2]^{2-}$. In fact the computed IR frequencies are in agreement with the experimental data and the optimized geometries have similarities with computed structures for related compounds.[27] The EPR-silent $[Fe(CN)_4(NO)_2]^{2-}$ intermediate also appears as the precursor of $[Fe(CN)_2(NO)_2]^-$, a

proposed new member of a well characterized series of paramagnetic, distorted tetrahedral complexes, $\{Fe(L)_2(NO)_2\}$, with different L ligands, described as $\{Fe(NO)_2\}^9$.[3a] These DNICs are known to be reversible, labile NO-carriers, effecting transnitrosylation processes.[17] Some of them, *viz*, L = thiolates and imidazole, activate sGC promoting vasodilation.[15h,40] The new cyano-derivative could be formed under biologically relevant conditions upon injection of NP, *even in the absence of thiolates*, although a fast interchange between cyanides and thiolates should be expected due to the labile character of DNICs.

The detection of dinitrosyl compounds as precursors of disproportionation is of fundamental concern in metal-NO coordination chemistry, most relevant to the enzymatic behavior of NO- and N_2O-reductases.[16,43] A very recent report on the NO inhibition of FUR (a non-heme ferric uptake regulator protein) describes the characterization of two dinitrosyl species with proposed $\{Fe(NO)_2\}^8$ and $\{Fe(NO)_2\}^9$ structures, affording surprisingly similar spectroscopic properties as reported here for intermediates I_1 and I_2, respectively.[44] Dinitrosyl formation, beyond the mononitrosyl coordination stage, has been ascribed as responsible of the conformational changes associated with NO inhibition of FUR. Some controversy still exists on related processes that seem to be present during the activation of sGC leading to smooth muscle relaxation.[39]

Acknowledgment. I gratefully acknowledge Prof Dr. Rudi van Eldik for providing access to his laboratory equipment and Prof. Dr. Valentín T. Amorebieta for the mass spectrometric experiments.

6.5. References

1. *Methods in Nitric Oxide Research*; Feelisch, M.; Stamler, J. S., Eds.; Wiley, Chichester: UK, 1996. (b) Wang, P. G.; Xian, M., Tang X.; Wu,

X.; Wen, Z.; Cai, T.; Janczuk, A. J. *Chem. Rev.* **2002**, *102*, 1091-1134. (c) *Nitric Oxide: Biology and Pathobiology*; Ignarro, L. J., Ed.; Academic Press: San Diego, 2000. (d) Butler, A. R.; Williams, D. L. H. *Chem. Soc. Rev.* **1993**, *22*, 233-241.

2. Moncada S.; Palmer, R. M. J.; Higgs, E. A. *Pharmacological Reviews*, **1991**, *43*, 109-142.

3. (a) Butler, A. R.; Megson, I. L. *Chem. Rev.* **2002**, *102*, 1155-1165. (b) Clarke, M. J.; Gaul, J. B. *Struct. Bonding (Berlin)*, **1993**, *81*, 147-181. (c) Butler, A. R.; Glidewell, C. *Chem. Soc. Rev.* **1987**, *16*, 361-380.

4. Enemark, J. H.; Feltham, R. D. *Coord. Chem. Rev.* **1974**, *13*, 339-406.

5. (a) Swinehart, J. H. *Coord. Chem. Rev.* **1967**, *2*, 385-402. (b) Westcott, B. L.; Enemark, J. H. In *Inorganic Electronic Structure and Spectroscopy*; Solomon, E. I., Lever, A. B. P., Eds.; Wiley-Interscience: New York, 1999; Vol. 2. Chapter 7, pp. 403-450.

6. Wolfe S. K.; Swinehart, J. H. *Inorg. Chem.* **1975**, *14*, 1049-1053.

7. Bottomley, F. In *Reactions of Coordinated Ligands*; Braterman, P. S., Ed.; Plenum Press: New York, 1989; Vol. 2, pp 115-222.

8. Masek, J.; Maslova, E. *Coll. Czech. Chem. Comm.* **1974**, *39*, 2141-2160.

9. (a) Szacilowski, K.; Wanat, A.; Barbieri, A.; Wasielewska, E.; Witko, M.; Stochel, G.; Stasicka, Z. *New J. Chem.* **2002**, *26*, 1495-1502. (b) Johnson, M.; Wilkins, R. G. *Inorg. Chem.* **1984**, *23*, 231-235.

10. Morando, P. J.; Borghi, E. B.; Schteingart, L. M.; Blesa, M. A. *J. C. S. Dalton Trans.* **1981**, 435-440.

11. Roncaroli, F.; Olabe, J. A.; van Eldik, R. *Inorg. Chem.* **2003**, *42*, 4179-4189.

12. Cheney, R. P.; Simic, M. G.; Hoffman, M. Z.; Taub, I. A.; Asmus, K. D. *Inorg. Chem.* **1977**, *16*, 2187-2192.

13. (a) Glidewell, C.; Johnson, I. L. *Inorg. Chim. Acta* **1987**, *132*, 145-147. (b) Shafer, P. R.; Wilcox, D. E.; Kruszyna, H.; Kruszyna, R.; Smith, R. P. *Toxicol. Appl. Pharmacol.* **1989**, *99*, 1-10. (c) Wilcox, D. E.; Kruszyna, H.; Kruszyna, R.; Smith, R. P. *Chem. Res. Toxicol.* **1990**, *3*, 71-76. (c) Bates, J. N.; Baker, M. T.; Guerra, R. Jr.; Harrison, D. G. *Biochem. Pharmacol.* **1991**, *42*, S157-S165. (d) Kruszyna, H.; Kruszyna, R.; Rochelle, L. G.; Smith, R. P.; Wilcox, D. E. *Biochem. Pharmacol.* **1993**, *46*, 95-102. (e) Rochelle, L. G.; Kruszyna, H.; Kruszyna, R.; Barchowsky, A.; Wilcox, D. E.; Smith, R. P. *Toxicol. Appl. Pharmacol.* **1994**, *128*, 123-128. (f) Kleschyov, A. L.; Sedov, K. R.; Mordvintcev, P. I.; Vanin, A. F. *Biochem. Biophys. Res. Commun.* **1994**, *202*, 168-173.

14. Butler, A. R.; Calsy-Harrison, A. M.; Glidewell, C.; Sorensen, P. E. *Polyhedron*, **1988**, *7*, 1197-1202.

15. (a) Lee, M.; Arosio, P.; Cozzi, A.; Chasteen, N. D. *Biochemistry*, **1994**, *33*, 3679-3687. (b) Vanin, A. F.; Serezhenkov, V. A.; Mikoyan, V. D.; Genkin, M. V. *Nitric Oxide: Biology and Chemistry*, **1998**, *2*, 224-234. (c) Reginato, N.; McCrory, C. T. C.; Pervitsky, D.; Li, L. *J. Am. Chem. Soc.* **1999**, *121*, 10217-10218. (d) Butler, A. R.; Glidewell, C.; Hyde, A. R.; Walton, J. C. *Polyhedron*, **1985**, *4*, 797-809. (e) Costanzo, S.; Menage, S.; Purrello, R.; Bonomo, R.; Fontecave, M. *Inorg. Chim. Acta* **2001**, *318*, 1-7. (f) Burlamaschi, L.; Martín, G.; Tiezzi, E. *Inorg. Chem.* **1969**, *8*, 2021-2025. (g) McDonald, C. C.; Phillips, W. D.; Mower, H. F. *J. Am. Chem. Soc.* **1965**, *87*, 3319-3326. (h) Ueno, T.; Yoshimura, T.

Jpn. J. Pharmacol. **2000**, *82*, 95-101. (i) Foster, M. W.; Cowan, J. A. *J. Am. Chem. Soc.* **1999**, *121*, 4093-4100. (j) Bryar, T. R.; Eaton, D. R. *Can. J. Chem.* **1992**, *70*, 1917-1926.

16. (a) Ford, P. C.; Lorkovic, I. M. *Chem. Rev.* **2002**, *102*, 993-1018. (b) Ford, P. C.; Laverman, L. E.; Lorkovic, I. M. *Adv. Inorg. Chem.* **2003**, *54*, 203-257.

17. Ueno, T.; Suzuki, Y.; Fujii, S.; Vanin, A. F.; Yoshimura, T. *Biochem. Pharmacol.* **2002**, *63*, 485-493.

18. *A Textbook of Quantitative Inorganic Analysis Including Elementary Instrumental Analysis*; Vogel, A.; 4th Edition, Longman Inc.; New York, 1978.

19. Szacilowski, K.; Stochel, G.; Stasicka, Z.; Kisch, H. *New J. Chem.* 1997, *21*, 893-902.

20. Roncaroli, F.; Olabe, J. A.; van Eldik, R. *Inorg. Chem.* **2002**, *41*, 5417-5425.

21. Sharpe, A. G. *The Chemistry of Cyano Complexes of the Transition Metals*; Academic Press: London, 1976.

22. Gutiérrez, M. M.; Amorebieta, V. T.; Estiú, G. L.; Olabe, J. A. *J. Am. Chem. Soc.* **2002**, *124*, 10307-10319.

23. Binstead, R. A.; Zuberbulher, A. D. Spectrum Software Associates: Chapel Hill, N. C., 1993-1999.

24. Schwane, J. D.; Ashby, M. T. *J. Am. Chem. Soc.* **2002**, *124*, 6822-6823.

25. Olabe, J. A.; Zerga, H. O. *Inorg. Chem.* **1983**, *22*, 4156-4158.

26. Lorkovic, I.; Ford, P. C. *J. Am. Chem. Soc.* **2000**, *122*, 6516-6517.

27. (a) Conradie, J.; Wondimagegn, T.; Ghosh, A. *J. Am. Chem. Soc.* **2003**, *125*, 4968-4969. (b) Patterson, J. C.; Lorkovic, I. M.; Ford, P. C. *Inorg. Chem.* **2003**, *42*, 4902-4908.

28. Franz, K. J.; Lippard, S. J. *Inorg. Chem.* **2000**, *39*, 3722-3723.

29. Shafirovich, V.; Lymar, S. V. *Proc. Natl. Acad. Sci.*, **2002**, *99*, 7340-7345.

30. Pearsall, K. A.; Bonner, F. T. *Inorg. Chem.* **1982**, *21*, 1978-1985.

31. (a) Lin, R.; Farmer, P. J. *J. Am. Chem. Soc.* **2001**, *123*, 1143-1150. (b) Yoshimura, T. *Inorg. Chim. Acta* **1984**, *83*, 17-21. (c) Settin, M. F.; Fanning, J. C. *Inorg. Chem.* **1988**, *27*, 1431-1435. (d) Ellison, M. K.; Schulz, C. E.; Scheidt, W. R. *Inorg. Chem.* **1999**, *38*, 100-108.

32. Lorkovic, I. M.; Ford, P. C. *Inorg. Chem.* **1999**, *38*, 1467-1473.

33. (a) Lorkovic, I. M.; Ford, P. C. *Inorg. Chem.* **2000**, *39*, 632-633. (b) Lim, M. D.; Lorkovic, I. M.; Wedeking, K.; Zanella, A. W.; Works, C. F.; Massick, S. M.; Ford, P. C. *J. Am. Chem. Soc.* **2002**, *124*, 9737-9743. (c) Kurtikyan, T. S.; Martirosyan, G. G.; Lorkovic, I. M.; Ford, P. C. *J. Am. Chem. Soc.* **2002**, *124*, 10124-10129.

34. Olson, L. W.; Schaeper, D.; Lancon, D.; Kadish, K. M. *J. Am. Chem. Soc.* **1982**, *104*, 2042-2044.

35. (a)Frisch, M. J.; Trucks, G. W.; Schlegel, H. B.; Scuseria, G. E.; Robb, M. A.; Cheeseman, J. R.; Zakrzewski, V. G.; Montgomery, J. A., Jr.; Stratmann, R. E.; Burant, J. C.; Dapprich, S.; Millam, J. M.; Daniels, A. D.; Kudin, K. N.; Strain, M. C.; Farkas, O.; Tomasi, J.; Barone, V.; Cossi, M.; Cammi, R.; Mennucci, B.; Pomelli, C.; Adamo, C.; Clifford, S.; Ochterski, J.; Petersson, G. A.; Ayala, P. Y.; Cui, Q.; Morokuma, K.;

Malick, D. K.; Rabuck, A. D.; Raghavachari, K.; Foresman, J. B.; Cioslowski, J.; Ortiz, J. V.; Baboul, A. G.; Stefanov, B. B.; Liu, G Liashenko, A.; Piskorz, P.; Komaromi, I.; Gomperts, R.; Martin, R. L.; Fox, D. J.; Keith, T.; Al-Laham, M. A.; Peng, C. Y.; Nanayakkara, A.; Gonzalez, C.; Challacombe, M.; Gill, P. M. W.; Johnson, B.; Chen, W.; Wong, M. W.; Andres, J. L.; Gonzalez, C.; Head-Gordon, M.; Replogle, E. S.; Pople, J. A. *Gaussian 98, Revision A.11*; Gaussian. Inc.: Pittsburgh, PA, 1998. (b) Stephens, P. J.; Devlin, F. J.; Cabalowski, C. F.; Frisch, M. J. *J. Phys. Chem.* **1994**, *98*, 11623. (c) Martí, M. A.; Scherlis, A. A.; Doctorovich, F. A.; Ordejón, P.; Estrin. D. A. *J. Biol. Inorg. Chem.* **2003,** 8, 595.

36. Schmidt, J.; Kühr, H.; Dorn, W. L.; Kopf, J. *Inorg. Nucl. Chem. Letters*, **1974**, *10*, 55-61.

37. Wanat, A.; Schneppensieper, T.; Stochel, G.; van Eldik, R.; Bill, E.; Wieghardt, K. *Inorg. Chem.* **2002**, *41*, 4-10.

38. Bonner, F. T.; Pearsall, K. A. *Inorg. Chem.* **1982**, *21*, 1973-1978.

39. Ballou, D. P.; Zhao, Y.; Brandish, P. E.; Marletta, M. A. *Proc. Nat. Acad. Sci.* **2002**, *99*, 12097-12101.

40. Vanin, A. F.; Stukan, R. A.; Mabuchkina, E. B. *Biochim. Biophys. Acta* **1996**, *1295*, 5.

41. Baraldo, L. M.; Forlano, P.; Parise, A. R.; Slep, L. D.; Olabe, J. A. *Coord. Chem. Rev.* **2001**, *219-221*, 881-921.

42. Kowaluk, E. A.; Seth, P.; Fung, H.L. *J. Pharmacol. Exp. Ther.* **1992**, *262*, 916-922.

43. (a) Wasser, I. M.; de Vries, S.; Moënne-Loccoz; Schröder, I.; Karlin, K. D. *Chem. Rev.* **2002**, *102*, 1201-1234. (b) Averill, B. A. *Chem. Rev.* **1996**, *96*, 2951-2964.

44. D´Autréaux, B.; Horner, O.; Oddou, J. L.; Jeandey, C.; Gambarelli, S.; Berthomieu, C.; Latour, J. M.; Michaud-Soret, I. *J. Am. Chem. Soc.* **2004**, *126*, 6005-6016.

7. Conclusiones generales

En una primera etapa se intentó profundizar sobre las relaciones estructura electrónica-reactividad en compuestos nitrosilados, investigando acerca de la influencia de los cambios redox en metales situados a distancias considerables respecto al centro reactivo. Se sintetizó por primera vez el compuesto *trans*-$[NCRu^{II}(py)_4(CN)Ru^{II}(py)_4(NO^+)](PF_6)_3$, que se caracterizó por varias técnicas espectroscópicas (IR, RMN, UV-vis, Raman) y electroquímicas. Este compuesto muestra una banda intensa en el espectro visible (555 nm, ε = 5800 $M^{-1}cm^{-1}$, acetonitrilo), asignada a una transición de transferencia de carga donor-aceptor, del Ru^{II} distante al sistema delocalizado $\{Ru^{II}\text{-}NO^+\}$. Por irradiación de esta banda se observó liberación de NO. La aplicación del modelo de Hush reveló un apreciable acoplamiento electrónico entre los dos centros, con H_{DA} *ca* 2000 cm^{-1}. Los espectros UV-vis e IR, así como los potenciales redox mostraron ser dependientes del solvente. El compuesto es electrofílicamente reactivo en solución, reaccionando con OH^- (k = 9.2 ± 0.2 x 10^3 $M^{-1}s^{-1}$, 25 °C, I = 1 M). Los parámetros de activación para la reacción de adición fueron $\Delta H^{\neq}$ = 90.7 ± 3.8 kJ mol^{-1} y $\Delta S^{\neq}$ = 135 ± 13 J K^{-1} mol^{-1}, siendo la constante de equilibrio para la formación del complejo final de nitrito, K = 3.2 ± 1.4 x 10^{15} M^{-2}. El complejo es capaz de reaccionar con cisteína a pH 4, (k = 7.00 ± 0.09 x 10^3 $M^{-1}s^{-1}$, I = 1 M, 25.0 °C). Por reducción a potencial controlado, se obtuvo un compuesto estable en ausencia de aire, que se caracterizó por espectrocopías UV-vis, IR y EPR. Se concluyó que puede describirse como *trans*-$[NCRu^{II}(py)_4(CN)Ru^{II}(py)_4(NO^{\bullet})]^{2+}$ La oxidación del Ru distante generó otro compuesto estable, que presentaba una reactividad nucleofílica frente al OH^- mucho mayor que el compuesto de partida, siendo la constante de equilibrio para la adición de OH^- ca. 10^{22} M^{-2}. Esta adición está acoplada a procesos irreversibles que no fueron estudiados en detalle.

Las reacciones con OH^- constituyen un tipo de adición nucleofílica relativamente simple, ya que no existen subsiguientes reacciones redox, como es el caso de otro nucleófilos (aminas, tiolatos). Sólo existían estudios previos para la reacción con OH^- en los complejos $[M(CN)_5NO]^{2-}$, (M = Fe, Ru, Os). Se estudió la cinética y el mecanismo de esta reacción para un número importante de nitrosilos de rutenio, que contenían gran variedad de coligandos, carga total, potenciales redox, etc. Primeramente se comprobó que el mecanismo que opera es el mismo que en los compuestos estudiados anteriormente. Este mecanismo consiste en una primera formación de un par iónico entre el complejo y el OH^-, seguida de la adición para generar el complejo de NO_2H, el cual se deprotona rápidamente generando el nitro complejo, que es el producto de la reacción. No se encontró correlación significativa entre la reactividad y la frecuencia de estiramiento del NO^-, ν_{NO}, tal como se proponía en la literatura. Sin embargo, se encontró una correlación entre la reactividad la constante de equilibrio de la reacción, y una buena correlación lineal entre la reactividad (logaritmo de la constante de velocidad para la adición) y el potencial redox de la cupla NO^-/NO°. La pendiente de dicha correlación es de *ca.* 20 V^{-1}, el cual es un valor encontrado en mecanismos asociativos. Además es cercano al predicho por la teoría de Marcus para la transferencia de átomos. Un análisis de los parámetros de activación mostró que al aumentar la velocidad de reacción, aumentaban la entropía y la entalpía de activación. De lo cual, se concluye que la entropía de activación gobierna la reactividad y que el paso más costoso energéticamente es la reorganización del nitrosilo, de una geometría lineal a una angular.

En el contexto de estudiar las adiciones de nucleófilos, se estudió la reacción con tioles, en particular con cisteína. Se postula que el nitroprusiato debe ser reducido por tioles presentes en los medios biológicos para luego liberar NO y ejercer su acción fisiológica. Por ello, la reacción del nitroprusiato con la cisteína ha sido estudiada por varios autores, sin que exista información alguna sobre la

reacción con otros complejos nitrosilados. El estudio se planeó en forma similar al de la reacción con OH^-, seleccionando un conjunto de complejos de rutenio que preanunciaban reactividades diferentes. En un primer paso de reacción se genera rápidamente un intermediario de estequiometría 1:1 (complejo cisteína) con una banda intensa en el visible entre 410 – 470 nm, que luego decae para generar un segundo intermediario de estequiometría 1:2, con una banda en *ca* 380 nm. Ambas reacciones son de primer orden en complejo y cisteína. Finalmente el segundo intermediario decae en la mayoría de los casos generando el correspondiente acuo-complejo y N_2O. El primer intermediario es análogo al producto primario de reacción que se obtiene con nitroprusiato. El segundo también fue propuesto, sin evidencia directa, en el mecanismo de la reacción entre este compuesto y la cisteína. En este trabajo, las medidas se hicieron a distintos pH, seleccionados según el caso, ya que las reacciones son muy rápidas para los compuestos más reactivos (pH's altos, 8 – 10), mientras que los compuestos menos reactivos no reaccionan a pH's bajos (4 – 7). Por esta razón las constantes de segundo orden para la formación de ambos intermediarios se corrigieron teniendo en cuenta el pH y la constante de disociación del grupo SH de la cisteína. Para la formación del primer intermediario, se encontró una correlación entre la reactividad y el potencial redox similar a la encontrada para la reacción con OH^-, pero sólo para los compuestos menos reactivos. Para los más reactivos, la constante de formación corregida es cercana al límite difusional (10^9 $M^{-1}s^{-1}$). Para la formación del segundo intermediario, más lenta, se observó dicha correlación con todos los complejos estudiados.

Un gran número de compuestos nitrosilados de rutenio fueron reducidos y caracterizados por EPR e IR. Estas determinaciones se planearon dado que los complejos de NO ejercen una labilización *trans* que puede llegar a la expulsión de un ligando, generando especies pentacoordinadas. Estos efectos *trans* presentan notable importancia en la activación de procesos enzimáticos por el NO. Se

encontró una notable constancia en los parámetros medidos de *g*, revelando una apreciable covalencia en el fragmento RuNO y la presencia exclusiva de especies hexacoordinadas, a diferencia de resultados de literatura para complejos nitrosilados de hierro, donde se encontraron mayores variaciones. La espectroscopia IR revela un gran decrecimiento de la frecuencia de estiramiento N-O, del orden de 300 cm^{-1}, consistente con los resultados de EPR.

En la última parte de la Tesis se estudió la descomposición de los productos de reducción monoelectrónica del nitroprusiato. Es generalmente aceptado que el nitroprusiato, una vez reducido por los tioles presentes en los medios biológicos, libera NO. Sin embargo, encontramos que la liberación de NO a pH > 5 es lenta, *ca* 5×10^{-5} s^{-1}, lo cual no está de acuerdo con la acción fisiológica que se manifiesta en el orden de minutos. A pH´s más bajos (4 – 5) la velocidad de descomposición y la liberación de NO aumentan en dos órdenes. Esto es suprimido por el agregado de CN^-. La presencia de iones metálicos en el medio (ej: Cu^{2+}) acelera la descomposición. Con estas evidencias, proponemos que la labilización de los cianuros induce la liberación de NO, a través de la intermediación de complejos lábiles. Durante la descomposición del producto de reducción del nitroprusiato, se determinó la presencia de un intermediario dinitrosilado. En base a medidas espectroscópicas (IR, UV-vis, EPR), de cálculos de DFT y a resultados en algunos sistemas similares de literatura, proponemos que dicho intermediario es el complejo *trans*-$[Fe(CN)_4(NO)_2]^{2-}$. El mismo se genera por reacción directa entre el NO liberado durante la descomposición y el $[Fe(CN)_4NO]^{2-}$ (uno de los reactivos que se genera rápidamente por labilización del CN^--trans). Finalmente, el intermediario desproporciona en nitroprusiato y N_2O en relación 2:1. A pH´s bajos (4 – 5), se genera además el complejo $[Fe(CN)_2(NO)_2]^-$ que tiene un espectro EPR característico. Este tipo de complejos pseudo-tetraétricos ha sido encontrado en los sistemas biológicos (proponiéndose la presencia de tiolatos o imidazoles en lugar

de los cianuros), y su acción suele vincularse con funciones de transporte y acumulación de NO.

Agradecimientos

Agradezco al Prof. José A. Olabe, por haber sido mi Director de Tesis, por haberme invitado a participar en su grupo cuando cursé Inorgánica II y por haber sido un guía durante todos estos años. Al Prof. Rudi van Eldik, quien brindó acceso a sus laboratorios en Alemania, por las valiosas discusiones y por estar siempre dispuesto para todo. A Luis M. Baraldo, que codirigió mis trabajos en los primeros años de Tesis. A Pablo Alborés, a quien siempre recurrí cuando necesitaba algo en el laboratorio. A Leonardo Slep por haberme ayudado mucho también en la primera parte de la tesis. A Alejando Parise y Mariela Videla, con quienes compartí el laboratorio, obteniendo muchas veces su colaboración cuando la necesitaba. A Mara E. Ruggiero por haber colaborado en las medidas de las reacciones con OH^- y haber sintetizado varios complejos. A Stephanie Frantz por realizar las medidas de EPR de los nitrosilos de rutenio. A Marcelo Martí y Darío Estrin por su ayuda con los cálculos de DFT. Al Prof. Valentín Amorebieta por las mediciones de espectrometría de masa. Al Prof. Douglas W. Franco, por facilitar la colaboración entre su grupo y el nuestro, lo que concluyó en varios trabajos en conjunto. Al Prof. Wolfgang Kaim, por propiciar los trabajos de colaboración con su grupo en Alemania, y por las discusiones sobre las mediciones de EPR

Agradezco a la Universidad de Buenos Aires por proveer un lugar para desarrollar mi Tesis, por haber financiado con subsidios la compra de materiales y por haberme otorgado tres becas en los primeros años de la tesis. Agradezco al CONICET por la Beca Doctoral Mixta de Tipo II, que me permitió viajar a Alemania numerosas veces. También a la Agencia Nacional para la Promoción Científica y Tecnológica por los subsidios que permitieron obtención de insumos, materiales, realizar viajes, etc.

También quiero agradecer a mis padres, por todo su apoyo en este tiempo.